Dissertation

Submitted to the
Combined Faculties for the Natural Sciences and for Mathematics
of the Ruperto-Carola University of Heidelberg, Germany

for the degree of
Doctor of Natural Sciences

presented by
Silvia de Juanes
born in: Madrid, Spain

Oral examination: 29.04.09

12R-LIPOXYGENASE DEFICIENT MOUSE SKIN MODELS FOR AUTOSOMAL RECESSIVE CONGENITAL ICHTHYOSIS

Referees:
Prof. Dr. Rainer Zawatsky
PD Dr. Karin Müller-Decker

To Alex

Part of this work was published in:

de Juanes S, Epp N, Latzko S, Neumann M, Fürsteberger G, Hausser I, Stark HJ and Krieg P. Development of an Ichthyosiform Phenotype in Alox12b-Deficient Mouse Skin Transplants. JID (2009).

de Juanes S, Epp N, Fürsteberger G, Müller K, Leitges M, Hausser I, Thieme F, Liebisch G, Schnitz G, Stark HJ and Krieg P. Knockout mouse models for the exploration of the role of epidermal Lipoxygenases in epidermal barrier formation and terminal differentiation in skin. Leopoldina symposium on Lipid Signalling (2008) Book of abstracts.

Krieg P, Epp N, Fürsteberger G, **de Juanes S**, Eckl KM, Hennies HC, Hausser I, Thieme F, Liebisch G, Schnitz G and Stark HJ. A novel eicosaneid pathway is essential for the epidermal barrier function: lessons from congenital ichthyosis and 12R-lipoxygenase deficient mice. Leopoldina symposium on lipid signalling (2008) Book of abstracts.

Epp N, Fürsteberger G, Müller K, **de Juanes S**, Leitges M, Hausser I, Thieme F, Liebisch G, Schnitz G and Krieg P. 12R-lipoxygenase deficiency disrupts epidermal barrier function. JCB (2007) 179(4):747-60.

Epp N, **de Juanes S**, Fürsteberger G, Müller K, Leitges M, Hausser I, Thieme F, Liebisch G, Schnitz G, Stark HJ and Krieg P. 12R-lipoxygenase deficiency disrupts epidermal barrier function. First World Conference on Ichthyosis (2007) Book of abstracts.

de Juanes S, Epp N, Fürsteberger G, Müller K, Leitges M, Hausser I, Thieme F, Liebisch G, Schnitz G, Stark HJ and Krieg P. 12R-Lipoxygenase is essential for the epidermal barrier function: lessons from 12R-lipoxygenase deficient mice. 37th Annual ESDR meeting (2007) Book of abstracts.

Eckl KM, Torres S, **de Juanes S**, Metze D, Krieg P and Hennies HC. Functional model systems for congenital ichthyosis: Basic and long way to therapy. 37th Annual ESDR meeting (2007) Book of abstracts.

Other publications:

Eckl KM , **de Juanes S**, Kurtenbach J, Natebus M, Lugassy J, Oji V, Traupe H, Preil ML, Martínez F, Smolle J, Harel A, Krieg P, Sprecher E and Hennies HC. Molecular Analysis of 250 Patients with Autosomal Recessive Congenital Ichthyosis: Evidence for Mutation Hotspots in *ALOXE3* and Allelic Heterogeneity in *ALOX12B*. JID (2009)

Table of contents

Abbreviations

4-OHT	4-hydroxy-tamoxifen
AP-1	Activating Protein-1
APS	Ammonium persulfate
ARCI	Autosomal Recesiv Congenital Ichthyosis
BSA	Bovine serum albumin
CE	Cornified Envelope
CE	Cornified envelope
CLE	Cornified Lipid Envelope
CLE	Cornified lipid envelope
Cre	Causes Recombination
Da	Dalton
del	Delete
DKFZ	Deutsches Krebsforchungszentrum
DNA	Deoxyribonucleic acid
DNase	Deoxyribonuclease
dNTP	Deoxynocleosidetriphosphate
ER	Estrogen Receptor
Erk	Extracellular-signalling regulated kinase
EtOH	Ethanol
Fig	Figure
Fil	Filaggrin
fl	Floxed
FLP	FliPase Recombianse
FRT	Flp Recognition Target
GAPDH	Glycerol-aldehyd-3-phosphat-dehydrogenase
h	Hour
HETE	Hydroxyeicosatetraionic acid
HODE	hydroxyoctadecadienoic acids
HPETE	Hydroxyperoxyeicosatetraionic acid
Inv	Involucrin
K	Kilo, 10^3
kb	Kilobasepair
KO	Knockout
LB	Lamellar Bodies
LBD	Ligand Binding Domain

LI	Lamellar Ichthyosis
LOX	Lipoxygenase
LoxP	Location of crossing-over in bacteriophage P1
M	Molar= mol/l
m	Meter
mAb	Monoclonal antibody
mg	Milligram
min	Minute
ml	Millilitre
mRNA	Messenger ribonucleic acid
NCIE	Non-bullous Congenital Ichthyosiform Erythroderma
n/u	Not used
o/n	Overnight
OD	Optic density
pAb	Polyclonal antibody
PAGE	Polyacrilamide gel electrophoresis
PBS	Phosphate buffered saline
PBS-T	Phosphate buffered saline – Tween 20
PCR	Polymerase Chain Reaction
PFA	Paraformaldehyde
RNA	Ribonucleic acid
RNase	Ribonuclease
ROS	Reactive Oxygen Species
rpm	Revolutions per minute
Rptn	Repetin
RT	Room temperature
RT-PCR	Reverse transcriptase- polymerase chain reaction
SDS	Sodium dodecyl sulfate
SPRR	Small PRoline Rich
Tam	Tamoxifen
TEMED	N,N,N',N'-Tetramethylethylenediamine
TEWL	Transepidermal Water Loss
TGM1	transglutaminase 1
Tm	Melting temperature
wt	Wild-type
µ	Micro, 10^{-6}

Summary

12R-lipoxygenase (12R-LOX) and epidermal LOX-3 (eLOX-3) are part of a recently identified eicosanoid pathway critically involved in skin terminal differentiation. Inactivating mutations in the genes of 12R-LOX and eLOX-3 are causally linked to the development of autosomal recessive congenital ichthyosis (ARCI). ARCI is an inherited skin disease associated with hyperkeratosis and impaired barrier function. To analyse the impact of 12R-LOX in epidermal barrier function and to investigate its physiological role a Cre-LoxP based mouse model for the targeted inactivation of 12R-LOX was generated in a previous study. Constitutive ablation of 12R-LOX leads to early neonatal death due to a severely impaired permeability barrier function. Disruption of barrier function is associated with ultrastructural anomalies in the upper granular layers, disordered composition of ester-bound ceramide species and impairment of profilaggrin processing but does not result in the development of a typical ichthyosiform phenotype in the neonatal skin.

The main focus of this thesis was to characterize the adult phenotype of 12R-LOX deficient skin by establishing skin grafts and conditional knockout models.

When transplanted onto the back of nude mice 12R-LOX$^{-/-}$ mouse skin developed a severe adult phenotype that closely resembles that seen in ichthyosis patients, with thickening of the epidermis, hyperproliferation, hypergranulosis, focal parakeratosis and marked hyperkeratosis. In contrast to the neonatal knockout phenotype, 12R-LOX deficiency did not affect profilaggrin processing in the adult transplanted skin but rather resulted in the over-expression of fully processed filaggrin monomers and other components of the cornified cell envelope such as involucrin and repetin.

In order to study the adult phenotype in more detail we established a temporally-controlled site-specific 12R-LOX knockout model by using a transgenic mouse line expressing a tamoxifen-dependent Cre recombinase under the control of the Keratin 14 promoter. In these *Alox12b*$^{fl/fl/K14\text{-}Cre\text{-}ERT2}$ (mutant) mice, Cre-mediated *Alox12b* inactivation was detected upon tamoxifen treatment but also spontaneously as early as day 17 after birth in K14-expressing tissues such as epidermis, tongue, cornea and thymus. 12R-LOX ablation resulted in the development of a severe phenotype associated with growth retardation, dramatic loss of body weight and premature death. Morphological changes observed in mutant mice included focal alopecia, scaling of the skin and palmoplantar keratoderma. Histological analyses of skin biopsies confirmed the development of an ichthyosiform phenotype mimicking that observed in ichthyosis patients.

Comparative gene expression profiling to identify disease-related downstream targets of the 12R-LOX/eLOX-3 pathway showed that 12R-LOX ablation is associated with deregulation of members of the activating protein-1, small proline rich protein and keratin gene families, known to be important for the epidermal differentiation.

This data documents a crucial role of 12R-LOX in the establishment and maintenance of the epidermal barrier function. Moreover, 12R-LOX knockout mice may be a suitable model to investigate molecular mechanisms of the LOX pathway related to diseased phenotype as well as for the development of novel strategies towards a therapy for ARCI forms associated with impaired LOX metabolism.

Zusammenfassung

Die 12R-Lipoxygenase (12R-LOX) und die Epidermis-Typ Lipoxygenase-3 (eLOX3) sind Schlüsselenzyme eines neuen Stoffwechselweges in der Haut, der bei der terminalen Differenzierung eine wichtige Rolle spielt. Eine genetische Inaktivierung einer dieser beiden LOX führt beim Menschen zur Ausbildung von autosomal rezessiver kongenitaler Ichthyose (ARCI), einer vererbten epidermalen Verhornungsstörung, die mit dem Verlust der epidermalen Barrierefunktion assoziiert ist.

Zur Untersuchung der physiologischen Funktion von 12R-LOX in der Haut und ihrer Rolle bei der Pathogenese von ARCI wurde in einer vorangegangenen Arbeit unter Verwendung der Cre/LoxP-Technologie ein Mausmodell für eine konstitutive und induzierbare 12R-LOX-Geninaktivierung etabliert. Der konstitutive 12R-LOX-Genknockout führt in den Mäusen zu einem frühen neonatalen Tod, der auf einer massiven Beeinträchtigung der epidermalen Barriere beruht. Der Verlust der Barrierefunktion geht einher mit Störungen der Filaggrin-Prozessierung und des Ceramid stoffwechsels, führt aber in der neonatalen Haut nicht zur Ausbildung eines typischen ichthyosiformen Phänotyps.

Ziel meiner Arbeit war die Untersuchung des adulten 12R-LOX-Knockoutphänotyps anhand von Hauttransplantaten und eines konditionellen Knockoutmodells.

Nach Transplantation auf den Rücken immundefizienter Nacktmäuse bildeten die Häute der 12R-LOX-Knockoutmäuse eine vielschichtige Epidermis aus, die mit Acanthose, Hypergranulose und Hyperkeratose typische Merkmale eines ichthyosiformen Phänotyps aufweist. Im Gegensatz zum neonatalen Knockout-Phänotyp war in der transplantierten Haut keine Störung der Filaggrinprozessierung zu beobachten, viel eher eine starke Überexpression von Filaggrinmonomeren und anderer Komponenten des „Cornified Cell Envelopes“.

Um den adulten Phänotyp im Detail studieren zu können, wurde unter Verwendung von K14-Cre-ER^{T2}-Mäusen, die eine Tamoxifen-induzierbare Cre-Rekombinase unter Kontrolle des Keratin-14-Promoters exprimieren, ein Mausmodell für eine gewebspezifische und zeitlich kontrollierte Inaktivierung des 12R-LOX Gens hergestellt. In den doppeltransgenen Mutanten kam es Tamoxifenbehandlung, aber auch spontan ab einem Alter von 17 Tagen, zu einer Inaktivierung des 12R-LOX-Gens in Epidermis und anderen K14-exprimierenden Geweben, was mit der Ausbildung eines ausgeprägten Phänotyps assoziiert war, gekennzeichnet

makroskopisch durch Fellveränderungen mit fokaler Alopezie, einer starken Schuppung der Haut und ausgeprägte Palmoplantarkeratose sowie durch einen dramatischen Gewichtsverlust und einen vorzeitigen Tod. Histologische Analysen der Haut belegten die Ausprägung eines typischen ichthyosiformen Phänotyps.

In meiner Arbeit konnte ich weiterhin durch genomweite Expressionsanalyse mittels Illumina-Bead-Arrays zeigen, dass die Deletion von 12R-LOX mit einer Deregulierung von Mitgliedern der „Activating Protein-1“ (AP-1), der „Small Proline Rich Proteins“ (SPRR) und der Keratin-Genfamilien assoziiert ist.

Die Ergebnisse dieser Arbeit belegen eine essentielle Funktion der 12R-LOX für die Entwicklung und Aufrechterhaltung der epidermalen Barrierefunktion. Mit der Etablierung und Charakterisierung einer konditionellen 12R-LOX-Knockout-Mauslinie habe ich ein geeignetes Modellsystem zur Verfügung gestellt für weitergehende Analysen der molekularen Mechanismen des 12R-LOX/eLOX-3-Stoffwechselwegs, die für die Entstehung des Ichthyose-Phänotyps von Bedeutung sind. Das Modellsystem könnte darüber hinaus auch für die Entwicklung neuer Ansätze zur Therapie von Ichthyosen von Bedeutung sein.

1. Introduction

1.1. The Skin

The skin is the largest organ in the human body, contributing more that 10% of the body mass. Its large mass is equal to its wide range of biological functions, forming a dynamic interface between our body and its external environment. It serves as a protective barrier preventing internal tissues from exposure to trauma, ultraviolet radiation, temperature extremes, toxins and bacteria. Other important functions include sensory perception, immunological surveillance, thermoregulation, and control of fluid loss. The skin consists of two mutually dependent layers known as the epidermis and dermis. The major cell type of the epidermis is the keratinocyte, making up about 90% of epidermal cells. In addition, the epidermis houses specialised cell types including the pigment containing melanocytes, antigen processing Langerhans cells, and pressure-sensing Merkel cells. The dermis contains collagen, elastic fibres, blood vessels, sensory structures and fibroblasts [1, 2]. The dermis also houses nail, hair follicles and sebaceous glands. Beneath the dermis lies the subcutaneous or fat layer.

1.1.1. Epidermis: structure and function

The epidermis is the outermost and thinnest layer of the body with a multilayered structure and self-renewing ability. The epidermis rests on the basement membrane and is divisible into the basal (stratum basale), the spinous (stratum spinosum), the granular layers (stratum granulosum) and the stratum corneum (Fig. 1). The epidermal keratinocytes have the function of producing, maintaining and renewing the most superficial and crucial compartment, the stratum corneum. The renewal process occurs by cell division of keratinocytes in the basal layer, which migrate towards the surface layer, a process known as keratinisation [2]. The stratum corneum architecture resembles a “brick and mortar” organization, where the cornocytes form the “bricks” attached together by desmosomes and the “mortar” of lipids sequestered in the extracellular domains. This layer of terminally differentiated keratinocytes provides the physical basis for several types of barrier functions including: barrier to water permeability, penetration of xenobiotics, and microbial and parasitic invasion. Additionally the stratum corneum barrier helps to maintain the integrity of other components by providing defence against UV radiation and free radical injury, the immune barrier and crucial skin functions such as thermoregulation, waste elimination and sensory transduction (heat, cold, pain etc…) [1].

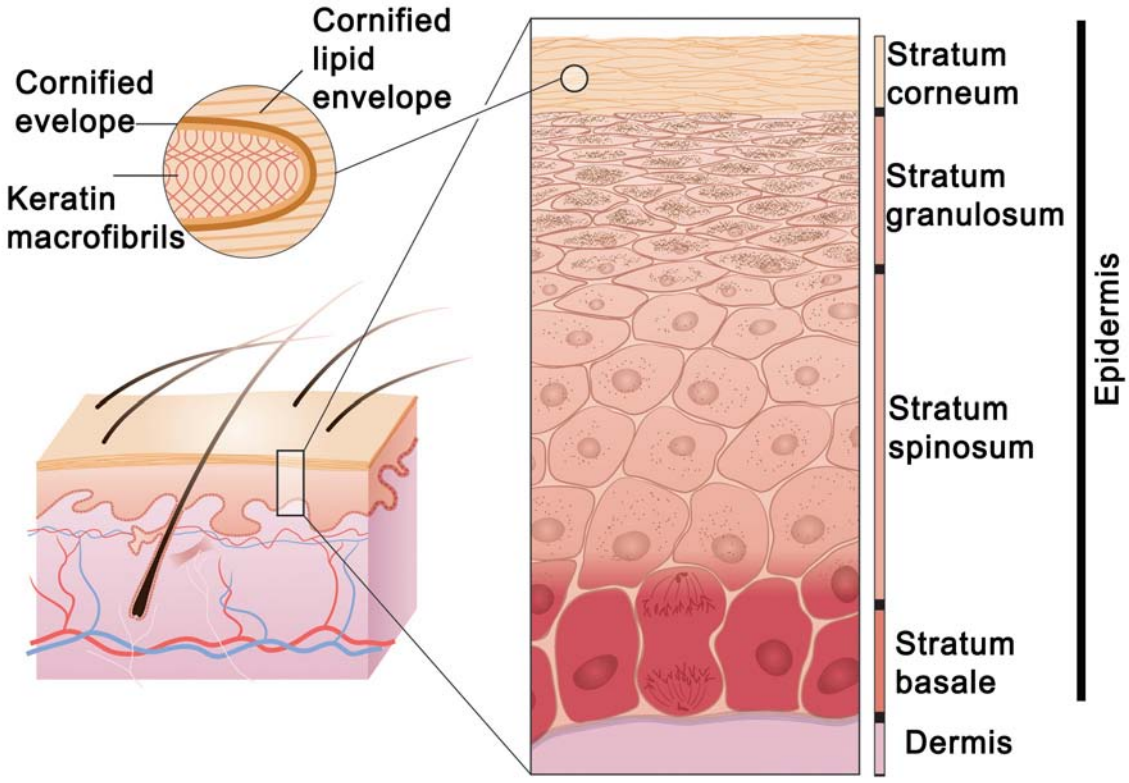

Figure 1: Schematic diagram of epidermal structure and differentiation
Picture adapted from Segre, 2006 [3]

1.1.2. Terminal differentiation of the epidermis

The basal layer keratinocytes are actively dividing and express keratin K5 (type II) and K14 (type I) as the predominant keratin pair. The process of terminal differentiation begins when basal cells lose their ability to adhere to the basement membrane. In the intermediate spinous layers, the cells reinforce a durable cytoskeleton framework of keratin filaments to provide the mechanical strength necessary to resist physical trauma. They then express K1 (type II) and K10 (type I) as the predominant keratin pair. In the granular layers, lipids are stored inside lamellar bodies (LB) and keratins are bundled into macrofibrils through their association with filaggrin. At this point the main keratinocyte proteins are keratin and filaggrin, which are the main components of the cornified envelope (CE). The CE is assembled by sequential incorporation of precursor proteins directly underneath the plasma membrane. As the cell membrane disintegrates, the subsequent calcium influx activates the transglutaminases (TGM), enzymes to irreversibly cross-link the CE proteins, such as filaggrin, loricrin and keratins, creating a tough, insoluble sac that surrounds the keratin fibres. Finally, the nucleus breaks down and the lipids are extruded into the intercellular space forming the cornified lipid envelope (CLE) onto the CE scaffold and the intercellular lipid lamellae [3, 4]. A broad number of diseases appear when the process of terminal differentiation is disturbed within these we find a group of keratinisations disorders known as ichthyoses.

1.2. Ichthyosis

The term 'ichthyosis' is derived from the Greek root 'ichthys' meaning fish and used for those disorders sharing generalized scaling of the skin. Ichthyoses are a clinically and genetically heterogeneous group of cornification disorders, characterized by generalized desquamation of the skin, usually with erythema (Fig. 2) [5, 6].

Ichthyoses can be inherited or acquired, presenting at birth or later in life, can be limited to the skin, then called non-syndromic, or be an element of a multisystem disorder, then called syndromic. It is necessary to distinguish the congenital ichthyoses, which at birth typically exhibit a collodion membrane phenotype or ichthyosiform erythroderma, from vulgar ichthyoses, which manifest after birth. Thus all types of ichthyoses can be grouped into four major groups namely; non-syndromic vulgar or noncongenital ichthyosis, syndromic vulgar or noncongenital ichthyosis, non-syndromic congenital ichthyosis, syndromic congenital ichthyosis.

The subgroup of non-syndromic Autosomal Recessive Congenital Ichthyoses (ARCI) conformed by Lamellar Ichthyosis (LI) and Non-bullous Congenital Ichthyosiform Erythroderma (NCIE) is characterized by non-bullous hyperkeratosis. The more severe phenotype LI has an estimated prevalence of 1:200,000-300,000. Most patients (~90%) are born encased in a tight shiny covering, described as collodion membrane, and often show erythroderma. During the first weeks of life, the membrane is gradually replaced, and patients develop large, dark or plate-like scales, sometimes with marked palmoplantar hyperkeratosis. In contrast, individuals with NCIE show a more pronounced erythroderma with fine, white scaling [5]. The presence of hyperkeratosis with an increase in stratum corneum thickness, a normal or prominent granular layer and increased mitoses suggest a hyperproliferative epidermal defect in NCIE [6].

To date, six genes for LI/NCIE (type1-6) have been localized and five of them identified [7-10]. In about 35-40% LI/NCIE is caused by homozygous or compound heterozygous mutations in *TGM1* (LI/NCIE type 1 ,MIM 190195). *TGM1* (encoding transglutaminase 1) is implicated in the crosslinking of structural proteins and lipids forming the cornified cell envelope. *ABCA12* mutated in lamellar Ichthyosis type 2 (MIM 607800) and harlequin Ichthyosis encodes a lipid transporter critically involved in the maturation and secretion of lamellar bodies (LB). The other recently identified ARCI genes including the lipoxygenase (LOX) genes *ALOX12B* (MIM 603741) and *ALOXE3* (MIM 607206), a novel cytochrom P450 gene *CYP4F22* (MIM 611495) and a putative receptor gene *ichthyin* (MIM 609383) have been suspected to be part of a common lipid pathway [6].

Figure 2: ARCI patients
(a) generalized dark, large scaling in LI. (b) collodion membrane.
Patients from Dr. Hans Christian Hennies and Prof. Dr. med. Heiko Traupe [5].

1.3. Lipoxygenases

Lipoxygenases are widely distributed in plants, fungi, and animals. They are a heterogeneous family of non-heme iron dioxygenases that catalyze the stereo- and regio-specific oxygenation of polyunsaturated fatty acids with 1-cis, 4-cis-pentadiene structures (Fig. 3). About 40 LOX have been cloned and sequenced from plants and mammals [11-13] and one isoform, an 8*R*-lipoxygenase, from a marine invertebrate *Plexura homomalla* [14]. LOX convert Arachidonic Acid (AA) to labile hydroperoxy intermediates that are converted along both enzymatic and non-enzymatic pathways to their reduced analogs hydroxy-eicosatetraenoic acids (HETEs) and other molecules such as leukotrienes, lipoxins and hepoxilins, [15]. LOX-derived eicosanoids play important roles in inflammatory processes, blood clotting, leukocyte chemotaxis, and distinct inflammatory skin diseases [16]. The LOX products may act as discrete signalling molecules or give rise to the production of Reactive Oxygen Species (ROS) and oxidative degradation products of HETEs and HODEs [17].

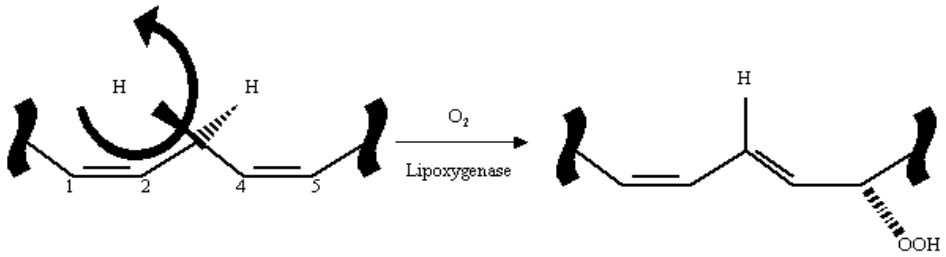

Figure 3: Oxidation catalyzed by lipoxygenases

Mammalian LOX are categorized according to the positional specificity of oxygen insertion into arachidonic acid [18]. Four positional LOX isoforms have been identified in mammalian tissue, comprising the 5-, 8-, 12-, and 15-LOX, which insert oxygen to yield the corresponding S-enantiomeric hydroperoxyeicosatetraenoic acid as primary products (Fig. 4). A further increase of LOX diversity was found due to the existence of isozymes with identical positional specificity such as leukocyte-type (*l*), platelet-type (*p*), and epidermis-type (*e*) 12S-LOX [19]. An additional complexity is introduced by the identification of a mammalian LOX generating products with R-chirality [16].

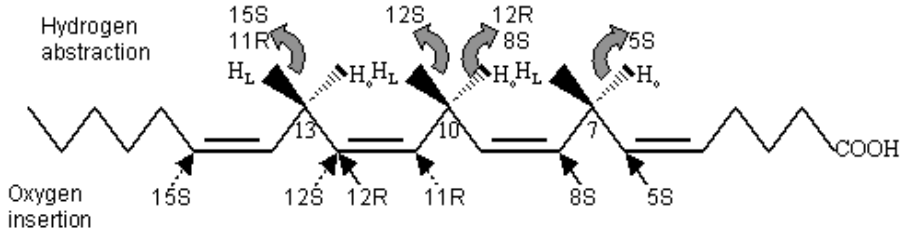

Figure 4: Stereochemical control of the LOX reaction

Six different human LOX isoenzymes have been cloned by several groups including 5S-LOX [20], two 12-LOX isoforms, *p* 12*S*-LOX [15] and 12*R*-LOX [21], two 15-LOX-isoforms, 15-LOX-1 and 15-LOX-2, , and *e*LOX3 [22] while in mice seven isoforms have been identified, 5-LOX, 8S-LOX [19], *p*- and *l*-12S-LOX, 12R-LOX and *e*LOX3.

1.3.1. Structure

LOX proteins consist of single polypeptide chains with molecular masses of 75-80 kDa in animals and up to 94-104 kDa in plants. The proteins are composed of a N-terminal β-barrel domain and a larger catalytic domain containing a single atom of non-heme iron. The iron atom is coordinated by three conserved histidines, a conserved isoleucine at the C terminus of the protein [18], water and by a variable sixth ligand. The sixth ligand is either histidine or asparagine with the exception of 15-LOX-2 and 8S-LOX in which a serine is present [19].The N-terminal β-barrel domain

shares significant homology with a similar domain located at the C terminus of mammalian lipases, suggesting that these domains may have similar functions in vivo [23]. Inactive enzymes contain iron in the ferrous form. Oxidation to the active ferric enzyme is required for catalysis.

Although they are four crystal structures available, there is no consensus on how substrate gains access to the catalytic center of the protein [18]. In addition, little information is available regarding the sequestration of the fatty acid substrate. In general, the positional specificity of LOX is determined by the overall size and shape of the arachidonic acid binding pocket.

1.3.2. Function

LOX are key enzymes that generate a great variety of bioactive eicosanoids. The LOX products HPETEs or its reduced hydroxy derivative HETEs have numerous biological activities: 12-HETE is described to be a modulator of neurotransmissions [24], 5-HETE has been shown to exert receptor-mediated action on calcium fluxes [25] and 12S-HETE has potent effects on cell adhesion and metastasis in prostate carcinoma [26]. Some HETEs such as 8S-HETE have also been described as ligands for nuclear receptors [27, 28].

LOX catalyze as well the peroxidation of membrane lipids, thus inducing structural and physical changes in the cell implicated in cell differentiation and maturation. In this regard, LOX have been discussed to play a potential role in red cell maturation [29], as well as in the maturation of erythroid cells [30], keratinocytes [31, 32], lens epithelium [33], macrophages and adipocytes [27, 34].

The overexpression of distinct LOX isoforms or the accumulation of LOX products in some tissues is related to the development of pathologies. This relation has been documented in Alzheimer [24], arthritis [35], atherosclerosis [36, 37], asthma and other chronic inflammatory diseases [38], and cancer [17].

1.3.3. Classification

The different isoforms in mammals share about 40-90% amino acid sequence identity, with one isoform in different animals being more similar than different isoforms in the same animal. Based on sequence identity a phylogentic tree has been constructed that subdivides the LOX family into four subfamilies (Fig. 5), the 5-LOX, the platelet-type 12-LOX, the 12/15-LOX enzymes exhibiting a dual positional specificity, and the epidermis-type LOX which are predominantly expressed in the skin [39]. Members of this family are the 15S-LOX-2 and its mouse and rat ortholog,

the 8S-LOX, as well as the 12R-LOX and *e*LOX3. Another epidermis-type LOX isoform in mouse, *e*12S-LOX is more related to the 12S/15S-LOX family.

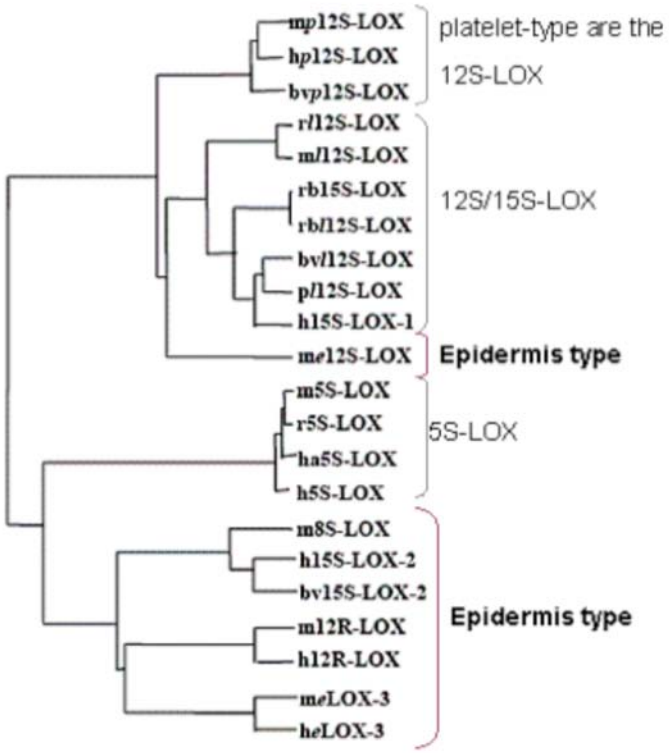

Figure 5: Phylogenetic tree of mammalian LOX

1.3.4. Epidermal lipoxygenases

The epidermis-type LOX form the most heterogeneous LOX subfamily. Their genes map close together within a gene cluster on human chromosome 17p13.1 that was also found to be highly conserved within a syntenic region in the central region of the mouse chromosome 11 [40]. Although the epidermis-type LOX are phylogenetically closely related sharing about 50% amino acid identity, the different enzymes exhibit a rather heterogeneous regio- and stereospecifity. Besides the epidermis-type LOX, 15-LOX-2 and 8-LOX in mice, 12R-LOX and e-LOX-3, other LOX isoforms including p12-LOX and 5-LOX have been found in human and mouse epidermis. The distinct LOX exhibit a differentiation-dependent pattern in the epidermis indicating that they may have different functions. 15-LOX-2, 8-LOX, 12R-LOX and *e*LOX-3 are predominantly expressed in the suprabasal keratinocytes.

1.3.5. 12R-LOX and *e*LOX-3

12R-LOX and *e*LOX-3 differ from all other mammalian LOX by unique structural and enzymatic properties. Both proteins contain an extra domain that is located at the surface of the catalytical unit. 12R-LOX is the only known mammalian LOX, which forms products with R chirality. Unlike all other LOX, *e*LOX-3 has been shown to transform 12R-HPETE, the product of the 12R-LOX to a hepoxilin-like epoxyalcohol, 8R-hydroxy-11R,12R-epoxyeicosatrienoic acid. Thus, *e*LOX3 is a hydroperoxide isomerase rather than a conventional LOX and a component of novel LOX pathway that consists of the sequential activities of the 12R-LOX and *e*LOX3 converting arachidonic acid into epoxy alcohols (Fig. 6). There is increasing evidence that this pathway plays an important role in terminal differentiation of keratinocytes.

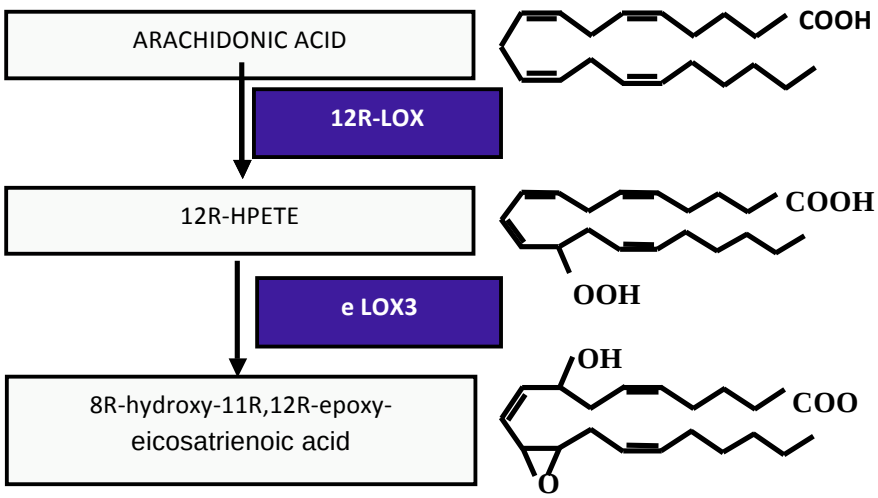

Figure 6: Schematic diagram of 12R-LOX and *e*LOX3 activity

The evidence that the 12R-LOX/*e*LOX3 pathway is involved in terminal differentiation is based on the following observations. First, both enzymes were found to be concomitantly expressed in the stratum granulosum of human and mouse epidermis. Second, recent genetic studies have identified mutations in the coding regions of 12R-LOX and *e*LOX3 genes in patients with ARCI. The examination of the molecular data revealed allelic heterogeneity for *ALOX12B* and two mutational hotspots in *ALOXE3*. Functional analysis of all missense mutations and a splice site mutation demonstrated that complete loss of function of the enzymes underlies the ARCI phenotype [41].

To investigate the role of 12R-LOX in epidermal differentiation and its implication for the development of ichthyoses several genetically modified animals were developed in our group in the last years.

1.4. Genetically modified animals

A genetically modified animal provides a powerful approach for elucidating gene function in the whole animal. Genes can be completely deleted, but this often leads to embryonic lethality, making it impossible to study the gene function in later developmental stages or in adults. This problem can be overcome by making conditional knockout (KO) mice, which allows a gene to be inactivated in a specific tissue or time. Since this technique was first described in 1987, it has been used in many cases to study protein function *in vivo*.

1.4.1. Conditional Knockout

The conditional KO technology is based on the Cre-LoxP recombination system. Typically, a conditional KO allele is made by inserting LoxP sites into two introns of a gene or at the opposite ends of a gene. Expression of Cre recombinase in mice carrying this allele catalyzes recombination between the LoxP sites and inactivates the gene. By expressing Cre recombinase from a tissue-specific promoter, the gene can be inactivated in a cell-type-specific fashion. The timing of Cre expression can also be controlled using inducible Cre expression systems.

1.4.1.1. Inducible conditional Knockout

To generate somatic mutations in a defined gene, at a given time of the life of the animal and in a specific cell type, inducible Cre recombinases have been generated using natural gene expression regulators. Steroid hormones such as estrogen, progesterone, androgen and glucocorticoid regulate the gene expression directly through classical intracellular steroid hormone receptors and possibly indirectly through novel unconventional membrane bound receptors belonging to the G protein coupled receptor superfamily [42, 43]. The intracellular steroid hormone receptor possesses a ligand binding domain (LBD), which can be used for posttranslational control of the Cre activity. A fusion protein containing Cre and the LBD can be expressed under the control of any given cell type specific promoter. In the absence of steroid hormone, the LBD are bound by heat shock proteins (Fig. 7), which inactivate recombinase activity. After binding the hormone, the receptors translocate from the cytoplasm to nucleus and activate or repress transcription of their target genes, which is mediated through binding to special palindromic HRE sequences (hormone responsive element). Until recently, posttranslational inducible recombinase systems used wild type LBDs of steroid hormone receptors fused to Cre [44, 45]. However, these chimeric recombinases are activated by endogenous steroids of the LBD and are therefore of limited use for applications in mice. Consequently, mutations were introduced into the LBDs of chimeric Cre recombinases that abolish the activation by natural ligands while retaining the ability to be activated by synthetic hormone antagonists. Mutated LBDs of the glucocorticoid receptor [46], the androgen receptor [47], the progesterone receptor [48] and the estrogen receptor [49] have been used to regulate Cre activity at posttranslational

level.

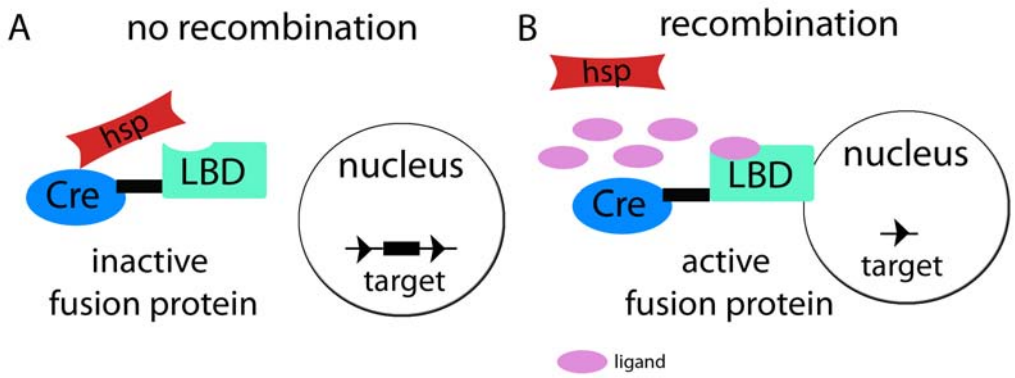

Figure 7: Posttranslational control of Cre activity
(A) Cre is fused to the Ligand Binding Domain (LBD) of a steroid hormone receptor. (B) Upon Tamoxifen (Tam) binding the complex dissociates and Cre-LBD translocates to the nucleus and mediates recombination.

Through time several posttranslational system of Cre fused to the LBD of the estrogen receptor (ER) have been made including LBDs of the a mutant human ER [50] which possess reduced affinity to endogenous estrogen and high affinity to the synthetic ligand tamoxifen.

Two different mutant hER LBDs, termed ER^{T1} and ER^{T2}, each containing three different amino acid substitutions, which result a 10-fold higher affinity to synthetic ligands were developed. The chimeric molecule between Cre and the triple mutant ER^{T2} can be activated by 10 nM 4-OHT. The activation characteristics of the Cre-ER^{T2} *in vivo* were confirmed in 1999. A transgenic mouse strain with Cre-ER^{T2} expression restricted to keratinocytes (K14-Cre-ER^{T2}) requires 10-times lower doses of tamoxifen in order to activate Cre activity in comparison with a mouse strain, which expresses the Cre-ER^{T} single mutant controlled by the same promoter [51, 52]. Numerous Cre-ER^{T2} transgenic exist today which express the fusion protein ubiquitously [53], or restricted to muscle [54], skin [51], and to several other tissues.

1.5. 12R-LOX deficient mouse

To investigate the physiological role of 12R-LOX and to analyze the molecular mechanisms that underlie the ichthyosiform skin phenotype, mice with targeted inactivation of the 12R-LOX gene were generated in our lab by using the Cre-LoxP system.

The goal of the targeting strategy for the inactivation of the 12R-LOX was to delete an essential exon 8. To this end mice with a floxed *Alox12b* allele were generated, in which a resistance cassette flanked by two LoxP sites is located upstream of exon 8 and a third LoxP site is inserted downstream of exon 8. By

crossing these mice with CMV-Cre deleter mice, which express the Cre recombinase ubiquitously mice were obtained with a disrupted *Alox12b* allele. The constitutive deletion of exon 8 leads to a complete lack of 12R-LOX protein expression in the skin of homozygous mutant mice. At birth, *Alox12b*$^{-/-}$ mice are hard to distinguish from wild-type and heterozygous littermates upon macroscopic inspection. However, their skin soon begins to develop a red, shiny appearance and becomes somewhat sticky to the touch. All homozygous mutant mice die within 3–5 h after birth.

The lethal phenotype of the 12R-LOX–deficient mice results from water loss as a result of impaired epidermal barrier function. Homozygous *Alox12b*$^{-/-}$ mice loos ~30% of their body weight within 3 h and they have an 8-fold increased transepidermal water loss (TEWL) compared with wild-type and heterozygous littermates. As shown by dye penetration assays the inside-out as well as the outside-in water barrier function is severely affected in the epidermis of 12R-LOX–deficient mice.

The epidermis of newborn *Alox12b*$^{-/-}$ mice does not exhibit overt abnormalities in the stratified organization of keratinocytes but some ultrastructural anomalies at the granular layer. The cells of the granular layer regularly contained vesicular structures of variable sizes, which are electron-lucent with some smaller vesicles inside and with some lamellar structures adhering to the surrounding membrane. Lipid metabolism disorders may be associated with the observed phenotype. The levels of total fatty acids, cholesterol, and total free ceramides are similar between control and 12R-LOX–deficient mice. Significant differences were found in the subfractions of ester-bound lipids between wild-type and KO mice.

The level of expression of the following terminal differentiation markers; keratin 5 and 10, loricrin, and involucrin are not altered in the *Alox12b*-null versus control mice. However, there is a complete loss of filaggrin monomer in KO epidermis, which is associated with enhanced levels of proteolytically derived intermediates, indicating that proteolytic processing of profilaggrin is impaired.

These data confirms that 12R-LOX has a crucial role in the establishment of the epidermal barrier [55].

1.6. Aim of the project

As already described, mutations in the epidermal lipoxygenases genes that lead to inactivation of 12R-LOX and *e*LOX3 have been associated with epidermal differentiation disorders. To learn more about the role of the epidermal lipoxygenases in skin differentiation our group developed a 12R-LOX KO-mouse model. Constitutive 12R-LOX KO mice die rapidly after birth due to dehydration and leave us a very small window of time to analyze the cutaneous phenotype. The aim of this study is to analyse the adult 12R-LOX KO phenotype by using techniques such as skin grafting and by developing a conditional mouse model with inducible 12R-LOX inactivation in the epidermis which furthermore will provide a useful animal model for a detailed analysis of mechanisms involved in ARCI forms which are associated with impaired LOX metabolism.

2. MATERIALS

2.1. Chemicals

Name	Company
Acetic acid (p.a. reagent)	FlukaChemie, Buch, Germany
Acetone (p.a. reagent)	FlukaChemie, Buch, Germany
Agarose	Sigma-Aldrich, Steinheim, Germany
Aprotinin	Sigma-Aldrich, Steinheim, Germany
ε-Amino-n-Capronsäure	Sigma-Aldrich, Steinheim, Germany
Ammonium peroxidisulphate (APS)	Merk, Darmstadt, Germany
β-mercaptoethanol	Sigma-Aldrich, Steinheim, Germany
Boric Acid	Calbiochem, Merck KG, Darmstadt, Germany
Bovine serum albumin, BSA	Roth, Karlsruhe, Germany
Bromophenolblue	Amerscham Biosciences, Freiburg, Germany
Chloroform	J.T. Backer, Deventer, Netherlands
Coomassie brilliant blue R	Gerbu, Gaiberg, Germany
Eosin	Merk, Darmstadt, Germany
Ethanol	DKFZ, Heidelberg, Germany
Ethidium bromide	Sigma-Aldrich, Steinheim, Germany
Ethylenediaminetetraacetic acid, EDTA	Roth, Karlsruhe, Germany
Food pellets	ProvimiKliba, Swizerland
Glycerin	Merk Biosciences, Schwalbach, Germany
Hydrocloric acid, HCl	Merk, Darmstadt, Germany
Hydrogen peroxide, H_2O_2	Roth, Karlsruhe, Germany
4-hydroxy-tamoxifen	Sigma-Aldrich, Steinheim, Germany
Isopropanol (p.a. reagent)	Sigma-Aldrich, Steinheim, Germany
LDS sample buffer	Invitrogen, Karlsruhe, Germany

Leupeptin	Sigma-Aldrich, Steinheim, Germany
Linoleic acid	Cayman Chamicals, Michigan, U.S.A.
α2-Macoglobulin	Roche Diagnostics, Mannheim, Germany
Magnesium chloride, $MgCL_2$	Merk, Darmstadt, Germany
Mayer´shemalum solution	Merk, Darmstadt, Germany
MES SDS Running buffer	Invitrogen, Karlsruhe, Germany
Methanol	DKFZ, Heidelberg, Germany
Milk powder	Fluka, Neu-Ulm, Germany
Mounting medium	DakoCytomation, Hamburg, Germany
N,N,N´,N´-Tetramethylethylenediamine (TEMED)	Applichem, Darmstadt, Germany
Norleucine	Sigma, Steinheim, Germany
Pap pen	Novocastra Novo, Newcastle, U.K.
Phosphate buffered saline (PBS)	Biochrome AG, Berlin, Germany
Phenylmethylsulfonamide fluoride (PMSF)	Sigma, Steinheim, Germany
Ponceau S	Sigma, Steinheim, Germany
2-Propanol p.A.	Sigma, Steinheim, Germany
Proteinase K	GerbuBiotechnik, Gaiberg, Germany
Reducing agent	Invitrogen, Karlsruhe, Germany
Rotiphorese gel 30 (37.5:1)	Carl Roth, Karlsruhe, Germany
Sodium dodecylsulphate (SDS)	GerbuBiotechnik, Gaiberg, Germany
Sodium chloride	J.T. Baker, Deventer, Netherlands
Sodium desoxycholate	Merk, Darmstadt, Germany
Sodium fluoride	Merk, Darmstadt, Germany
Sodium hydroxide	Merk, Darmstadt, Germany
Sodium orthovanadate	Sigma, Steinheim, Germany
Sunflower oil	Sigma, Steinheim, Germany

Tissue-embedding medium	Vogel, Giessen, Germany
Tissue Tek OCT compound	Vogel, Giessen, Germany
Transfer buffer	Invitrogen, Karlsruhe, Germany
Tris Base	Carl Roth, Karlsruhe
Trishydroxymethylaminomethane hydrochloride (Tris/HCl)	Sigma, Steinheim, Germany
Triton X-100	Sigma, Steinheim, Germany
Tween-20	Merk Bioscience, Schwallbach, Germany
Vitro-Clud (Eukitt)	R. Langenbrinck, Teningen, Germany
Water Aqua bidest-grade	Millipore, Eschborn, Germany
Xylol	Merk, Darmstadt, Germany

2.2. Kits

Name	Company
DC quick Lowry solutions A, B and C	Bio-Rad Laboratories, CA, U.S.A.
ECL reagent for western	Amersham Bioscience, Freiburg, Germany
QIAamp RNA Midi kit	Qiagen, Hilden, Germany
RedTaq™ DNA polymerase	Sigma, Seelze, Germany
RNeasymini kit	Quiagen, Hilden, Germany
RQ1 RNase-Free DNase	Promega, Mannheim ,Germany
Taq - DNA – Polymerase	Q-Biogene, USA

2.3. Antibodies

2.3.1 Primary antibodies

Name	Host/Type	Dilution used Immunofluorescence/ Western Blot	Source Company
12R-LOX (Y2)	Rabbit polyclonal	not used (n.u.)– 1:2000	P. Krieg
12R-LOX (12R-1)	Mouse monoclonal	1:300 – n.u.	P. Krieg
Anti c-Jun SC - 45	Rabbit polyclonal	n.u. - 1:1000	Santa Cruz Biotechnology, Heidelberg, Germany
Anti c-Fos #2250	Rabbit polyclonal	n.u. - 1:1000	Cell Signaling, MA, U.S.A.
Anti ERK-1,2 MAP Kinase #9102	Rabbit polyclonal	n.u. / 1:1000	Cell Signaling, MA, U.S.A.
Anti phospho-ERK-1,2 MAP Kinase #9101	Rabbit polyclonal	n.u. / 1:1000	Cell Signaling, MA, U.S.A.
Anti Filaggrin	Rabbit polyclonal	1:50 / 1:4000	Babco, Richmond, CA, U.S.A.
Anti GAPDH	Maus polyclonal	n.u. / 1:800	Santa Cruz Biotechnology, Heidelberg, Germany
Anti Involucrin	Rabbit polyclonal	1:50 / 1:1000	Babco, Richmond, CA, U.S.A.
Anti JunB SC-46	Rabbit polyclonal	n.u. / 1:1000	Santa Cruz Biotechnology,

			Heidelberg, Germany
Anti Keratin 5	Rabbit polyclonal	1:50 / 1:10000	Babco, Richmond, CA, U.S.A.
Anti Keratin 6	Rabbit polyclonal	1:50 / 1:1000	Covance, Princeton, NJ U.S.A.
Anti Keratin 10	Rabbit polyclonal	1:50 / 1:10000	Babco, Richmond, CA, U.S.A.
Anti Keratin 14	Guinea pig polyclonal	1:50 / 1:10000	Babco, Richmond, CA, U.S.A.
Anti Ki-67	Rabbit monoclonal	Ready to use / n.u.	Innovative Diagnostik-systeme, Hamburg, Germany
Anti Loricrin	Rabbit polyclonal	1:400 / n.u.	Dr. Stark, DKFZ Heidelberg, Germany
Anti Repetin	Rabbit polyclonal	1:200 / 1:2000	Dr. Stark
Anti SAPK/JNK #9252	Rabbit polyclonal	n.u. / 1:1000	Cell Signaling, MA, U.S.A.
Anti phospho-SAPK/JNK #9251	Rabbit polyclonal	n.u. / 1:500	Cell Signaling, MA, U.S.A.

2.3.2. Secondary antibodies

Name	Company
Donkey anti-guinea pig IgG(peroxidase-coupled)	Jackson/ Dianova, Hamburg, Germany
Goat anti-guinea pigIgG (Cy3)	Jackson/ Dianova, Hamburg, Germany
Goat anti-mouse IgG (peroxidase-coupled) SC-2005	Santa Cruz Biotechnology, Heidelberg, Germany
Goat anti-mouse IgG (Alexa Fluor 488)	Invitrogen, Karlsruhe, Germany
Goat anti-rabbit IgG (Cy3)	Jackson/ Dianova, Hamburg, Germany
Goat anti-rabbit IgG (peroxidase-coupled)	Jackson/ Dianova, Hamburg, Germany
Goat anti-rabbit IgG (Alexa Fluor 488)	Invitrogen, Karlsruhe, Germany

2.4. Equipments and devices

Name	Company
- 80°C freezer	Heraeus AG, Zürich, Switzerland
- 20°C freezer	Liebherr, Ochsenhausen, Germany
4°C fridge	Liebherr, Ochsenhausen, Germany
24-well plates	Greiner, bio-one, Frickenhausen, Germany
96-well plates	Greiner, bio-one, Frickenhausen, Germany
Autoclave Vakulab HP	MedizinMechanik GmbH, München, Germany
Avanti J25 centrifuge	Beckman, CA, U.S.A.
Balance BL 6100	Zeiss, Goettingen, Germany
Bis-Tris gels (10%)	Invitrogen, Karlsruhe, Germany

Blotting paper	Schleichter&Schuell, Dassel, Germany
Cell culure flasks	Greiner, bio-one, Frickenhausen, Germany
Cell scraper	Greiner, bio-one, Frickenhausen, Germany
Centrifuge GPR	Beckman, CA, U.S.A.
Centrifuge Z33M	Hermle, Wiesloch, Germany
Cover slips	Thermo Scientific, Braunschweig, Germany
Cryomold Intermediate	Sakura Finitek, CA, U.S.A.
Cryotome CM 3050	Leica, Bensheim, Germany
Developing machine OptimaxTyp TR	M&S Laborgeräte, Wiesloch, Germany
Electrophoreisis power supply	Biotec Fischer, Reiskirchen, Germany
ELISA-Reader ELX-800	Bio-Tek Instruments, Winoski, U.S.A.
Films for Western	Fujifilms, Germany
Glass slide (SuperFrostPlus)	ThermoScientific, Braunschweig, Germany
Glass slide box	Neolab, Heidelberg, Germany
Ice machine	West End Lumber, Lorain, CL, U.S.A.
Heating water bath	Lauda, Groton, CT, U.S.A.
Horizontal gel electrophoresis unit	BioRad Laboratories, Munich, Germany
Hybridiezer HB-1000	Peqlab, Erlangen,
Kodak boman x-ray cassette	Eastman Kodak Company, Rochester, U.S.A.
Liquid scintillation vials	Wheaton, Millvillle, NJ, U.S.A.
Photomicroscope	Zeiss Axioplan2, Göttingen, Germany
Magnet stirrer	Janke& Kunkel, Staufeni.B. , Germany
Mega - Cassette	Sakura Finitek, CA, U.S.A.
Microscope	Leica, Bensheim, Germany
Microtome blades R35/C35	Feather, pfm, Köln, Germany
Microtome EM	Philips EM 400, Eindhoven, The

	Netherlands
Microtome RM 2155	Leica, Bensheim, Germany
Microwave	Bosch, Stuttgart, Germany
Multi-image light cabinet	Alpha Innotech Corporation, CA, U.S.A.
Multisteper	Eppendorf, Hamburg, Germany
Nano Drop	Kisker-Biotech, Steinfurt, Germany
Needles 21G	BD Microlance™,Nußloch, Germany
Nitrocellulose membrane	BioRad, Hercules, CA, U.S.A.
Parafilm	Pechiney plastic packaging, Chicago, U.S.A.
Petridishes	BD Bioscience, Heidelberg, Germany
Pipetboy	Fischer BioBlockScientific, IllirchCedex, France
NuPagewesern apparatus	Invitrogen, Karlsruhe, Germany
PCR reaction tubes	BiozymDiagnostik, Hess. Oldendorf
Peltier thermal cycler PTC 200	BiozymDiagnostik, Hess. Oldendorf
pH Meter pH 330	Fischer BioBlock Scientific, IllirchCedex
Precision pipettes 10µL	Gilson, WI/U.S.A.
Precision pipettes 100µL	Gilson, WI/U.S.A.
Precision pipettes 200µL	Gilson, WI/U.S.A.
Precision pipettes 1000µL	Gilson, WI/U.S.A.
Reaction tubes 1.5mL	BiozymDiagnostik, Hess. Oldendorf
Reaction tubes 1.5mL safe lock	Eppendorf, Hamburg, Germany
Reaction tubes 2mL safe lock	Eppendorf, Hamburg, Germany
Septa for 0,5mL Sample Tubes	Applied Biosystems, CA, U.S.A.
Shaker	Heidolph, Darmstadt, Germany
Shaker for Western Blot analysis	Neolab, Heidelberg, Germany
Single-use syringes 1mL	Henke Sass Wolf, Tuttlingen, Germany
Steril surgical blades	C. Bruno Bayha, Tuttlingen, Germany

Sterilgard Hood	Kojair, Uilppula, Finland
Tewameter	Courage and Khazaka, Cologne, Germany
Tips for PCR purposes (0,1-10)µL	Starlab, Ahrensburg, Germany
Tips for PCR purposes (1-20)µL	Starlab, Ahrensburg, Germany
Tips for PCR purposes (1-200)µL	Starlab, Ahrensburg, Germany
Tips for PCR purposes (101-1000)µL	Starlab, Ahrensburg, Germany
Tips (white, yellow, blue)	Eppendorf, Hamburg, Germany
Ultramicrotome	Reichert Ultracut E, Depew, NY, U.S.A.
Ultrasoung, sonoplus	Bandelin, Berlin, Germany
Vortex mixer	Heidolph Instruments, Schwabach, Germany
Warm plate HI 1220	Leica, Bensheim, Germany
Water bath	Kottermann, Haenigsen, Germany
Yellow capped centrifuge tubes 15mL	Techno Plastic products TPP, Trasadingen, Switzerland
Yellow capped centrifuge tubes 50mL	Techno Plastic products TPP, Trasadingen, Switzerland

2.6. Oligonucleotids

Code N°	Sequence
708	TCT GAG TGG GAC TGG CTG TTG G
709	AGA GAC CTC CCT TGT TGA GAA G
1231	CC CTC CCC TGC TGC TGT TGC
2275	ACCCTCCCCTGCTGCTGTTGCTA
2277	CTG CTC AAC AGA CTC CCT TAC TT
2583	ACCAGCCAGCTATCAACTCG
2584	TTACATTGGTCCAGCCACC

2585	CTAGGCCACAGAATTGAAAGATCT
2586	GTAGGTGGAAATTCTAGCATCATCC

2.6. DNA and Protein Ladders

Name	Company
DNA - 1kb Ladder Plus	MBI Fermentas, St. Leon-Roth, Germany
DNA – 100bp Ladder Plus	MBI Fermentas, St. Leon-Roth, Germany
PageRuler TM #SM0671, Prestained protein laddder	Fermantas, St. Leon-Rot, Germany

2.7. Mouse strains

Official name	Creator/Company
129S6/SvEvTac	Taconic, lilleSkensved, Denmark
NMRI	Charles River Laboratories, Sulzfeld, Germany
K14-Cre-ER^{T2}	D.Metzger,P.Chambon [56]
129;B6-*Alox12b*$^{tm1.1dkfz}$ (del)	P.Krieg [55]
129;B6-*Alox12b*$^{tm1.2dkfz}$(flox)	P.Krieg

2.8. Computer Software

Name	Company
Adobe® Photoshop® CS3	Adobe Systems Incorporated
EndNote X.0.2	Thomson ReseachSoft, CA, U.S.A.
GraphPadPrism5	GraphPad software
Husar	DKFZ, Heidelberg
Microsoft® Excel 2007	Microsoft Corporation
Microsoft® PowerPoint® 2007	Microsoft Corporation
Microsoft® Word 2007	Microsoft Corporation
NanoDrop 3.1.0	Coleman Technologies Inc., U.S.A.

pDraw	AcaClone software
Sequencing Analysis 3.7	PE Biosystems
WS FTP Pro	Ipswitch INC., Lexington, U.S.A.
Texts and abstracts	www.ncbi.nml.nhi.gov

3. METHODS

3.1. DNA analysis

3.1.1. Extraction of genomic DNA from tail biopsy

Tail biopsies are incubated overnight at 56°C in lysis buffer (50 mMTris-HCl, pH 7,5; 100 mM EDTA; 100 mMNaCl; 1% SDS; 0,2 mg/ml proteinase K). DNA is precipitated by adding an equal volume of isopropanol, pelleted by centrifugation, and the pellet is washed in 70% EtOH, and resuspended in EB-buffer (10 mMTris-HCl, pH 8).

3.1.2. DNA concentration

To determinate the concentration of DNA we measure the absorbance at 260 nm and 280 nm using the NanoDrop ND-1000 spectrophotometer. The Beer-Lambert equation is used to correlate the calculated absorbance with the concentration. An OD_{260} of 1 corresponds to 50µg/ml of double-stranded DNA.

The relation between OD_{260}/OD_{280} is used to evaluate protein contamination. A clean DNA solution has a quotient between 1.8 and 2.0. To use the nanodrop we only need to determine the blank with 1µL of elution buffer, and then measure 1µL of the DNA.

3.1.3 Amplification of DNA

The Polymerase Chain Reaction (PCR) is used to make a high number of copies of a DNA fragment. Therefore two antiparallel primers are needed that enclose the region to be replicated. Because both strands are copied during PCR, the technique allows a small amount of DNA to be amplified exponentially. For genotyping we use the Taq DNA polymerase from Qbiogene, it has 5'-3' exonuclease activity with no 3'-5'proofreading activity.

For standard amplification of DNA we use 100ng template DNA, 2.5µL puffer (10mM Tris-HCl pH 9.0, 50mM KCl, 1.5mM $MgCl_2$, 0.1% Triton X-100, 0.2 mg/ml BSA), 0.5µL dNTP´s (10mM from each nucleotide), 1µL from each 3´- and 5´-primers (10pmol/µL), 18.5µL water and 0.5µL Taq DNA polymerase (5U/µL, Qbiogene). For the amplification we use the Taq56 program in the Peltier Thermal Cycler PTC-200 (MJ research): it starts at 95ºC for 5 minutes to be sure that the DNA template as well as the primers have melted, then each replicating cycle starts with 94ºC for 1:50 minutes (denature), 56ºC for 1:30 minutes (annealing) and 72ºC for 2:30 minutes (elongation), this cycle is repeated 30 times. The last cycle has an elongation of 10 min at 72ºC. The annealing temperature can be different depending on the length of the primers used.

	Taq54	Taq56	Time
1. Initialisation	95°C	95°C	5 min.
2. Denaturising	94ºC	94ºC	1:50 min
3. Annealing	54°C	56°C	1:30 min
4. Elongation	72°C	72°C	2:30min
5. Cycles	Go to 2	Go to 2	30 times
6. Reaction end	72ºC	72ºC	10 min

3.1.4. Agarose gel electrophoresis

Agarose gel electrophoresis is used to separate DNA strands by size, and helps estimating the size of the separated strands by comparison to known marker fragments (DNA ladder). Loading buffer is added to the DNA in order to allow the sample to sediment in the gel well (glycerol) and to visualize the DNA fragments (indicators). The negatively charged indicators, such as Xylenecyanol and Bromophenol blue, keep track of the position of the DNA, as they run about 5000 bp and 300bp respectively (this precise position varies with percentage of the gel). For visualisation of the gel ethidium bromide is used, due to the property of fluorescing under UV light when intercalated into DNA. The buffer used is TBE that consist of a mixture of Tris base, boric acid, and EDTA Agarose powder is mixed with the electrophoresis buffer (TBE). By using different concentration of Agarose (0,7 – 1,4%) different sizes of DNA fragments can be resolved. Agarose is dissolved at the desired concentration in bidistilled water and boiled in the microwave. Once the agarose is complete dissolved add 10mg ethidium bromide per mL buffer and swirl to mix. Pour the gel slowly into the horizontal gel rack (8 x 10cm, 15 x 10 cm, 15 x 30 cm), which already has the desired well-forming comb. Let it cool down to polymerize. Once it is polymerized, put the rack in a full electrophoresis tank, load the samples and start the electrophoresis, it takes around 1 – 2 hours at 10V/cm to be done. At the end take a photo under UV light to see the results.

Buffer	Composition
1 x TBE	100 mMTris base, 89mM Boric Acid, 1mM EDTA. pH 8.5
Loading dye	50% Glycerol, 15mM EDTA, 0.15% Bromophenol blue, 0.15% Xylenecyanol, pH 7 - 8

3.2. Preparation of epidermis extracts

Tissues stored at -70˚C are transferred into liquid nitrogen for pulverization with a dismembrator. Meanwhile the teflon mortar and ball are cooled down (also in liquid nitrogen). Then the sample is placed within the teflon mortar, and pulverized using the dismembrator at 2500 rpm for 30 seconds. Tissue powder is suspended in the designated pre-cooled buffer solution.

3.3. RNA analysis

mRNA is prepared from pulverized mouse epidermis using the RNeasy mini kit (QIAGEN, Hilden, Germany) according to the manufacture's protocol. DNA was removed by DNaseI digestion (Promega, Mannheim, Germany).

Microarrays analysis was done by our cooperation partner Dr. Hans Christian Hennies from the Cologne Center for Genomics, using IlluminaGUI [57].

3.4 Protein analysis

3.4.1. Protein extraction

Protein from mouse epidermis powder is transferred with 2mL pre-cooled RIPA buffer to a glas-glas-homogenizer. The tissue suspension is then homogenized in ice for 2 minutes, separated in 2 equal aliquots and stored at -20°C for further analysis.

Buffer	Composition
RIPA	50 mMTris-HCl; pH 7.5; 150 mMNaCl; 0.5 % Sodium deoxycholate; 0.1 % SDS; 2 mM EDTA; 1 % Triton X-100; 10 % Glycerol; 1 mM PMSF; 1 µg/mL Aprotinin; 1 µg/mL Leupeptin; 1 µg/mL α2-Macroglobulin.

3.4.2. DC quick Lowry for measuring protein concentrations

Following solubilisation of tissues with detergent-containing buffers, protein concentrations may be assessed by means of the DC quick Lowry assay. In this colorimetric assay, proteins react with an alkaline copper tartrate solution and Folin reagent. Within a two-steps reaction sequence a blue color develops with a maximum absorbance at 750nm. Using a stock solution of 80 mg bovine serum albumin (BSA) per ml HP-buffer as a starting solution, eight standards are prepared with concentrations of 0, 0.125, 0.25, 0.5, 1, 2, 4, and 8 mg/mL. 37,5 µL of solution A ´(a mixture of 1000 µL quick Lowry solution A and 20 µL quick Lowry solution S) are placed into an Eppendorf tube for each standard and sample to be analyzed. 7.5 µL of each standard or sample are then added and vortexed immediately. Afterwards an

additional volume of 300 µL of quick Lowry solution B is mixed to each standard or sample. Preparations are then incubated for 15 minutes at room temperature. Into a 96 well plate, 200 µL of each mixture are transferred per well and the optical density is read at 750 nm using an ELISA reader. A standard curve is established for BSA with the optical density (y-axis) versus the BSA concentration (x-axis). With the aid of this curve the concentration of proteins is calculated.

3.4.3. Discontinuous SDS-polyacrilamide gel electrophoresis

Proteins within a mixture are resolved by polyacrylamide gel electrophoresis in order to visualize the mixtures composition or to evaluate its purity. With sodium dodecylpolyacrylamide gel electrophoresis (SDS-PAGE), proteins are separated according to their molecular weights. A reducing agent (mercaptoethanol or dithiothreitol) is supplied to the proteins to reduce the disulfide bridges formed by cystein residues. Furthermore, SDS is complexed to proteins to mask any intrinsic charges. SDS-protein complexes are anionic and have in general a constant net negative charge per gram protein. In an electric field all proteins migrate towards the anode and the electrophoretic mobility of these denatured and reduced proteins depends mainly on their molecular weights. For discontinuous SDS-PAGE, two types of gels are needed: 4.0 % stacking gel, and a separation gel with a concentration varying from 7.5 % to 15 % depending on the pore size required. Both are prepared by polymerising acrylamide monomers, and the cross-linker reagent N,N-methylenebisacrylamide. The polymerization reaction is started with ammonium peroxodisulfate (APS) as a catalyst, and N,N,N,´N-tetramethylethylenediamine (TEMED) as a radical donor. The separation gel is first poured between two clean glass plates, which are initially prepared and separated by 1.5 mm spacers. Few drops of aqua bidest are added and then removed (after the gel has polymerized) with a small piece of a whatmann paper. Only then the stacking gel can be poured, and a comb with the requested number of teeth is inserted. Whenever the stacking gel polymerizes, the whole system is fixed into a vertical gel electrophoresis unit filled with 1X SDS-PAGE buffer. The comb is removed and the samples are loaded along with a molecular weight standard proteins (Pre-stained marker, Invitrogen). Electrophoresis is carried out overnight at 9mA.

3.4.4. Immunoblot analysis – western transfer

After separation of proteins in a SDS gel, they are electrically transferred to the hydrophobic PJDF immobilon membrane. But before usage, the membrane is activated by rinsing in 100 % ethanol for few minutes. Transfer is performed with the aid of a semi-dry electrophoretic unit onto which the transfer sandwich is placed. This sandwich is made by: wetting 6 Whatmann 3 MM filter papers in anode buffer 1 to be placed onto the anode, soaking 3 Whatmann3 MM filter papers in anode buffer 2 to be added over the first stack of papers, equilibrating the membrane in anode buffer 2 to be placed over the pile, equilibrating the separation gel in cathode buffer to be also

added, and finally wetting 6 Whatmann 2 MM filter papers in cathode buffer to complete the sandwich. To start the transfer of proteins, the cathode is placed onto the top of the stack, the apparatus is burdened with 1 kg weight, and the electrodes are connected to the power suppler. Transfer is performed with 0.8 mA/cm^{2}gel for 2 hours at room temperature.

After completion, transfer efficiency can be verified by transient staining of proteins with Ponceau S dye for 2 to 5 minutes, followed by destaining in aqua bidest for 2 to 5 minutes.

Buffer	Composition
Anode Buffer 1	0.3 M Tris-HCl, pH 10.4; 20% Methanol
Anode Buffer 2	25 mMTris-HCl, pH 10.4; 20% Methanol
Cathode Buffer	25 mMTris-HCl, pH 9.4; 40mM Norleucin; 20% Methanol

3.4.5. Immunoblot analysis – incubation with antibodies

In order to be able to label and visualize the protein(s) of interest, the membrane is first blocked to minimize any background that may develop by non-specific binding of the antibodies. The blocking solution used is 7.5% milk powder in 1x PBS and 0.1 % Tween 20 (PBST). Membranes are blocked for 2 hours at room temperature. After blocking, a primary antibody specific to the protein of interest is diluted in the blocking solution and the membrane is incubated overnight at 4˚C. On the next day, the primary antibody solution is discarded, the membrane is washed 3 x 10 minutes with 1x PBST solution, and the secondary antibody (peroxidase-coupled) diluted appropriately in the blocking solution is added to the membrane for 45 min at room temperature. After that, the membrane is washed again 3 x 10 minutes with PBST. All steps are carried with continuous shaking. Dilutions used to prepare primary and secondary antibodies are given in materials.

For the signal detection the ECL western detection kit is used, having solutions A and B as substrates. After incubation of the membrane with this substrate for 1 minute, excess substrate is drained, the membrane is wrapped with a foil, and is applied for chemiluminescence detection. Signals are detected by exposing Fuji super RX medical X-ray films (for up to one hour). Films are developed in the dark room as necessary by means of a film developing machine.

3.5 Preparation and staining of skin sections

3.5.1. Preparation of skin cryo-sections

Once the animal is killed by cervical dislocation, its skin is embedded in Tissue Tek and is immediately placed on top of dried ice. All samples are then stored at -70˚C. Whenever sections are needed for staining procedures, the embedded organ is cut at -25°C into 5µm sections using a Cryotome, with two sections placed per glass slide (SuperFrostPlus). The sections dry at room temperature (RT) for 4-6 hours and are then stored at -70˚C for future use. Samples are defrosted for two hours before staining.

3.5.2. Immunohistochemical staining

For staining immerse the slides 5 times in PBS then fix in -20°C precooled acetone for 10 minutes, let them dry and orbit the tissue with Novopen. Shake 10 seconds in PBS/0,5%TritonX-100. Block in 1% BSA/PBS (30µL per tissue) in a humid chamber for 20 min at RT. Incubation with first antibody is done for 1hour RT in 5%milk/PBS (30µL per tissue). Wash by immersing 3 times in PBS and incubate by shaking 2 times 5 minutes in PBS. Incubate with the second antibody for 30 min RT in 1%BSA/PBS (30µL per tissue) in a dark humid chamber. Wash by immersing 3 times in PBS and incubate by shaking 2 times 5 minutes in PBS. Immerse shortly in distilled water and incubate 1 minute in 100% ethanol p.a. Let the sections air dry and cover them with fluorescein mounting medium.

3.5.3. Preparation of paraffin sections

Once the animal is killed by cervical dislocation, its skin is fixed overnight in filtrated 4% Paraformaldehyde solution. The next day the skin probes are hydrated at least 2 h under running water, then dehydrated o/n and embedded in paraffin blocks, which can be stored at room temperature. Whenever sections are needed for staining procedures, the embedded organ is cooled down to -20°C and cut into 5µm sections using a microtome. The fresh cut sections are transferred to a 38 °C water bath. Two sections are placed per glass slide (SuperFrostPlus). The sections dry at a 50°C warm plate for two hours and are stored at room temperature (RT) until use.

3.5.4. Hematoxylin and Eosin staining

This is the most conventional stain for formalin fixed paraffin sections. The hematoxylin stains negatively charged nucleic acids (nuclei and ribosomes) blue. The eosin stains proteins pink. Before staining the slides are deparaffinised in 2 x 10 minutes changes of xylene and hydrated by placing twice in 100 % ethanol for 3 minutes each, then passing a series of decreasing ethanol concentrations (95 % - 70 % - 50 % - 30 %) for 2 minutes each. Slides are then immersed in hematoxylin staining solution for 2 to 10 minutes, and washed under running tap water for 1 minute. After that, slides are placed in a solution of HCl/Alcohol (25 % HCl/ 70 %

EtOH v/v) for 20 seconds. Before proceeding, slides are washed 10 minutes under running tap water, and then stained in eosin for 1 minute. All slides are then washed in aqua bidest for 1 minute and dehydrated by passing in a series of increasing ethanol concentrations (70 % - 96 % - 100 %) for 2 x 2 minutes in each. Finally the sections are immersed twice in xylol for 5 minutes, and then mounted with Eukitt.

3.5.5. Electron microscopy

All specimens were fixed for at least 2 h at room temperature in 3% glutaraldehyde solution in 0.1. cacodylate buffer, pH 7.4, cut into pieces of approximately 1mm^3, washed in buffer, postfixed for 1 h at 41 °C in 1% osmium tetroxide, rinsed in water, dehydrated through graded in ethanol solutions, transferred into propylene oxide, and embedded in epoxy resin (glycidether 100). Ultrathin sections were cut with an ultramicrotome (Reichert Ultracut E),treated with uranyl acetate and lead citrate, and examined with an electron microscope (Philips EM 400).

3.6. Animal work

3.6.1. Mouse maintenance

The animal experiments were performed in accordance with the guidelines of the Arbeitsgemeinschaft der Tierschutzbeauftragten in Baden-Württemberg (Officials for Animal Welfare) and were approved by the Regierungspräsidium Karlsruhe, Germany. All animals used for this study were kept at the central animal facility of the German Cancer Research Center. Animals were maintained under pathogen-free conditions, an artificial day/night rhythm and were feed standard food pellets (ProvimiKliba), with sterile water available ad libitum.

3.6.2. Transepidermal water loss measurement

For the measurement animals are shaved the day before. The rate of TEWL from the skin transplants was determined using a Tewameter (Courage and Khazaka) under normal conditions. Data are expressed in gm^{-2}per hour.

3.6.3. Epidermis isolation from newborn mice

Wash mice in PBS before decapitation. Cut off limbs above the wrist and ankle joints. Cut off tail close to body, these will be lately used for DNA extraction and genotyping. Grasp the body between the fingers, insert a small scissors through the hole at the head and cut the skin along the ventral midline of the boy to the tail. Loss skin gently and pull it away from the body. Immerse the skin in 56°C preheated PBS for 30 seconds. Place the skin on the surface of a culture dish, dermis side up. Spread out the skin completely flat. Dermis can then be separated from the epidermis that remains at the bottom. Epidermis is then frozen at -80°C until further need [58].

3.6.4. Epidermis isolation from adult mice

Skin is extended on paper and immediately frozen in liquid nitrogen. The skin is placed on a cooled plate and epidermis is mechanically separated from the dermis by scratching. Epidermis is then frozen at -80°C until further need.

3.6.5. Skin grafting

We transplanted full-thickness dorsal skin grafts from neonate donors onto athymic nude recipient mice as squares using the skin-flap technique [59].

General anesthesia is essential for grafting operations on mice. Grafts should be kept awaiting use by laying them raw side down in small Petri dishes fitted with filter papers damped with sterile 4 x MEM solution (were it remains viable for at least 4 days). The recipient area is sterilized and a rectangular area smaller than the donor (for a better fitting) skin is removed, this skin is shortly incubated in liquid nitrogen and will be use as a protection cover for the skin graft. Donor skin graft is placed on this area, covered by the dead skin and it is fixed through 4 staples and 4 reabsorbable stitches.

After 2 weeks of grafting the staples are removed and the cover skin gets lose and falls. The grafted skins are fully visible after 3 weeks of grafting. At 4 weeks after transplantation they were harvested for the analysis.

3.6.6. Tamoxifen treatment

The Cre-ER^{T2}recombinase is activated by injecting 4-hydroxy-tamoxifen (Sigma) intraperitoneally into mice at the age of 6 and 8 weeks The administration schedule consisted of five consecutive daily injections of 0.1mg tamoxifen dissolved in 100µL sunflower oil. Animals were sacrificed after tamoxifen treatment at the age of 9 weeks.

4. RESULTS

4.1. Characterization of 12R-LOX$^{-/-}$ adult skin phenotype

To investigate the pathomechanism of ARCI and the function of 12R-LOX we recently generated a 12R-LOX KO model [55]. 12R-LOX deficient mice die rapidly after birth from severe barrier dysfunction without exhibiting an obvious cutaneous phenotype. Thus, we analysed the adult phenotype of 12R-LOX$^{-/-}$ skin transplanted onto nude mice.

4.1.1. Genotyping strategy for detection of 12R-LOX$^{-/-}$ neonates

In order to identify the 12R-LOX$^{-/-}$ neonates for the skin transplants, we developed a PCR-genotyping strategy using the primer combination 2275/2277 (Fig. 8). These primers recognise intron 7 and 8 respectively, that flank exon 8 in the wild-type allele producing a 930bp product, but flank only the LoxP-site in the deleted allele amplifying a 320bp product. The DNA was isolated from tail biopsies.

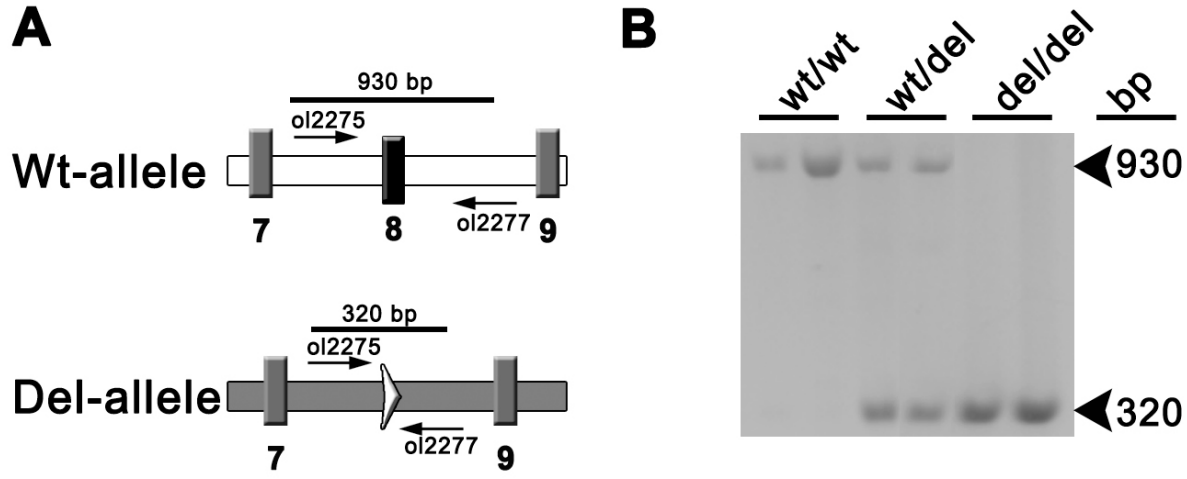

Figure 8: Genotype analysis of *Alox12b* allele
(A) PCR strategy for identification of wild-type and deleted alleles. Primer combination flanks the exon 8 in wild-type and the LoxP-site in the deleted allele. Triangle: LoxP-site.
(B) DNA was extracted from tail biopsies. 100ng DNA template was subjected to PCR using the primer pair 2275/2277 producing a 930bp product in wild-type and 320bp product in deleted allele.

4.1.2. Macroscopical characterisation of 12R-LOX skin grafts

After genotypic identification, a total of 15 12R-LOX$^{-/-}$ neonates and 17 controls (12R-LOX$^{+/+}$ as well as 12R-LOX$^{+/-}$) were transplanted onto the back of nude mice. Four weeks after transplantation, the grafts were covered with normal hair

(Fig. 9 A, B). Macroscopically no significant differences were apparent between KO and control grafts. At the level of haematoxylin-eosin–stained paraffin sections the histology of control skin grafts on nude mice was similar to that of normal adult mouse skin with a thin epidermis that consists of 2-3 nucleated cell layers without visible stratum granulosum (Fig. 9 C). In contrast, skin grafted from *Alox12b* deficient neonates was considerably thicker exhibiting a hyperplastic phenotype with epidermal acanthosis and pronounced hyperkeratosis (Fig. 9 D).

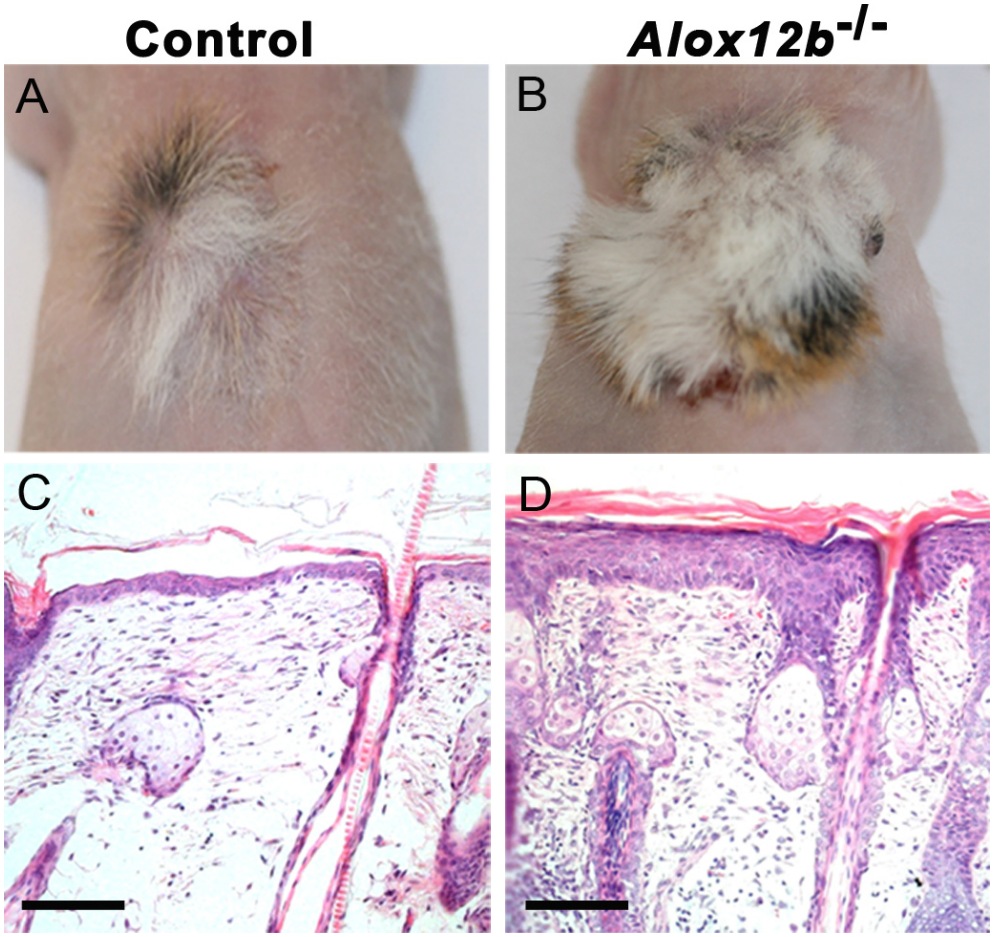

Figure 9: Phenotype analysis of control and 12R-LOX$^{-/-}$ skin grafts
(A and B) Morphological examination showed no differences of the control and 12R-LOX$^{-/-}$ mouse skin grafted.
(C and D) Dorsal skin of 4 week old grafted skin was embedded in paraffin. 5µm sections were made and stained with hematoxylin and eosin. Representative sections are depicted. The control skin graft is almost identical to normal adult mouse skin. In contrast, the grafted 12R-LOX$^{-/-}$ mouse skin shows epidermal acanthosis and severe hyperkeratosis.

4.1.3. Ultrastructural analysis

Electron microscopy analysis confirmed hyperkeratosis at the ultrastructural level. As compared with control skin grafts, the stratum corneum of skins grafted from

KO mice was markedly piled up in over 30 layers (Fig. 10 A, B). Lipid droplets and occasionally remnants of cellular components, e.g. of nuclei were observed in corneocytes of the mutant skin grafts but not of the control grafts (Fig. 10 C, D). In addition, deposits resembling extruded contents of lamellar bodies in the transient zone were seen in the intercellular spaces of higher stratum corneum levels of mutant skin grafts suggesting disturbed extrusion or processing of lamellar bodies. Furthermore, both the size and the number of keratohyaline granules were increased indicating hypergranulosis in mutant skin grafts (Fig. 10 E).

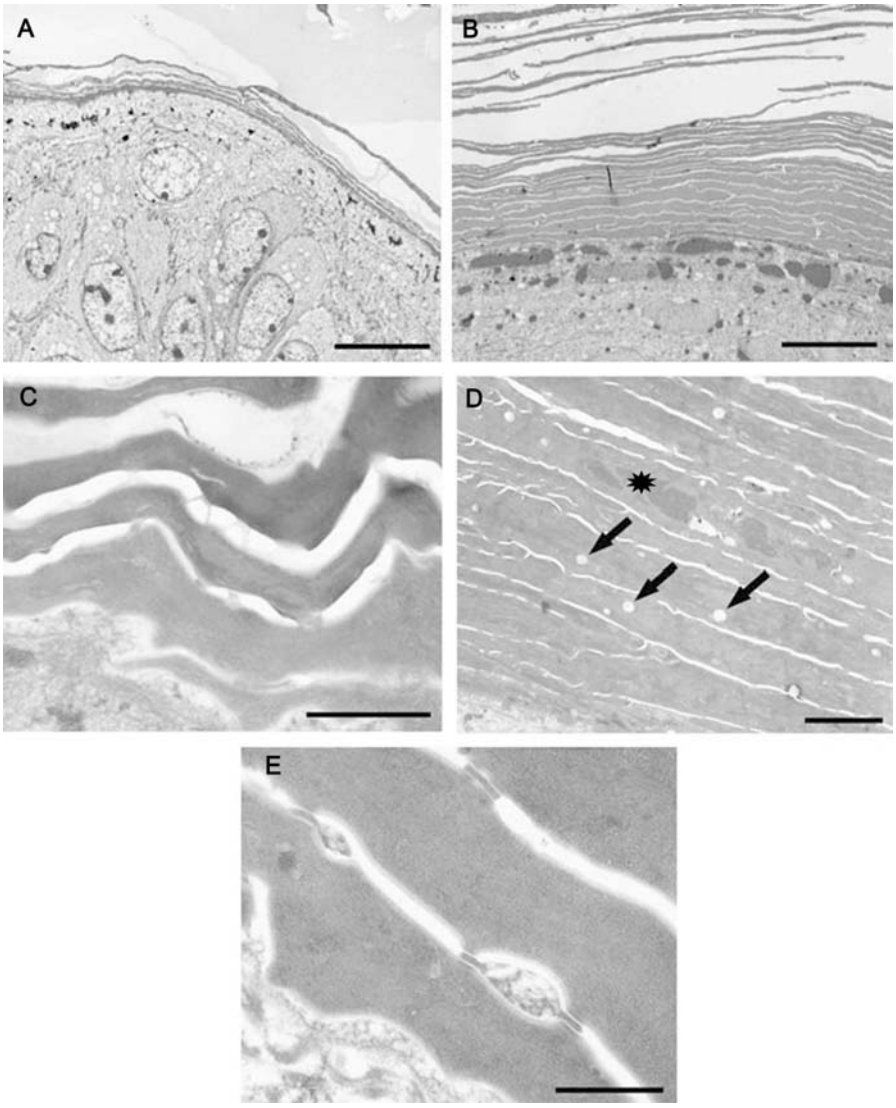

Figure 10: Ultrastructural analysis of grafted control and knockout skin
(A and C) ultrastructure from control grafted skin.
(B) Epidermis of mutant skin graft showed marked hyperkeratosis and increased size and number of keratohyaline granules. In the stratum corneum lipid droplets (D, arrows) and nuclear remnants (D, star) as well as remnants of cytoplasmatic organelles (E) were found. Scale bars: (A and B) = 10 μm, (C) = 1 μm, (D) = 2 μm, (E) = 50nm.

4.1.4. Hyperproliferation in skin grafted epidermis

Epidermal hyperplasia in mutant skin is associated with a markedly increased basal cell proliferation. The epidermal proliferation index of the grafted skin was determined by immunofluorescence analysis as the percentage of Ki67 staining nuclei in the epidermis (Fig. 11 A, B). Ki67 positive cells were significantly increased in the mutant grafts as compared to the control grafts (63.4%+/-3.2 vs. 46.4 % +/- 0.6 in KO and control mice, respectively), which indicated a significant hyperproliferation of the epidermis. While in control grafts all Ki67 positive cells remained restricted to the basal cell layer, Ki67 staining nuclei in mutant skin grafts were occasionally observed in the first suprabasal layer (Fig. 11 B). Consistently with epidermal hyperproliferation, a strong expression of keratin 6 (K6) was observed in basal and suprabasal layers of the mutant skin graft as compared to a more focal pattern in those of control grafts (Fig. 11 C, D).

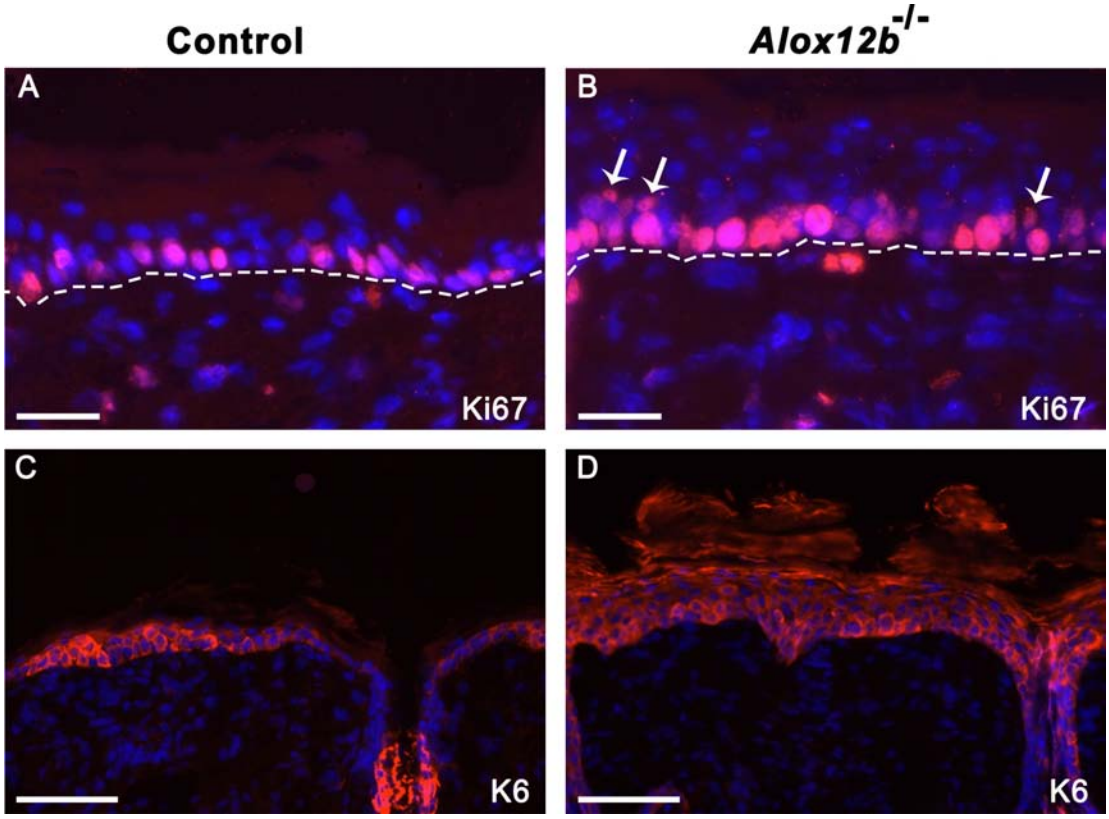

Figure 11: Hyperproliferation markers in control and knockout grafted skin

(A and B) Immunostaining with Ki67 specific antibody showed an increased number of positive nuclei in the 12R-LOX-/- skin grafts.

(C and D) Immunostaining against K6 showed a strong up-regulation in mutant skin grafts. Nuclei were counterstained with Hoechst 33258. The dashed line shows the epidermal/dermal junction. Bars (A and B) = 20 μm, (C and D) = 25 μm.

4.1.5. Comparative analysis of differentiation markers

The expression levels of epidermal keratin and terminal differentiation markers in the skin grafts were evaluated by immunofluorescence and western blotting. Basal cell-specific keratin K14 was present at similar levels showing a comparable immunostaining pattern in mutant and control skin grafts (Fig. 12 a, b). Strong expression of keratin K10 was observed in all living suprabasal cell layers of control and *Alox12b* deficient skin transplants. In the latter the stained area was much broader according to the expanded suprabasal compartment (Fig. 12 c, d). Similarly, proteins of the cornified envelope (CE) such as involucrin, repetin and filaggrin were seen in their typical localizations in both control and mutant skin grafts, with the consistent difference, however, that the staining was stronger and the number of cell layers showing immunostaining of these proteins was higher in the grafts from *Alox12b* deficient mice (Fig. 12 e-j).

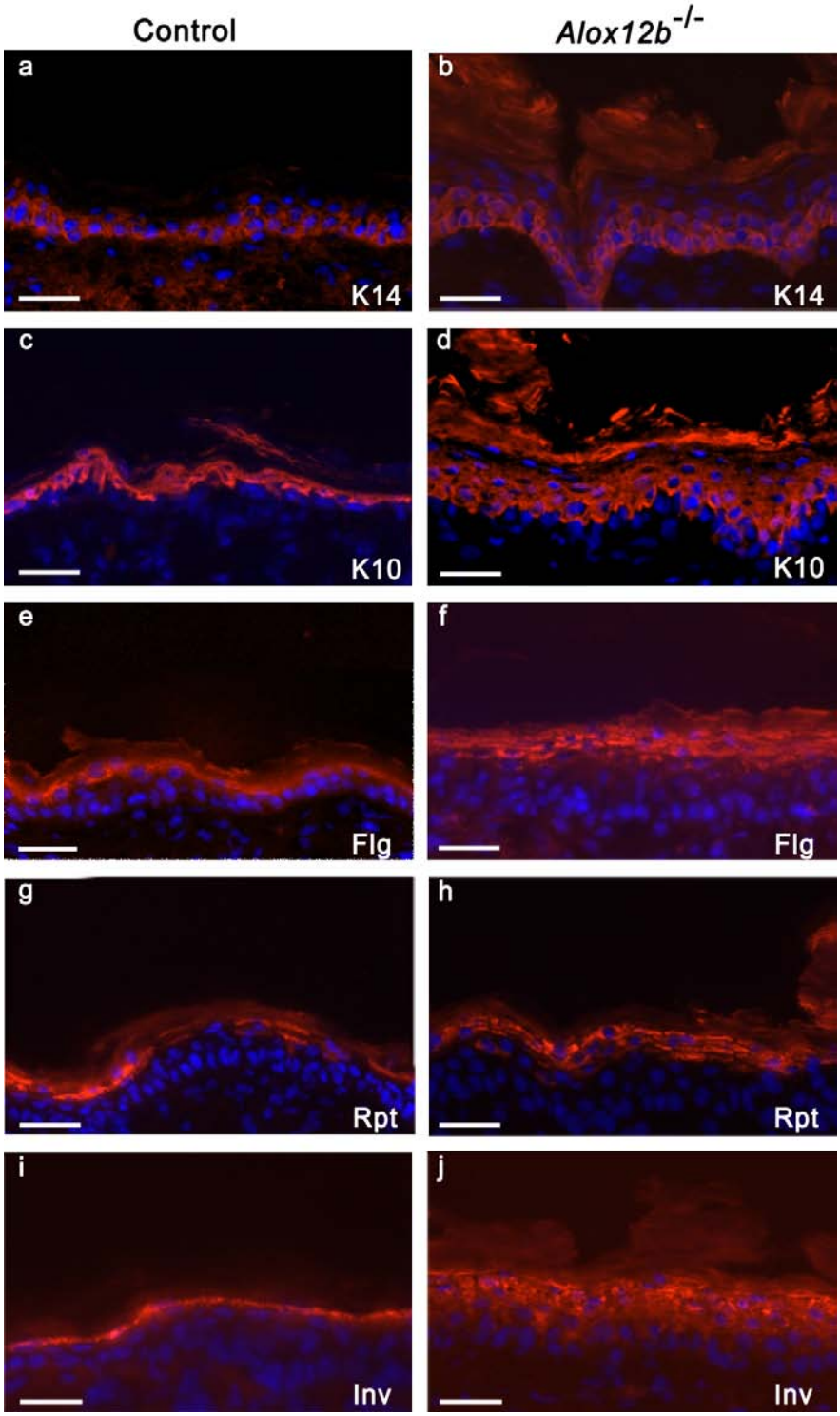

Figure 12: Analysis of epidermal differentiation markers in control and mutant grafted skin

Skin section were immunostained with specific differentiation markers for the basal K14 (a and b), seen in similar levels, and the suprabasal cell layer (c and d) K10, the staining of which is found in the typical localisation but is broader in the transplants from KO skin. This same distribution was also seen with immune staining of the cornified envelope proteins filaggrin (e-f), repetin (g-h) and involucrin (i-j). Nuclei were counterstained with Hoechst 33258. Bars (a-j) = 20µm.

Consistently with these observations, Western blot analysis demonstrated a markedly increased expression of these CE proteins and K6 in extracts from mutant skin grafts as compared to wild-type transplants, while the levels of K5 and K10 were similar in both genotypes (Fig. 13 A). Most interestingly, in addition to a strong overexpression of profilaggrin precursor intermediates, also highly increased levels of fully processed filaggrin monomers were detected both in control and mutant skin transplants, which indicates complete profilaggrin processing in the mutant adult skin grafts in contrast to the neonatal *Alox12b* deficient skin which has been shown previously to completely lack mature filaggrin monomers [55] (Fig. 13 B).

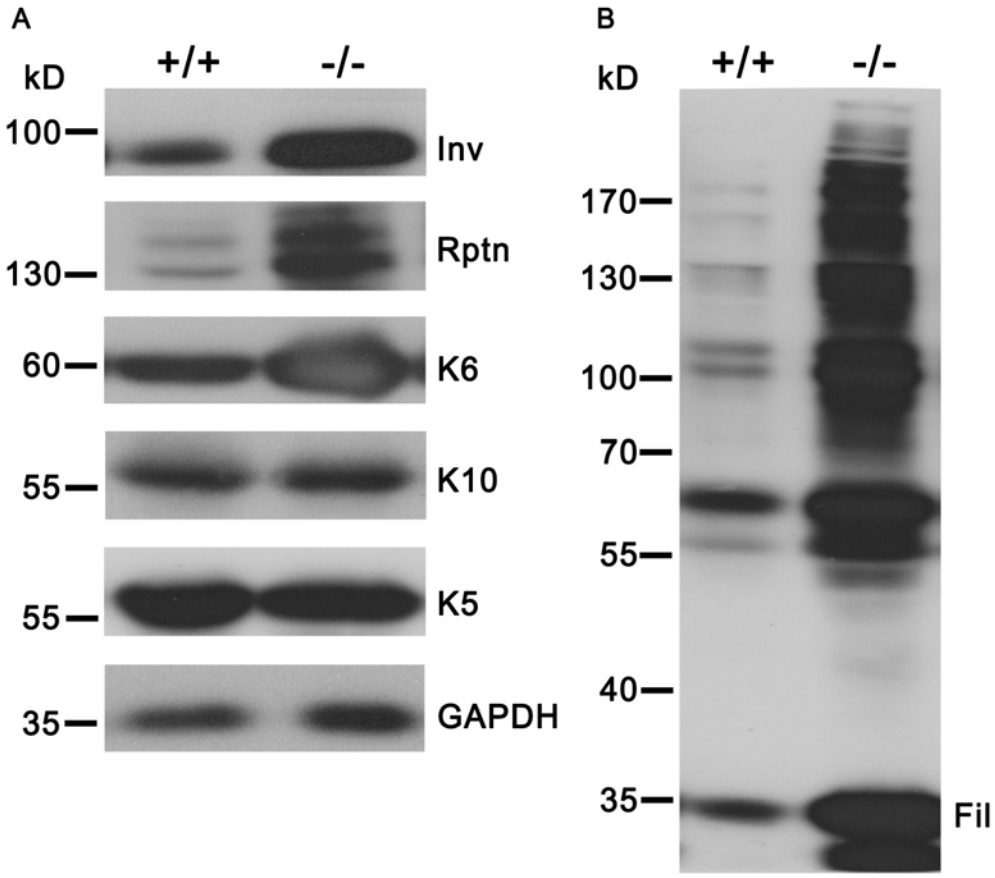

Figure 13: Protein expression level analysis

Equal amounts of extracts of epidermal proteins from control and KO skin grafts were separated through SDS-PAGE and subjected to Western blot using specific antibodies.

(A) Differentiation markers K5 and K10 show no expression differences. Cornified envelope protein such as involucrin (Inv) and repetin (Rptn) were expressed at higher levels in KO skin grafts as compared to controls. Glycerol-aldehyd-3-phosphat-dehydrogenase (GAPDH) was used as a loading control.

(B) Profilaggrin processing was unimpaired in mutant skin grafts and filaggrin precursors as well as filaggrin were significantly higher expressed in KO skin as compared to control skin.

4.1.6. Transepidermal water loss

The disturbance of barrier function, a characteristic feature of *Alox12b* deficient skin, was also displayed in mutant skin transplants as determined by measuring transepidermal water loss (TEWL) (Fig. 14). TEWL in the grafted control skin was 3.2 ± 0.2 g/m^2/h, a level similar to that found in normal neonatal skin (2.6± 0.2 g/m^2/h). The TEWL levels of grafted mature *Alox12b* deficient skin was about threefold higher (7.9 ± 0.3 g/m^2/h), but significantly reduced as compared to the levels of *Alox12b*$^{-/-}$ neonates (14,4± 0,3 g/m^2/h, [55]).

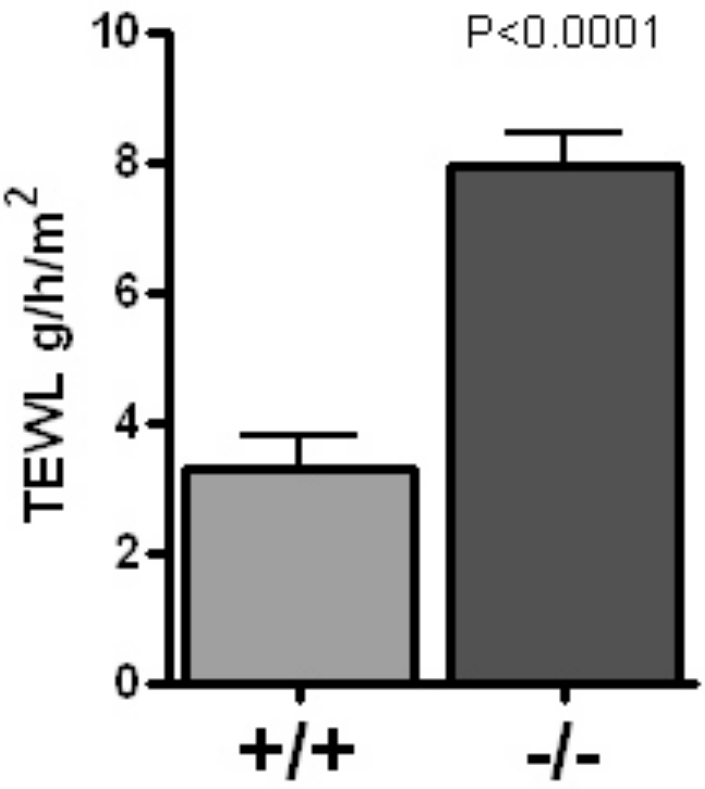

Figure 14: Transepidermal water loss on the skin grafts
Animals were shaved one day before measurement. TEWL was measured on the grafted surface after 4 weeks of transplantation. On the KO skin grafts TEWL was threefold higher than in controls.

4.1.7. Summary

Taken together this data demonstrate that *Alox12b* deficient neonatal mouse skin transplanted onto adult nude mice shows an impaired barrier function and develops an ichthyosiform phenotype with thickening of the epidermis, hyperproliferation, hypergranulosis, parakeratosis and severe hyperkeratosis.

4.2. Conditional inactivation of 12R-LOX in mouse skin

4.2.1. Strategy to generate temporally controlled inactivation of 12R-LOX in mouse epidermis

In order to determine the physiological role of 12R-LOX in the mouse we generated an inducible conditional KO model. To this end we took advantage of a previously in our lab established mouse strain harboring genetically modified *Alox12b* alleles designed for applying the conditional Cre/LoxP recombination system. The modified, so called "floxed" allele contains two LoxP-sites flanking an essential coding region of the *Alox12b* gene (exon 8) to be excised by the Cre recombinase. Ubiquitous Cre expression as achieved by mating the 12R-LOX$^{fl/fl}$ with a Cre-deleter strain (CMV-Cre) led to the generation of a null-allele, which, as previously described, resulted in early postnatal lethality [55].

To be able to determine the role of 12R-LOX in the development and maintenance of the barrier function, the 12R-LOX$^{fl/fl}$ animals were crossed with a K14-Cre-ER^{T2} transgenic line [51], ultimately leading to the conditional inactivation of 12R-LOX in the mouse epidermis after tamoxifen administration (Fig. 15). The K14-Cre-ER^{T2} transgenic mice express a chimeric Cre recombinase, which is fused to the mutated ligand binding domain of the human estrogen receptor that binds tamoxifen but not its natural ligands. While in an un-induced state, Cre is sequestered in the cytoplasm, nuclear translocation and subsequent Cre recombination is induced by exogenous tamoxifen but not by endogenous ligands of the estrogen receptor. Cre fusion protein is expressed under the control of the human keratin14 promoter (K14). The activity of the K14 promoter is essentially restricted to the dividing basal layer keratinocytes of the epidermis, the outer sheath of hair follicles, other stratified squamous epithelia such as oral and tongue epithelia, and epithelial cells of the thymus. However, the K14 promoter is also active in the epidermal layer during embryogenesis [60].

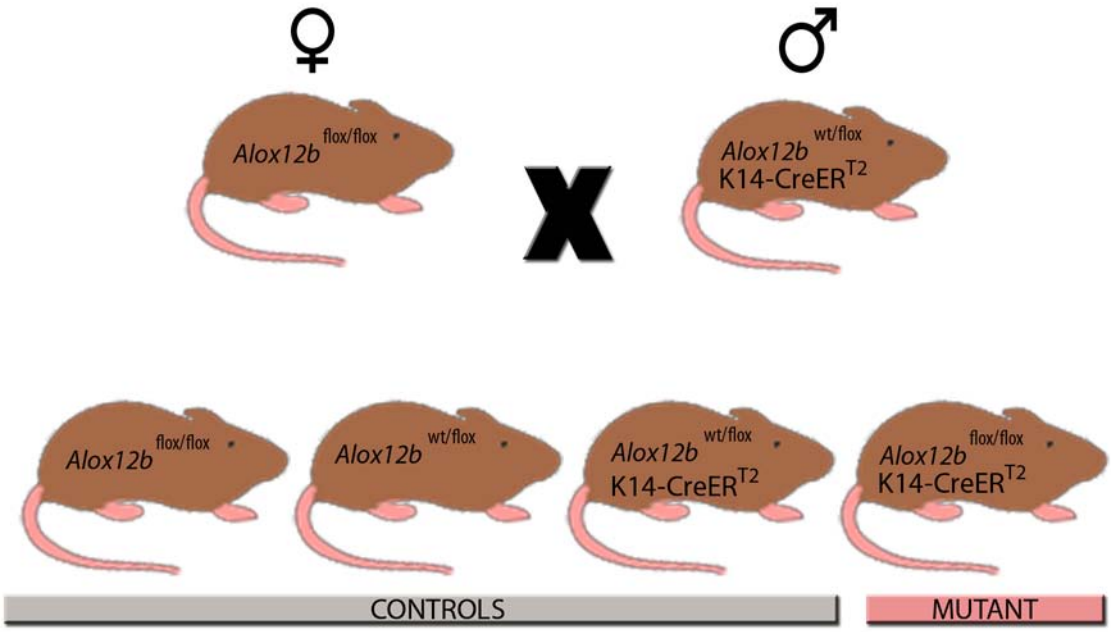

Figure 15: Breeding strategy for generating the conditional inactivation of *Alox12b* in mouse skin

According to the breeding strategy as outlined in figure 15 homozygous 12R-LOX$^{fl/fl}$ mice were crossed to K14-Cre-ER^{T2} transgenic mice to obtain mutant mice for tamoxifen-inducible 12R-LOX inactivation in the adult skin.

Genotype analysis of 419 offspring from 53 matings indicated a ratio of 21% *Alox12b*$^{fl/fl/K14\text{-}Cre\text{-}ERT2}$ mice (mutants) among 46% males and 54% females (Fig. 16). The data demonstrated that mutant and control mice were born in the expected Mendelian ratio, indicating no embryonic lethality of the mutant mice.

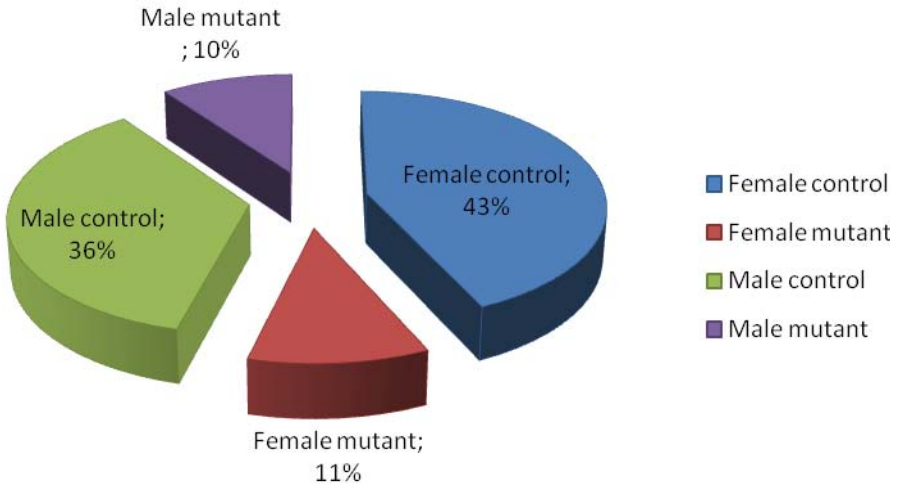

Figure 16: Genotype and sex distribution of mutant and control mice
After genotyping 419 offspring 21% of mutants were identified, following Mendel´s law.

4.2.2. Genotyping of *Alox12b*$^{fl/fl}$ and K14-Cre-ER^{T2} via PCR of genomic DNA

Briefly, exon 8 of the "floxed" *Alox12b* allele is flanked by two LoxP-sites placed 230 bp upstream and 84 bp downstream of exon 8. *Alox12b*$^{fl/fl}$ mice were generated by intercrossing heterozygous floxed mice. Mice homozygous for the "floxed" *Alox12b* allele showed no gross phenotypic abnormalities, indicating that *Alox12b*$^{fl/fl}$ is functionally fully active. Genotyping was performed by PCR using 100ng DNA isolated from tail as a template and primers 708 and 709 to distinguish the 310 bp wild-type allele band from the 344 bp floxed band. (Fig. 17 A, B). For the identification of K14-Cre-ER^{T2} transgene a duplex PCR was applied using primer combination 2585/2586, which amplifies a Cre-specific product of 199bp and a p48-specific primer pair 2583/2584 as internal positive control.

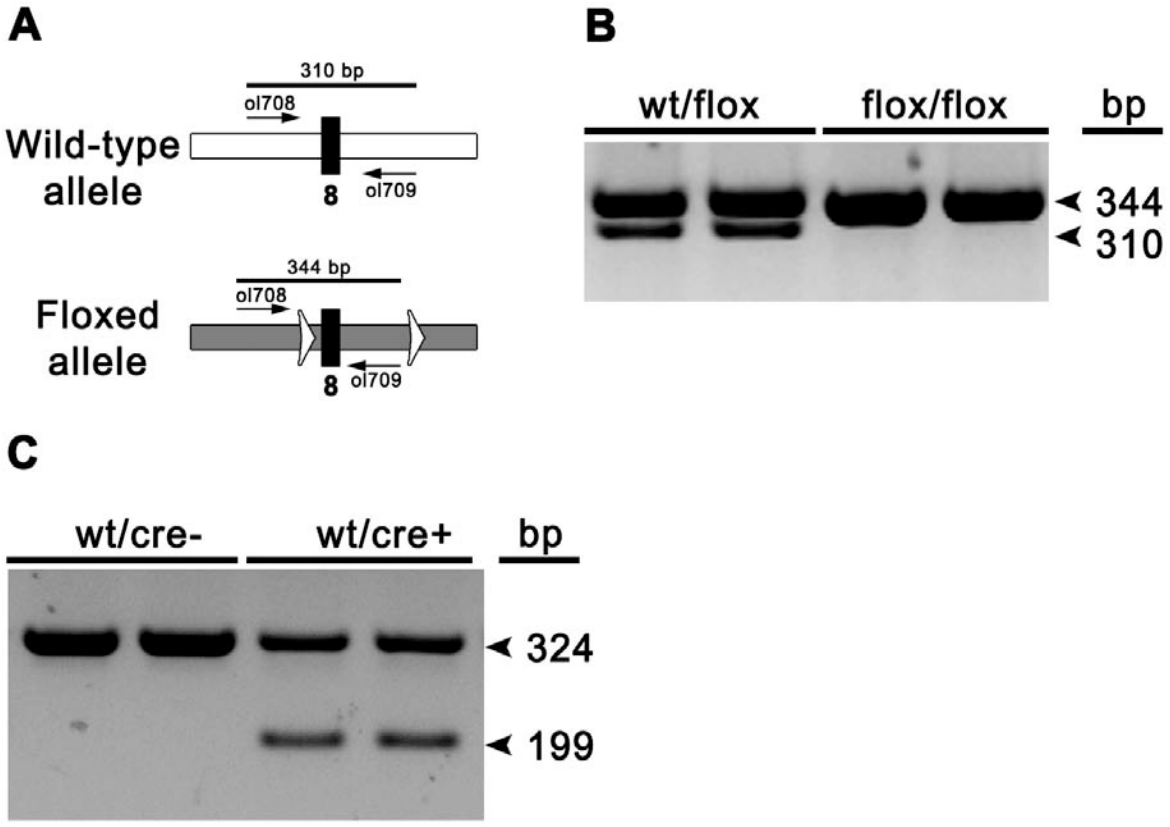

Figure 17: PCR genotyping analysis of tail DNA
(A) PCR Strategy to distinguish the wild-type from the floxed allele.
DNA is extracted from tail biopsies. 100ng DNA template was subjected to PCR for genotyping using different primers combinations.
(B) Primer combination 708/709 amplified a 310bp product from the wild-type and a 344bp product from the floxed allele.
(C) Primer combination 2583/2584 amplified a 324bp product for the internal control and primer pair 2583/2584 amplified a 199bp product from the Cre transgene.

Cre-mediated recombination within the *ALOX12b* allele was monitored by the already described standardized PCR genotyping strategy using primer pair 2275/2277 (Skin grafting genotyping).

4.2.3. Development of mutant 12R-LOX$^{fl/fl/K14\text{-}Cre\text{-}ERT2}$ mice

All control animals, i.e. heterozygous mice expressing the wild-type *Alox12b* allele in the presence or absence of Cre transgene as well as 12R-LOX$^{fl/fl}$ mice that are homozygous for the targeted allele but do not express the Cre transgene, developed normally and did not show any gross abnormalities. Mutant 12R-LOX$^{fl/fl/K14\text{-}Cre\text{-}ERT2}$ mice, that were homozygous for the floxed allele and carrying the Cre transgene, in contrast, were consistently smaller than their control littermates by the age of 3 weeks indicating abnormal development already in the absence of tamoxifen treatment.

To investigate the retardation in post-natal development and growth of the *Alox12b*$^{fl/fl/K14\text{-}Cre\text{-}ERT2}$ mice (mutants) in more detail, we analyzed a group of 103 animals generated from matings as outlined in figure 15, of which 75% of the animals were controls and 25% mutants.

4.2.3.1 Body Weight

Mutant and control littermate mice were weighed daily from birth. All animals developed normally until day 17. From day 17 on the controls continued gaining weight steadily while the mutants showed a significantly reduced weight gain (Fig. 18).

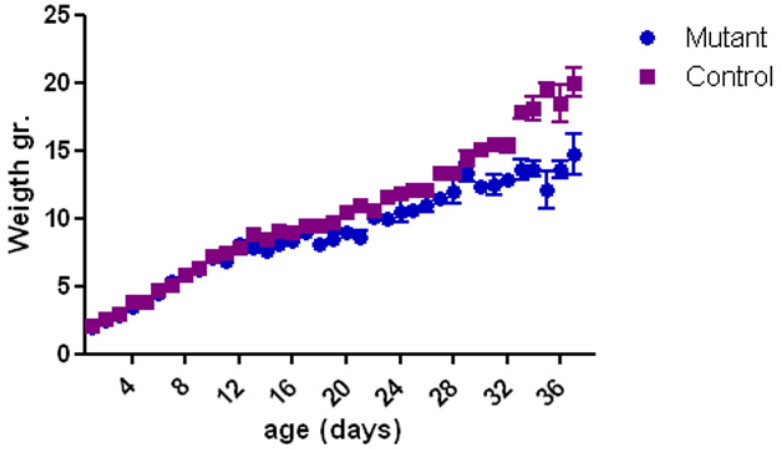

Figure 18: Weight development of mutant 12R-LOX$^{fl/fl/K14\text{-}Cre\text{-}ERT2}$ and control mice
Before day 17 after birth no differences can be appreciated between controls and mutants. After day 20 mutants show a significant ($p<0,05$) reduced growth as compared to control littermates. $n_{control} = 77$ $n_{mutant} = 26$

For a more precise comparison of the mutant and control animals we chose randomly a minimum of three animals from day 14 every third day until day 32 and made a thorough anatomical characterization. Before animal preparation, body weight and size was determined. Consistent with our first observations the mutants began to show reduced body weight in comparison with the controls at day 17. The differences became significant after day 26. Body size, in contrast, as measured by snout-anus length was not different. The bone length of the animals was approximately equal in controls and mutants (Fig. 19 A, B). While femoral (Fig. 19 C, D) and tibial (data not shown) length was not different the bone weight was significantly reduced in mutants as compared to the controls.

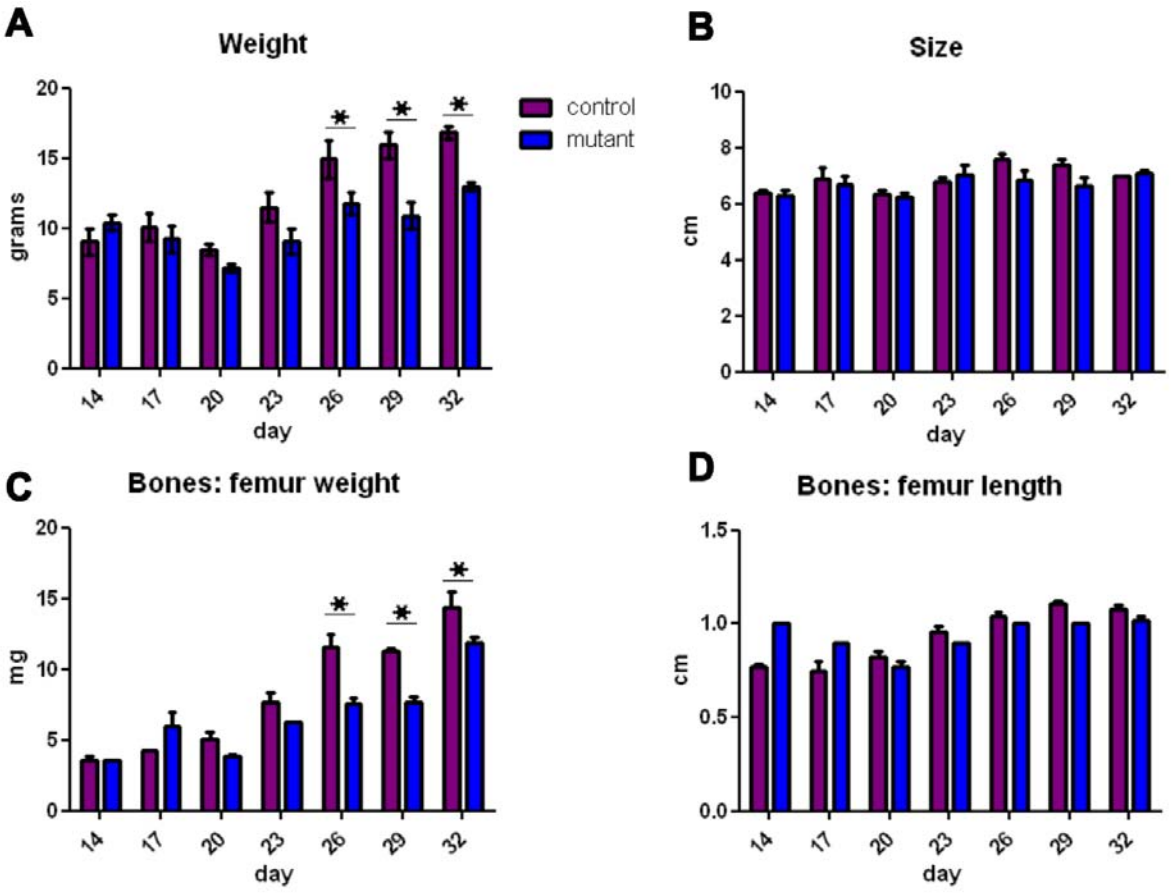

Figure 19: Weight and size development of controls and mutants
(A) Control and mutant mice were monitored for their body weight every third day. Weight differences between controls and mutants became apparent at day 17, and after day 23 the differences became significant (n=3, * $p<0.05$)
(B) Body size as measured by snout-anus length showed no significant differences between controls and mutants (n=3)
(C) Femur bones were lighter in mutants after day 20 than in controls (n=3, * $p<0.05$)
(D) Femur length was not significantly different (n=3)

4.2.3.2. Morphological examination

Postnatal mutant mice were indistinguishable from their respective control littermates and developed normally without showing any signs of skin abnormalities. After day 17 they began to show a growth delay, which was macroscopically discernable by day 23. However, differences between mutants and control were appreciated macroscopically starting at day 26 in more ventral regions of the body (Fig. 20). The mutant mice developed a different, somehow greasy coat appearance exhibiting local alopecia but without showing any scaling. During animal preparation it became apparent that the skin of mutant mice was considerably thinner and more fragile making it more easily to be dissected. Differences in internal organs could also be seen after day 26. Most noticeable, the amount of white adipose tissue was reduced and was almost completely absent by day 32. Spleen and thymus showed a reduced size in mutant mice when comparing to littermates while the lymph nodes were enlarged (data not shown). Other internal organs such as liver, kidney, lung and heart showed no significant differences.

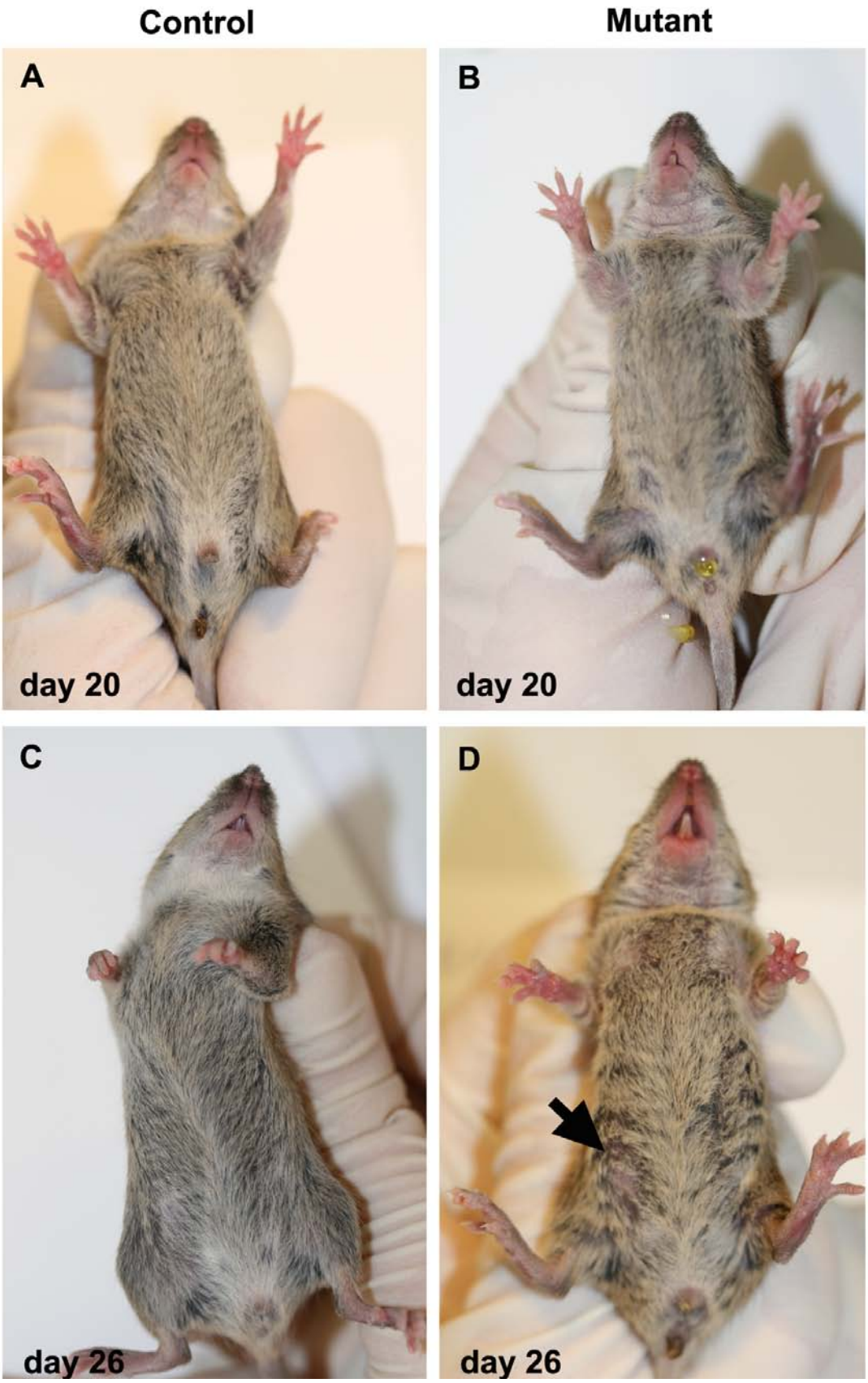

Figure 20: Macroscopic ventral examination of control and mutant mice
(Legend in the next page)

(A-B) At day 20 no morphological differences could be observed
(C-D) Examination of control and mutant at day 26 showed differences in coat appearance and focally reduced hair density (arrow)

4.2.3.3 Skin histology

The histological analysis was made on hematoxylin/eosin-stained paraffin sections of dorsal skin from control and mutant mice. The skin of control animals developed normally exhibiting the typical appearance of adult mouse skin, which is characterized by a thin epidermis consisting of 2-3 nucleated cell layers without a visible stratum granulosum. In contrast, the mutant skin developed from a normal histological appearance at day 17 to a hyperplastic phenotype at day 29, showing pronounced epidermal acanthosis and hyperkeratosis (Fig. 21).

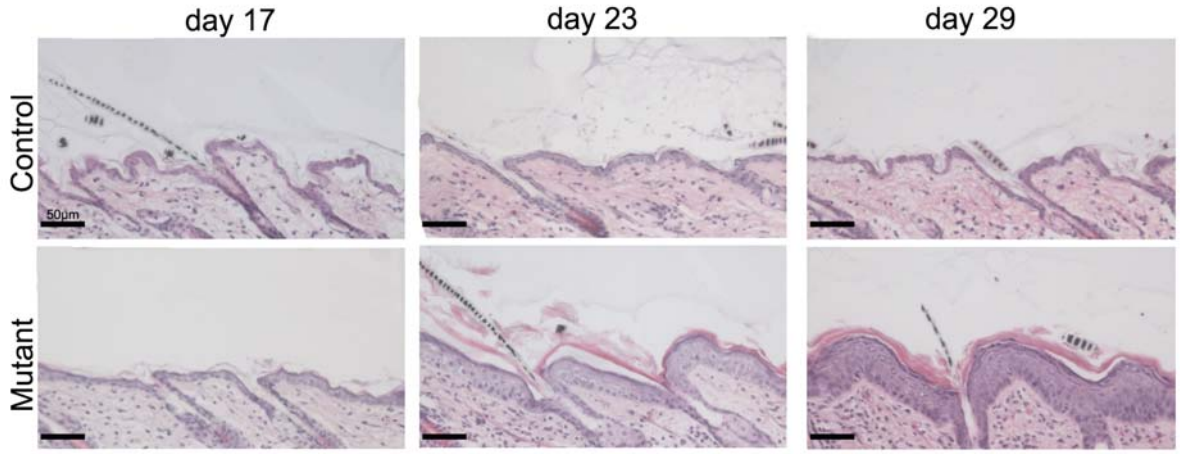

Figure 21: Histological analysis of control and mutant dorsal skin
Dorsal skin was embedded in paraffin. 5µm sections were made and stained with hematoxylin and eosin. Representative sections are depicted.
In contrast to control epidermis, mutant epidermis developed hyperkeratosis and epidermal acanthosis. Scale bar, 50µm.

In contrast with the observation made on paraffin sections, at an ultrastructural level a mild hyperkeratosis could be already observed at day 17 in the mutant skin. Control skin has a stratum corneum with an average of 5 to 8 layers (Fig 22 A, C). As compared with the control skin, the stratum corneum of the mutant mice at day 17 contained from 10 to 15 layers and at day 32 the stratum corneum was markedly piled up in over 50 layers. At either time point morphological anomalies were obsesrved in the mutant skin (Fig. 22 B, D). In addition, deposits resembling extruded contents of lamellar bodies were seen in the intercellular spaces of the mutant stratum corneum (Fig. 22 E, F).

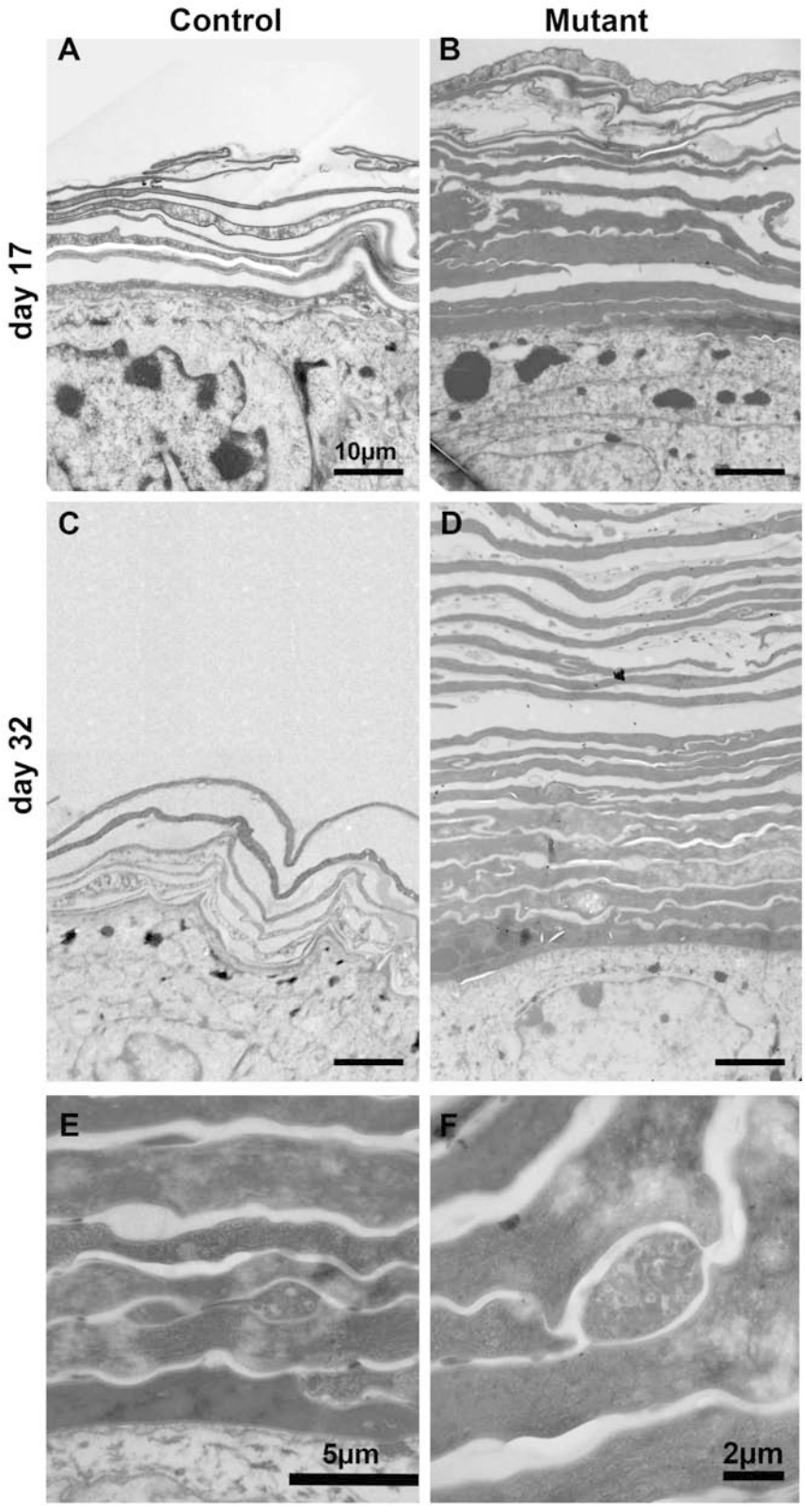

Figure 22: Ultrastructural analysis of control and mutant dorsal skin
Skin biopsies were fixed in 3% glutaraldehyde solution and embedded in epoxy resin. Ultrastructure of dorsal skin from control and mutant mice at day 17 (A and B) and at day 32 (C and D). Remnants of cytoplasmatic organelles in the intracellular space of

mutant animals (E and F). Data are representative of those obtained using three mice of each genotype for each time point. Bars: (A-D) 10 µm; (E) 5 µm; (F) 2µm

4.2.3.4 Molecular analysis of spontaneous activation of the Cre recombinase

4.2.3.4.1. Spontaneous Cre-mediated inactivation of 12R-LOX in the epidermis of mutant mice

The appearance of the morphological abnormalities in the mutant mice suggested that spontaneous Cre recombination had occurred in the absence of tamoxifen. To proof this hypothesis, DNA was isolated from the epidermis of mutant and control mice at different age and Cre-mediated deletion of exon 8 of the *Alox12b* gene was analyzed by PCR (Fig. 23). No deletion could be seen over this period of time in the epidermis of control animals (*Alox12b*$^{fl/fl}$ and *Alox12b*$^{fl/wt}$) not containing the Cre transgene. As detectable by the presence of a 250 bp PCR product, Cre-mediated deletion in the epidermis of mutant mice (*Alox12b*$^{fl/fl/K14\text{-}Cre\text{-}ERT2}$) was observed for the first time at day 17. Amplification of the 920 bp fragment indicated concurrent presence of the uncut floxed *Alox12b* allele until day 23. By day 26, however, no wild-type band could be amplified indicating complete *Alox12b* inactivation in the epidermis of the mutants.

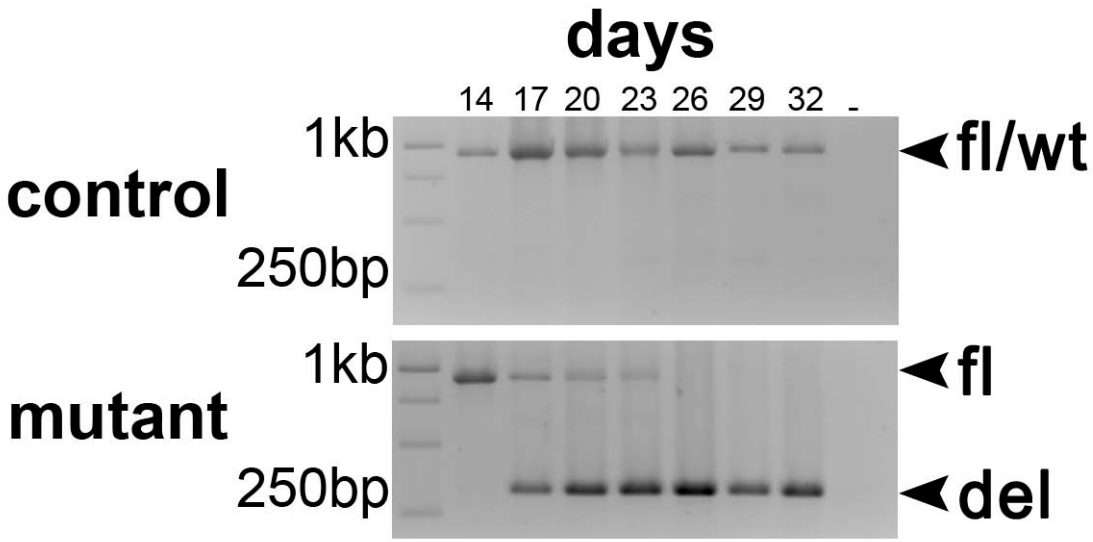

Figure 23: PCR analysis of epidermal DNA of control and mutant mice
DNA was extracted from epidermis of control and mutant animals. 100ng DNA template was subjected to PCR using primer combination 2275/2277, amplifying a 920 bp product for the floxed, 938 bp for the wt allele, and a 320 bp product for recombined *Alox12b* allele. PCR analysis of the mutant showed a partial spontaneous Cre-mediated deletion at day 17 and complete deletion at day 26.

4.2.3.4.2. Spontaneous loss of 12R-LOX protein expression in mutant mice epidermis

To evaluate the impact of the spontaneous Cre recombination on the 12R-LOX protein expression Western blot analysis was performed using protein extracted from dorsal skin epidermis and a polyclonal antiserum raised against a12R-LOX specific peptide (Fig. 24). Wild-type 12R-LOX Protein (68KDa) was detected in all control (*Alox12b*$^{fl/fl}$, *Alox12b*$^{fl/wt}$ and *Alox12b*$^{fl/wt/K14\text{-}Cre\text{-}ERT2}$) protein extractions. Mutant mice (*Alox12b*$^{fl/fl/K14\text{-}Cre\text{-}ERT2}$), in contrast, showed complete loss of 12R-LOX protein expression from day 23 onwards.

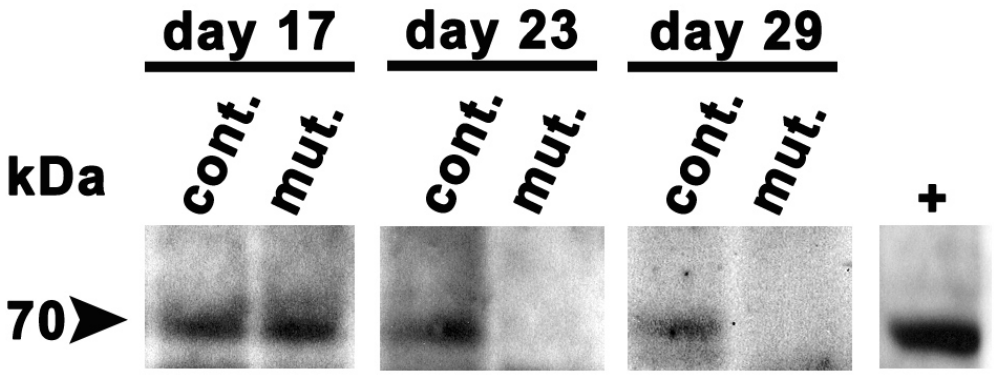

Figure 24: Loss of 12R-LOX protein expression in the dorsal epidermis of mutant mice
Protein was extracted from dorsal epidermis of mutant and control mice at different time points after birth as indicated. 15µg of total lysis proteins were applied to 7.5% SDS-PAGE. The Western blot was developed using a polyclonal antiserum raised against a 12R-LOX-specific peptide. As a positive control, the cell lysate of HEK 293 transfectants expressing m12R-LOX was used. In mutant mice the complete loss of 12R-LOX expression could be detected at day 23.

Spontaneous loss of 12R-LOX protein expression in the mutant mice was furthermore confirmed by immunofluorescence. Since in the adult mouse the epidermis and in particular the granular layer is very thin 12R-LOX protein is hardly to be detected by immunofluorescence in the adult mouse skin. Therefore, immunofluorescence analysis using a 12R-LOX-specific monoclonal antibody was performed on tongue epithelia containing multiple granular layers. In control mice, persistent 12R-LOX expression was detected in the plasma membranes of the granular keratinocytes giving a net-like staining pattern. In the mutant mice, in contrast, only focal expression could be detected at day 17. At day 29 a complete loss of the specific 12R-LOX staining was observed in mutants (Fig. 25).

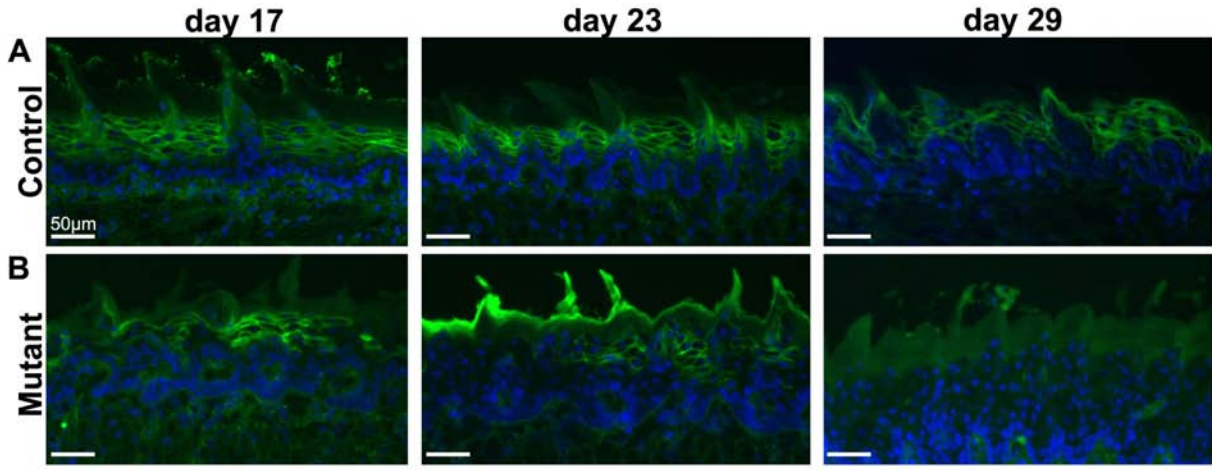

Figure 25: Expression of 12R-LOX in tongue epithelium of control and mutant mice

5µm transversal cryosections of the tongue were made and immunostained.
(A) Immunostaining using a 12R-LOX-specific mAb showed staining of the plasma membranes of the keratinocytes in the granular layers.
(B) Immunostaining of mutant mice showed a patchy staining pattern at day 17 and 23. At day 29 the staining appeared negative.
Nuclei were counterstained with Hoechst 33258. Scale bar, 50µm.

4.2.4. Summary

We report the generation and development of a new conditional 12R-LOX KO transgenic line. No prenatal death was detected of the mutant mice, however a leakiness of the system could be detected at day 17 after birth. Although a sustained growth delay was evident after day 26, the length of the skeleton was not affected, only the mass. Reduced size of internal organs (spleen, thymus) were measurable at day 26. Hematoxylin and eosin staining of the mutant dorsal epidermis showed development of an ichthyosiform phenotype, which is characterized by hyperplasia and hyperkeratosis. At the molecular level, Cre mediated deletion of exon 8 of *Alox12b* started to be identified via PCR at day 17 and a complete loss of 12R-LOX protein in the epidermis was observed at day 23. These results demonstrate a severe leakiness of our inducible conditional 12R-LOX KO system from day 17 on.

4.3. Tamoxifen induced deletion of 12R-LOX in *Alox12b*$^{flox/flox}$ K14-Cre-ER^{T2} mice

In order to achieve a complete simultaneous inactivation of 12R-LOX in the skin of mutant mice Cre activity was induced by tamoxifen administration. Tamoxifen (0.1 mg dissolved in 100 µl sunflower oil) was injected intraperitoneally into 6 weeks old mutant (n=6) and control (n=9) mice daily on 5 subsequent days. After 1 week of rest period we performed a second tamoxifen treatment [56]. Due to the observation that mutant animals were strongly affected and became moribund, we examined the animals immediately after the second treatment at the age of 9 weeks. As already described, before tamoxifen treatment, at the age of 6 weeks, mutant animals were approximately half the weight of control littermates. During treatment mutant animals lost additional 16.6 % of their weight whereas the control littermates gained 20.5% of weight (Fig. 26). Cre induction with tamoxifen shortened the lifespan of mutant animals considerably and all mutant animals died before reaching their 10th week of age.

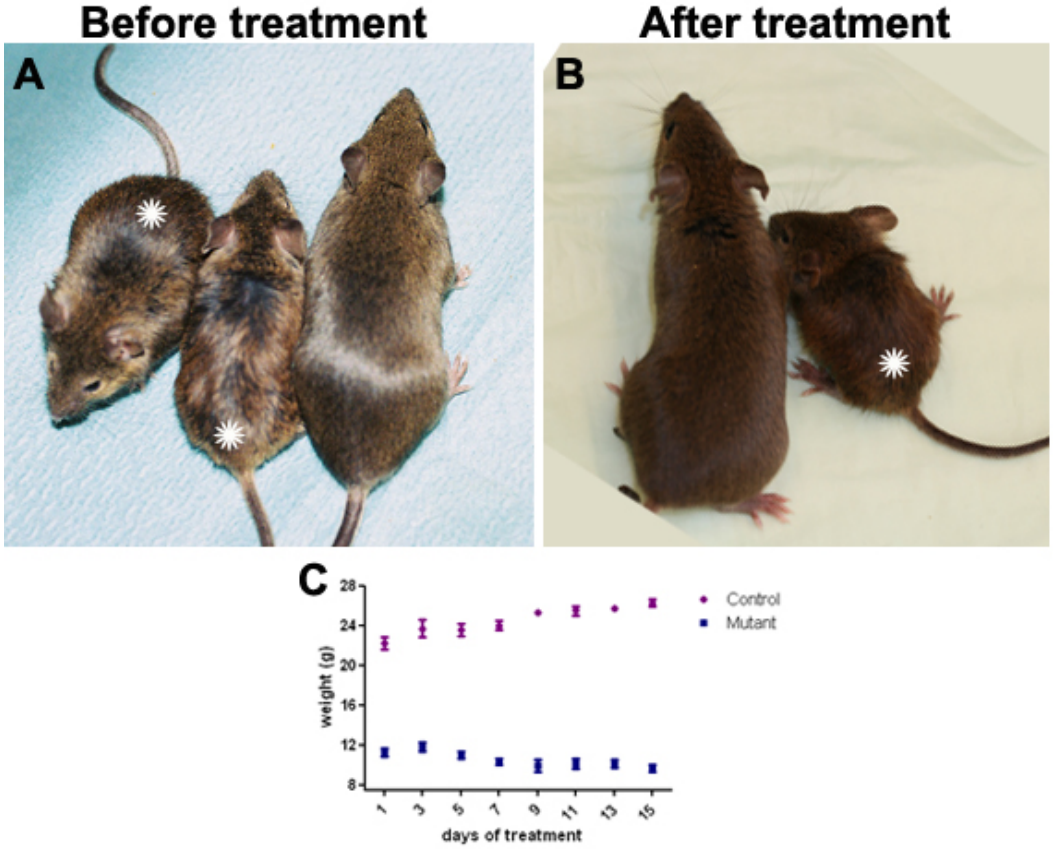

Figure 26: Macroscopic phenotype of control and mutant mice before and after tamoxifen treatment
Legend in next page

Animals were weighed daily before tamoxifen treatment.
(A) Before treatment, mutants were considerably smaller as control littermates.
(B) After tamoxifen treatment (1mg Tam per day injected intraperitoneally) differences in body weight increased furthermore.
(C) Body weight development after tamoxifen treatment. Mutant mice lost on average 2 g of body weight while control mice gained 5 g of body weight during this period. (Asterisk = mutant).

4.3.1 Morphological examination

Following tamoxifen administration mutant animals began to exhibit discretely thickening flaky plaques on their throat, breast and around the snout skin. These lesions subsequently became enlarged and developed into hyperkeratotic, focally ulcerated plaques at the throat, breast and sometimes extending to the arms (Fig. 27). Observations of the mutant mice revealed frequent scratching indicating that the skin lesions were apparently itching. The affected mice fed and drank frequently until they became moribund. At the time of death, all mutant animals displayed a cachectic appearance exhibiting adipose and muscular atrophy, kyphosis (humped back) and failing locomotor functions (Fig. 27 b). In addition, examination of lymphoid organs in the tamoxifen treated mutants revealed a smaller spleen and thymus and enlarged lymph nodes. Other internal organs such as liver, kidney, lung and heart showed no significant differences. Pathological changes induced upon tamoxifen treatment occurred faster and to a more severe extent as observed in the non-induced mutant mice. No similar pathological changes were observed in control mice treated with tamoxifen.

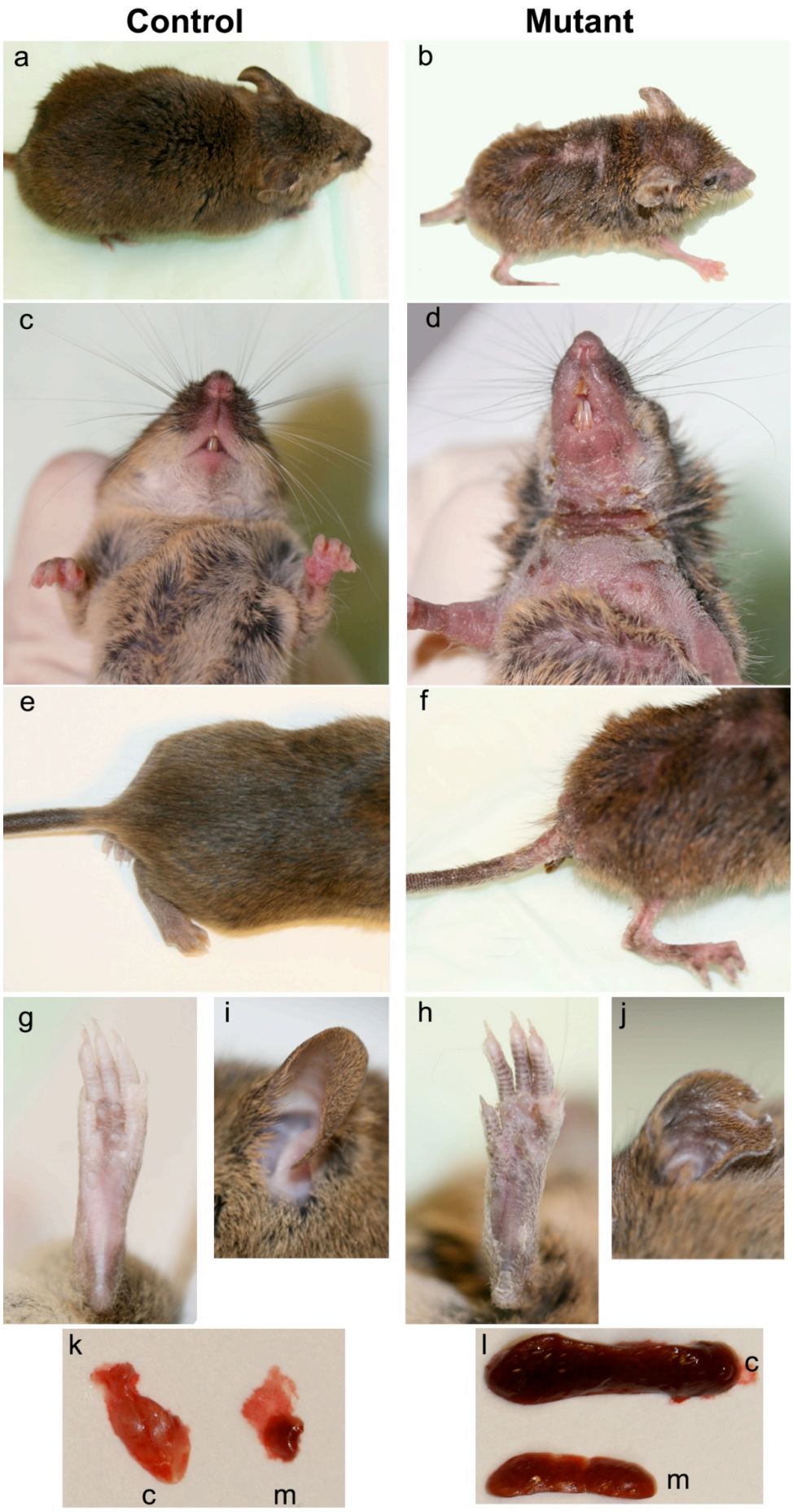

Figure legend in next page

Figure 27: Macroscopic analysis of control and mutant mice after tamoxifen treatment

Phenotypic alterations by tamoxifen-induced deletion of *Alox12b*. a,b, dorsal view. c,d, ventral view. e,f, rear dorsal view and tail. g,h, footpad. i,j, ear. k thymus. l spleen c: control m: mutant. Mutant animals developed, after tamoxifen treatment, severe scaling on their body skin (b), tail (f), footpads (h), and ears (j), moreover scaling was more intensely at mechanical stress regions (throat) where also local alopecia developed (d). Mutant spleen and thymus were smaller than in control animals (k,l).

4.3.2 Histological analysis

Dorsal skin of the treated animals was isolated and stained with hematoxilin and eosin for histological examination (Fig. 28). The epidermis of treated mutant mice showed acanthosis, hypergranulosis and severe hyperkeratosis (arrow).

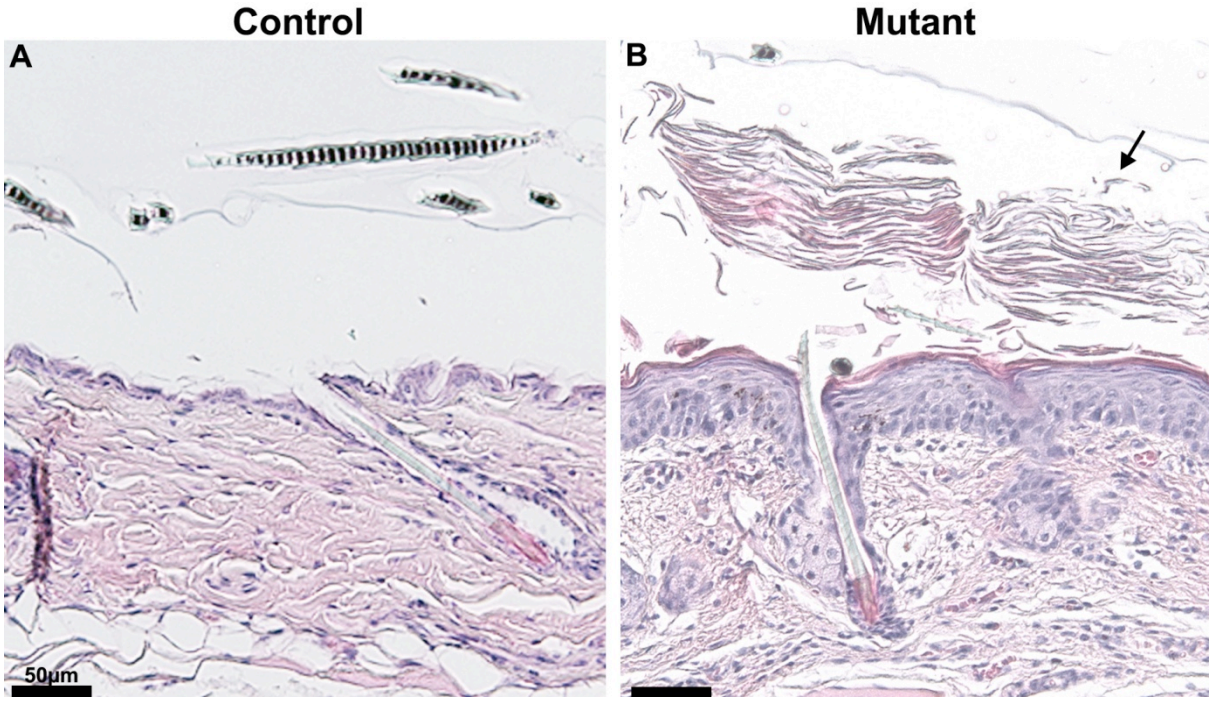

Figure 28: Histological examination of control and mutant dorsal skin after tamoxifen administration

Dorsal skin of 9 week old mice was embedded in paraffin. 5µm sections were made and stained with hematoxylin and eosin. Representative sections are depicted.
(A) Dorsal skin from tamoxifen-treated control animals.
(B) Dorsal skin from tamoxifen-treated mutant animals. Severe hyperkeratosis (arrow) and epidermal hyperplasia could be observed. Scale bars: 50µm

4.3.3. Cre-mediated deletion of *Alox12b* is restricted to Keratin 14-expressing tissues

To investigate the tissue-specifity of the K14-Cre-ER^{T2} activity, we isolated DNA from a large number of different tissues including different stratified epithelia (oesophagus, tongue, skin…) as well as other K14-expressing tissues and non-expressing tissues. Cre-mediated recombination was monitored by PCR using primer pair 2275/2277 (Fig. 29). DNA extracted from control animals (*Alox12b*$^{fl/fl}$ and *Alox12b*$^{fl/wt}$) produced only the floxed (920 bp) band. In tamoxifen-treated mutant animals (*Alox12b*$^{fl/fl/K14\text{-}Cre\text{-}ERT2}$) the floxed as well as the deleted (320bp) band could be detected in the following tissues: thymus, eye lid, salival glands, cornea, tongue, snout, ear and foot pad. A complete loss of the floxed allele was observed in DNA extracted from tail epidermis, dorsal and ventral skin and dorsal isolated epidermis. No deletion was detected in other epithelia such as oesophagus, forstomach and others (Fig. 29).

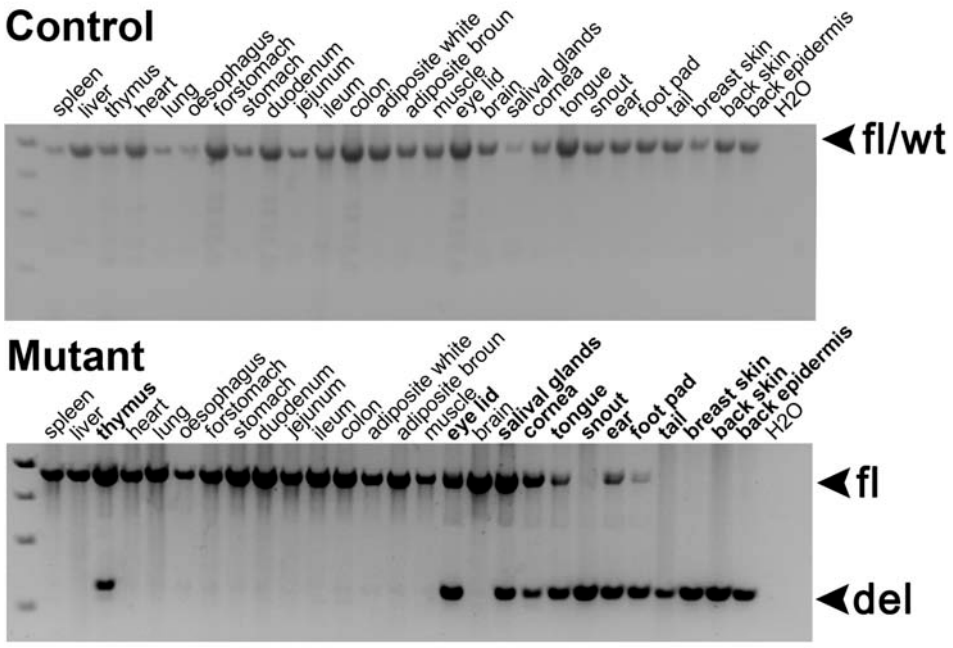

Figure 29: Tissue-specificity of K14-Cre-ER^{T2}tamoxifen-mediated *Alox12b* disruption

DNA was extracted from various organs of tamoxifen-treated control and mutant mice. 100ng DNA template was subjected to PCR using the primer pair 2275/2277. PCR products of 920bp from the floxed (fl) allele, 938bp from the wild-type (wt) allele and 320bp from the deleted (del) allele were obtained. Products were analyzed on a 1% agarose gel. Complete deletion of *Alox12b* could only be detected in snout, tail, breast and dorsal skin and in the isolated dorsal epidermis.

4.3.4. Epidermal differentiation and proliferation markers

To investigate if the loss of 12R-LOX in adult mice induces defects in skin differentiation and proliferation, we analyzed the level of expression of various differentiation and proliferation markers via Western blot analysis in epidermal extracts (Fig. 30). The higher levels of Keratin 6 (K6) expression that could be detected in the Western blot, is consistent with the hyperproliferation of the mutant skin when comparing to the control. The Western blot also revealed that the levels of Keratin 5 (K5) and Keratin 10 (K10) used as a basal and suprabasal marker were not altered. We also analyzed the expression levels of a group of cornified envelope proteins. Involucrin (Inv) showed no significant differences between control and mutants, however repetin (Rptn), however, exhibited a much higher expression levels in mutants than in controls.

Because skin from 12R-LOX constitutive knock-out has been associated with a block in the processing of profilaggrin to filaggrin [55], western blot analysis was made to ascertain this processing in tamoxifen-treated mutant mice. Both, profilaggrin as well as fully processed filaggrin levels were significantly higher in mutants when comparing to control protein levels and no signs of impaired processing could be detected.

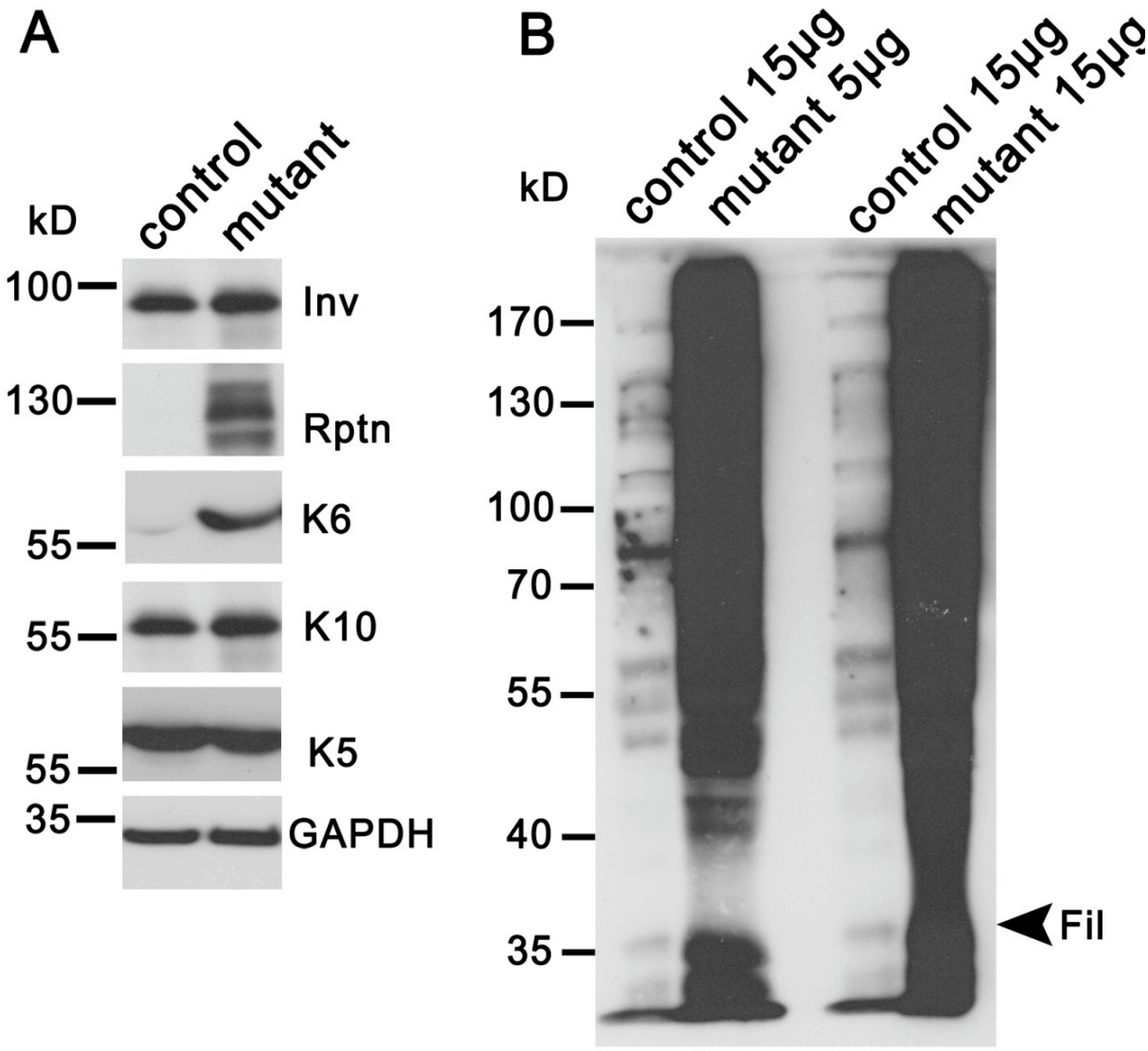

Figure 30: Protein expression analysis after tamoxifen treatment on control and mutant mice.

Protein was extracted from tamoxifen treated control and mutant epidermis by using RIPA buffer. 15µg protein were loaded per line on a 7,5% SDS-PAGE and subjected to Western blot analysis using specific antibodies.

(A) Differentiation markers Keratin 5 (K5) and Keratin 10 (K10) showed no expression differences. Hyperproliferation marker Keratin 6 (K6) as well as cornified envelope protein repetin (Rptn) was expressed at higher levels in mutants (but not involucrin (inv). Glycerol-aldehyd-3-phosphat-dehydrogenase (GAPDH) was used as a loading control.

(B) Filaggrin precursor expression was much higher in mutants than in controls and no disturbance of the profilaggrin processing could be detected.

4.3.5. Summary

The results demonstrate that intraperitoneal administration of tamoxifen to mutant mice produces a much more severe phenotype than the spontaneous deletion of *Alox12b*. Mutant mice lost 20,5% of their weight during tamoxifen treatment and developed severe scaling of the whole epidermis. Internal organs such as spleen and thymus were also affected. However, *Alox12b* deletion could only be detected in tissues with endogenous K14 expression, including thymus but not spleen. The phenotypical changes were also associated with large structural changes of the epidermis. The mutant epidermis developed hyperplasia and an acute hyperkeratosis. Proteins of the cornified envelope such as involucrin, filaggrin and repetin were up-regulated in the mutant epidermis. Differentiation markers (K5 and K10) showed no alteration in expression levels whereas hyperproliferative keratin K6 was over-expressed in mutants.

4.4. Insights in the 12R-LOX molecular pathway

In this study we have demonstrated that the deletion and inactivation of 12R-LOX in the adult mouse skin leads to the development of an ichthyosiform phenotype, which is a typical compensatory pathological mechanism of the epidermis to counteract increased water loss through the skin. We were also able to confirm that 12R-LOX plays a significant role in terminal differentiation of mouse epidermis and maintenance of the barrier function. At the present little is known about the mechanism of the action of the 12R-LOX pathway. In order to investigate at a molecular level, how 12R-LOX deficiency affects the expression state of a large number of genes, we performed a gene expression profiling using cDNA microarray technology.

4.4.1 Gene expression profile of 12R-LOX deficient mice

Animals were obtained from 12R-LOX heterozygous mating directly after birth. After genotyping and separation of epidermis, RNA was extracted from 6 newborn mice of each genotype. As not all RNAs had the quality necessary for gene analysis a total of 6 RNAs from wild-type, 5 from heterozygous and 5 from KO epidermis were further used for microarray analysis. cDNA synthesis and hybridization to the Illumina bead-array as well as bioinformatical data analysis was done by our cooperation partners in Dr. Hennies laboratory (Fig. 31).

As expected, the RNA expression pattern was found to be different between control and 12R-LOX-deficient epidermis. No significant differences were observed between wild-type and heterozygous animals which do not express a skin phenotype, as they clustered together and apart from KO epidermis.

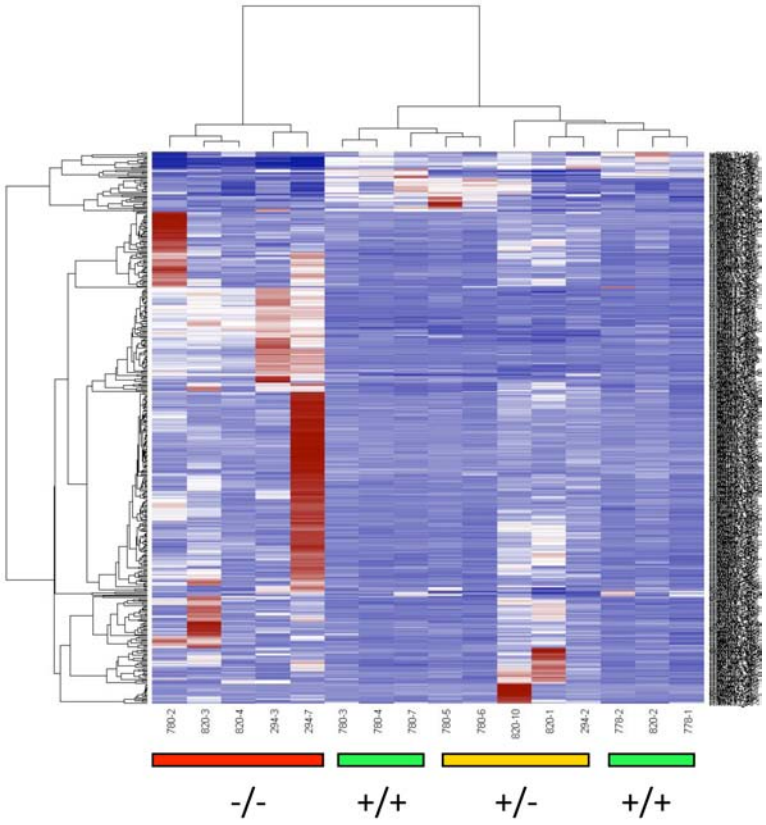

Figure 31: Alterations in RNA expression profiles between knockout and control epidermis.
Red denotes high level expression and white denotes low expression.

Although all KOs are clustered together, significant differences between individual KO animals were observed and therefore further experiments are needed. Yet, gene candidates showing the same expression pattern in all KO animals could already be identified. Although these results remain to be verified by Real-time PCR, some candidate genes that are known to play an important role in skin proliferation and differentiation could be seen to share the same pattern in all individual animals. More than 200 genes were differentially expressed between KO and littermate control epidermis (Supplementary Table 1). Differentially expressed genes with known functions that have potential roles in epidermal differentiation are shown in Table 1. Not only were there differences in the expression of several keratins, important members of the cytoskeleton, but also higher expression levels of Small Proline Rich (SPRR) proteins, constituents of the cornified cell envelope and important components of the skin barrier function. Genes with consistently increased expression levels in the KO also include transcription factors such as JunB and Fos. They are members of the activating protein-1 (AP-1) family, which are known as regulators of keratinocytes proliferation and differentiation (table1).

Symbol	Gene name	Mean Knockout	Mean control	Difference
Sprr2e	small proline-rich protein 2E	2134,82	103,62	20,6
Sprr2g	small proline-rich protein 2G	2557,37	135,11	18,93
Sprr1b	small proline-rich protein 1B	9671,02	557,06	17,36
Krt16	keratin complex 1, acidic, gene 16	3904,18	320,87	12,17
Krt6b	keratin complex 2, basic, gene 6b	611,79	202,75	3,02
JunB	Jun-B oncogene	2973,14	442,21	6,72
Fos	FBJ osteosarcoma oncogene	3366,45	1598,28	2,11
Fosb	FBJ osteosarcoma oncogene B	635,3	200,33	3,17

Table 1: Selection of Up-regulated candidate genes in the 12R-LOX deficient epidermis compared to control (wild-type and heterozygotes) epidermis

4.4.2 Up-regulation of AP-1 complex proteins

Among the deregulated genes observed in absence of 12R-LOX, the AP-1 members *JunB* and *Fos* particularly attracted our attention because of their involvement in cell proliferation and differentiation. The activating protein-1 (AP-1) is a transcription factor principally composed of dimers between the Jun, Fos and ATF (activating transcription factor) protein families. AP-1 is at the receiving end of signaling cascades elicited by a various number of physiological and pathological stimuli, including cytokines, growth factors, stress signals, bacterial and viral infections as well as oncogenic stimuli and it regulates, upon activation, numerous target genes [61]. The distinct expression pattern of the Jun and Fos proteins in the epidermis suggests a general role for individual AP-1 subunits in cell proliferation and differentiation [62]. As shown by gene array analysis at the transcriptional level, *Fos* was found to be 2 fold and *JunB* 6 fold up-regulated in the epidermis of 12R-LOX deficient mice as compared with controls. To verify altered gene expression at the protein level we furthermore performed Western blot analysis. Both the expression c-Fos and JunB was increased in KO protein extracts compared with extracts from wild-type and heterozygous epidermis (Fig. 32 A), thus, correlating with the mRNA transcript levels. The cDNA microarray analysis also revealed genes the expression

of which was consistently decreased in mutant skin. Interestingly, c-Jun was down-regulated in KOs, which also could be confirmed by Western blot analysis. There is strong evidence from tissue culture experiments and KO mice that specific members of the MAP kinase family (Erk 1/2, JNK/SAPKs, p38-kinase) selectively regulate AP-1 proteins depending on the extracellular stimuli [63]. Since Fos expression is induced by extracellular-signalling regulated kinase (Erk) signalling, we measured the levels of phosphorylated Erk in 12R-LOX KO epidermis (Fig. 32 B). Western blot analysis revealed robustly increased levels of phosphorylated Erk in KO epidermis. Therefore, enhanced Erk signalling presumably account for elevated Fos levels. In contrast, no change in the expression or phosphorylation of the Jun-N-terminal kinases (JNK-1, -2, -3) was seen in KO epidermis. These results are in accordance with the absence of phosphorylated c-jun in the epidermis of any genotype (data not shown). JNK also known as stress-activated kinases (SAPK), which are strongly activated, by cytokines and environmental stress phosphorylate and therefore regulate c-Jun activity (Fig. 32 C).

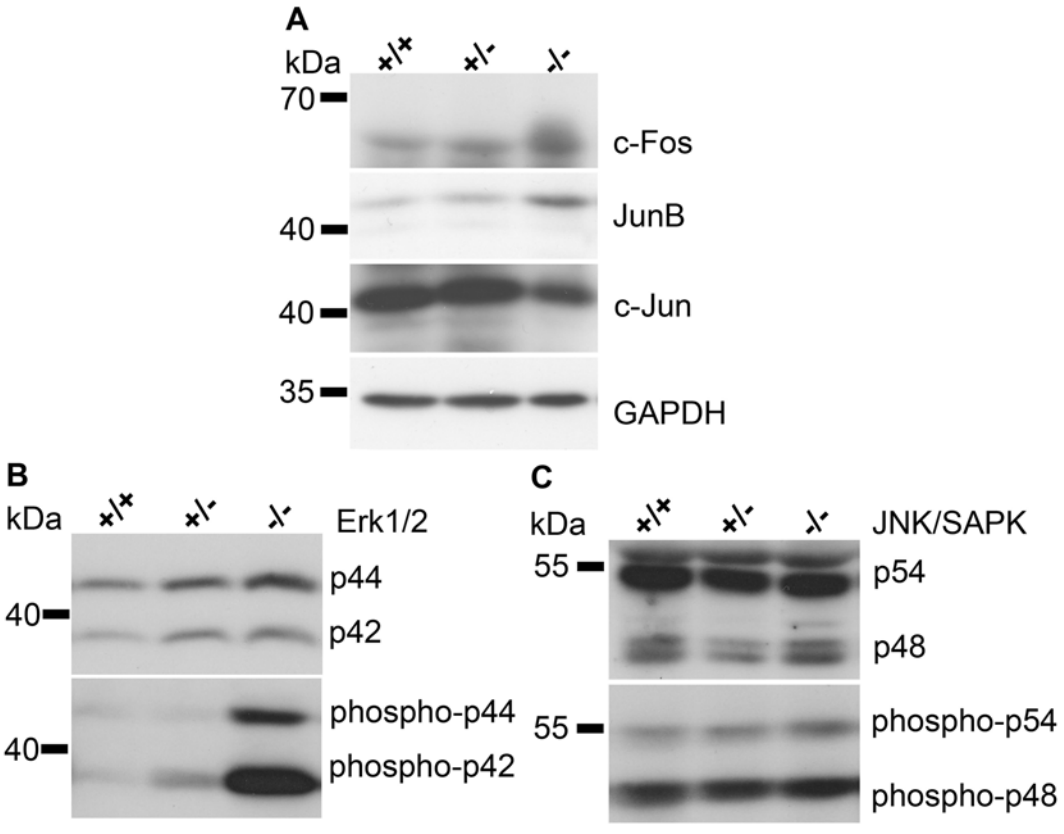

Figure 32: Protein expression levels of AP-1 family members and their activators

Proteins were extracted from newborn epidermis. 15µg protein were loaded per line on a 7,5% SDS-PAGE and subjected to Western blot analysis using specific antibodies.

(A) Higher levels of JunB and C-Fos protein expression were detected in the KO extracts. C-Jun was found to be down-regulated in KOs. Glycerol-aldehyd-3-phosphat-dehydrogenase (GAPDH) was used as a loading control.
(B) Levels of phosphorylated Erk1/2 were increased in KO epidermis, while Erk1/2 expression levels remained unaffected.
(C) Expression and phosphorylation of JNK isoforms showed no differences between genotypes.

4.4.3 Summary

In conclusion, 12R-LOX KO epidermis showed a large number of differentially regulated genes. Among them, member of the AP-1 gene family appeared as very interesting candidate genes due to there implication in skin biology and stress. We could confirm major differences in mRNA transcript and protein levels of AP-1 between wild-type and 12R-LOX knock-out epidermis. While increased Erk signalling was presumably responsible for enhanced Fos expression, levels of JunB were as well elevated in the absence of 12R-LOX. By contrast, Jun expression was diminished in 12R-LOX deficient epidermis.

5. Discussion

Autosomal recessive congenital ichthyosis (ARCI) is a clinically and genetically heterogeneous group of skin disorders that are associated with impaired skin barrier function. In non-syndromic ARCI six different genes have been identified to date that underlie the phenotype. The corresponding proteins are involved in the production, transport or assembly of components of the stratum corneum that constitute the permeability barrier of the skin. The more recently identified ARCI genes including *ALOX12B* and *ALOXE3* have been suspected to function in a common metabolic pathway.

ALOX12B and *ALOXE3* encoding the lipoxygenases (LOX) 12R-LOX and eLOX-3 are members of the epidermal subfamily of mammalian LOX with preferential expression in skin and few other epithelial tissues. 12R-LOX and eLOX-3 differ from all other LOX by unusual structural and enzymatic features. 12R-LOX represents the only mammalian LOX, which forms products with R-chirality and, unlike all other LOX, eLOX-3 does not exhibit dioxygenase activity but functions as a hydroperoxide isomerase. Both enzymes act in sequence to convert arachidonic acid via 12R-hydroperoxyeicosatetraenoic acid (12R-HPETE) to the corresponding hepoxilin-like epoxyalcohol, 8R-hydroxy-11R,12R-epoxyeicosatrienoic acid. Furthermore, spatial and temporal coexpression of 12R-LOX and eLOX-3 indicate a close functional relationship of both enzymes.

Genetic studies have shown that mutations in *ALOX12B* or *ALOXE3* which completely eliminate the catalytic activity of the LOX enzymes represent the second most common cause for ARCI. To date 23 different point mutations in *ALOX12B* and 7 in *ALOXE3* have been identified. The LOX catalysed step represents a key position at the start of a novel eicosanoid pathway in skin that seems to play an essential role in the establishment and/or maintenance of the epidermal barrier function. It has been suspected that other recently identified ARCI genes, *CYP4F22,* a putative ω-hydroxylase, and *ichthyin*, a putative hepoxilin or trioxilin receptor as well as two other genes associated with syndromic ARCI forms (*ABHD5*, a lipid hydrolase mutated in Chanarin-Dorfman Syndrom and *ALDH3A2,* a fatty aldehyde dehyrogenase mutated in Netherton Syndrom) may function as downstream elements of the 12R-LOX/e-LOX-3 sequence in the same eicosanoid pathway [41, 64, 65].

To analyze the impact of this pathway in terminal keratinocyte differentiation and in the development and/or maintenance of the epidermal barrier we have established mouse models with targeted inactivation of 12R-LOX and eLOX-3 by using the Cre/LoxP system.

Previous work was focused on the characterisation of a constitutive 12R-LOX KO mouse model. These *Alox12b* deficient mice die rapidly after birth as a result of severe dehydration. In fact, it has previously been demonstrated that gene defects

that disrupt barrier function are known to cause a more severe phenotype in the mouse than in human skin as a result of the much larger surface to volume ratio. Morphologically, however, the newborn KO mice did not exhibit an obvious cutaneous phenotype [55]. These findings revealed an essential role of 12R-LOX in the formation of the barrier function. Another mouse carrying a naturally occurring mutation in exon 14 of the *Alox12b* gene leading to a 12R-LOX deficiency [66] displayed the same phenotype, confirming our findings.

The aim of this study was to develop a mature 12R-LOX deficient mouse skin model in order to compare the adult mouse phenotype with the human ichthyosis phenotype and to study the responsible molecular mechanisms underlying this event, and consequently creating a suitable animal model for ARCI forms associated with an impaired LOX metabolism.

5.1. Animal models generated to study 12R-LOX deficiency in the adult stage

We developed two different experimental approaches: skin grafting of newborn 12R-LOX deficient skin onto the back of nude mice and the development of transgenic mice with inducible deletion of *Alox12b* in skin keratinocytes. Skin grafting is an excellent technique to overcome the difficulty of KO mouse models that die immediately after birth, however it also suffers from some significant limitations. The skin grafting procedure is not trivial and some technical assistance from an animal expert is needed, however if this small obstacle is overcome the skin rapidly grafts onto the adult skin with a normal phenotype. Indeed, skin grafts have other clear disadvantages mostly due to the limited sample size. Thus, certain analytical methods requiring large amounts of epidermis such as lipid analysis or gene arrays are not possible. Furthermore, skin grafts are not isolated systems but become part of the host animal thereby some processes can be overcome by the environmental compensating effects of the surrounding host tissue., Therefore, only the skin and no other organs or response to treatments can be studied. To overcome those skin grafting restrictions, we engineered as well an inducible, epidermis-specific 12R-LOX KO mouse model by crossing *Alox12b*$^{fl/fx}$ transgenic mice that harbour the 12R-LOX gene targeted by LoxP sites with mice expressing a tamoxifen inducible Cre recombinase under the control of the human keratin 14 (K14) promoter, whose activity is restricted to the basal layer of the epidermis [67]. Such mouse model would allow us to study the influence of 12R-LOX deletion in adult skin and its effects in other organs. In our model, we used the Cre-ER^{T2}, which is a fusion protein between a triple mutated ligand domain of the human estrogen receptor and the Cre recombinase. Its activity can be induced with 10 times less tamoxifen than its predecessor Cre-ER^{T} [51], reducing possible toxicity events due to a very high tamoxifen doses. We could demonstrate that the expression pattern and activity of K14-Cre-ER^{T2} was, as expected not only observed in skin and tail, but also in the

tongue, salivary glands, eye lid [60] and at very low levels in the thymus. In contrast to the K14-Cre-ER^{T2} study made by Indra et al [60], no recombination was detectable in stomach or oesophagus following tamoxifen treatment.

In contrast to previous studies where no or only minimal activity of Cre-ER^{T} or Cre-ER^{T2} was detected in the absence of tamoxifen [51, 68], a strong spontaneous Cre recombinase activity was observed in our mouse model indicating substantial leakiness of the system. Cre recombinase activity was firstly monitored in skin at 17 days after birth and a complete recombination of the *Alox12b* target was observed at day 26. In support to our observation, other conditional KO mice such as K14-Cre-ER^{T2} *IKK2*$^{fl/fl}$ showed spontaneous Cre activity. In this case, however, spontaneous Cre-mediated deletion of *IKK2* in the skin was later and first seen at 6 months of age [69]. No spontaneous deletion at all was described in K14-Cre-ER^{T2} RXR$\alpha^{fl/fl}$ [70] or at Fatp4$^{fl/fl}$ mice [71]. The striking differences in the extend of leakiness of the Cre system in the distinct conditional KO models could be due to different genetic background of the mice used. Indeed, while our conditional animals have been backcrossed over 10 generations into the 129SV background, the K14-Cre-ERT2 *IKK2*$^{fl/fl}$ as well as the *RXR*$\alpha^{fl/fl}$ models have a C57/B6 background. To verify this hypothesis we are currently backcrossing the *Alox12b*$^{fl/fl/K14\text{-}Cre\text{-}ERT2}$ into a C57/B6 background. Another explaination for the leakiness of our system could be Cre activation by diet-derived compounds capable of interacting with nuclear receptors. Indeed, it has been described that numerous dietary compounds, such as polyphenols (soy isoflavones genistein and daidzein), can modulate the activity of the estrogen receptors [72], therefore we are taking into consideration that changing the animal diet to a poor-polyphenols diet could reduce the leakiness of our system.

5.2. Ichthyosiform phenotype in skin grafts and *Alox12b*$^{fl/fl/K14\text{-}Cre\text{-}ERT2}$ mouse

In this study, we could demonstrate by skin grafting and conditional KO mouse approaches that *Alox12b* deficient mouse skin developes an ichthyosiform appearance with thickening of the epidermis, hyperproliferation, hypergranulosis, parakeratosis and severe hyperkeratosis. These features represent typical compensatory mechanisms observed in the adult epidermis of mice suffering from severe skin barrier defects and recapitulate the phenotype observed in skin from ichthyosis patients [5, 41, 73]. Compensatory pathological epidermal mechanisms, as observed in our model, primarily serve to counteract an increased loss of water through the skin. In fact, presumably due to the pronounced hyperkeratosis, the transepidermal water loss (TEWL) (of the adult transplants from *Alox12b* deficient skin is considerably decreased as compared to neonatal KO skin, but remained significantly higher than in the control skin grafts. In the *Alox12b*$^{fl/fl/K14\text{-}Cre\text{-}ERT2}$ mice we expect that TEWL will be high at day 17 after birth and reduced at day 32 or after tamoxifen treatment when hyperkeratosis is completely developed. While in many

mouse models with defective barrier function a cutaneous phenotype is already apparent at birth, the development of hyperplasia and thickening of the stratum corneum seen in the 12R-LOX KO skin grafts could represent later response processes, a feature that was also observed in *TGase1*-deficient mice [74]. Conversely, skin grafts from *TGase1*$^{-/-}$ mice and from other mice with barrier defects typically showed alopecia, marked erythema and massive scales [75-77]. 12R-LOX KO grafts, in contrast, exhibited normal hair growth, no erythema and mild scaling. This macroscopic appearance closely reproduce the mild phenotype seen in many patients with *ALOX12B* mutations which is characterized by moderate light scaling with no or moderate erythema [8, 41, 64, 78]. On the other hand, a more severe phenotype with intense lamellar scaling and large brown scales in addition to a self healing collodion baby phenotype [79] was observed in other patients with *ALOX12B* mutations confirming clinical heterogeneity of ARCI. Moreover, in a recent study, 13 out of 19 patients, showed a striking palmoplantar hyperlinarity with or without mild karatoderma. Remarkably, this phenomenon could also be seen in the tamoxifen treated conditional animals to an extreme of being unable to open their front claws.

Heterogeneity is also observed on the histopathological and even more so on the ultrastructural level. To date, only two reports in the literature describe the morphological features of skin biopsies from patients with *ALOX12B* mutations. Histologically, the 12R-LOX deficient mouse skin grafts closely resemble the phenotype of a patient exhibiting the clinical features of self-healing collodion membrane [79]. The skin biopsy taken 3 days after birth at the edge of the collodion membrane showed a thickened orthokeratotic stratum corneum containing numerous cytoplasmic droplets and increased prominence of the granular layer with underlying mild acanthosis. In another report, the histological analyses of two patients with *ALOX12B* mutations similarly showed orthokeratotic hyperkeratosis but reduced or absent stratum granulosum [78]. More comprehensive morphological analyses of skin biopsies from patients with *ALOX12B* mutations are needed to further clarify similarities and differences between the *Alox12b*-deficient mouse skin and human patient skin.

Although spontaneous Cre recombination of *Alox12b* was sufficient to elicit a clear ichthyosiform phenotype in the conditional model, the further stimulation with tamoxifen resulted in accelerated and more profound phenotype changes with a 100% recombination of *Alox12b* in all K14 expressing tissues. For K14-Cre-ER^{T2} Fatp4$^{fl/fl}$ mice representing another conditional KO model with barrier defects, in contrast, a persistent tamoxifen treatment for a long period of time was required to evoke an ichthyosiform phenotype that was much weaker as compared to mice with constitutive Fatp4 deficiency implicating a more important role of Fatp4 for the generation than for the maintenance of the epidermal barrier [71].

By the use of the skin graft approaches and epidermal specific 12R-LOX ablation, we demonstrated that the function of 12R-LOX in keratinocytes is essential

for the development and maintenance of a normal epidermal structure as well as for epidermal barrier function.

5.3. Ultrastructure of the 12R-LOX skin

A characteristic ultrastructural feature of the neonatal 12R-LOX KO skin is the presence of vacuole-like structures in the upper granular cells, the appearance of which resembles those functioning as reliable ultrastructural markers in a distinct group of ARCI patients [55, 80]. Our suggestion was that loss of barrier function might be caused by a disturbance of normal processing of lamellar bodies, which is essential for the formation of intercellular lipid structures. Consistent with a pathogenic role of a disturbed lipid metabolism, we furthermore observed significant alterations in the composition of ester-bound ceramides in the neonatal KO skin. A comprehensive lipid analysis was not feasible because of the small size of the skin grafts, however we now have to our disposal the *Alox12b*$^{fl/fl/K14\text{-}Cre\text{-}ERT2}$ mouse model, which will be used for further lipid analysis. In addition, electron microscopic examination of the adult skin grafts and *Alox12b*$^{fl/fl/K14\text{-}Cre\text{-}ERT2}$ adult skin does not reveal any of the above described vacuole-like structures suggesting that these might be caused by the rapid dehydratation after birth of the newborn deficient mice. We observe, however, occasionally deposits of cytoplasmatic material within the intercellular space of the stratum corneum lamellae of mutant skin grafts and conditional KOs at day 32, with the same appearance as extruded contents of lamellar bodies in the transition area supporting the proposed hypothesis that 12R-LOX deficiency might affect processing of lamellar bodies.

5.4. Other phenotypic changes observed in the 12R-LOX conditional mouse model

Not only changes of the skin morphology and ultrastructure could be observed in the skin of tamoxifen treated *Alox12b*$^{fl/fl/K14\text{-}Cre\text{-}ERT2}$ animals but also other organs were affected. After tamoxifen treatment gross phenotypic changes were observed including thymic atrophy, kyphosis, sarcopenia, and strongly reduced amount of fat tissue, which contributed to the cachectic appearance at the time of death. As the observed reduced size of spleen and thymus represent clear defects in the innate immune system, , it will be essential to investigate in more detail the subsequent impacts of 12R-LOX-deficiency on immune responses. Moreover, JunB deficient mice showed enlarged spleen [81] while 12R-LOX deficient mice expressed higher levels of JunB. Therfore, it might be of interest to clarify if the 12R-LOX conditional mice also have higher levels of JunB, which could explain the smaller spleen. Low bone mass (osteopenia) and higher bone fragility was registered in 12R-LOX conditional animals, therefore it will be very interesting to investigate the balance between osteoclast (cells that reabsorb old bone) and osteoblast (cells depositing

new bone), which is crucial for the correct bone remodelling. For osteoclast differentiation c-Fos is required, accordingly, mice that lack a functional c-Fos gene develop osteopetrosis (decreased bone resorption and increased levels of calcified bone matrix) [82]. In the one hand, 12R-LOX deficient mice as well as 12R-LOX conditional KO (data not shown) expressed c-Fos at a higher level, which could be a possible explanation for the osteopenia found in the conditional animals. A possible correlation between both events could be assessed by decreasing c-Fos levels upon interferon-ß treatment which in turn would slow down the excessive bone destruction [83]. On the other hand, there is substantial epidemiological evidence that many of the chronic inflammatory diseases are associated with systemic bone loss [84].

It has been described that different ways of tamoxifen delivery produce slightly different phenotypes [85]. To examine more localized changes in the skin and to get a milder phenotype and elongate the lifespan of the *Alox12b*$^{fl/fl/K14\text{-}Cre\text{-}ERT2}$ mice, tamoxifen should be topically applied to areas of shaved back skin, a site that is not easily accessible for self-grooming, scratching and mechanical irritation. If we manage to induce in the mice a milder phenotype, as observed in human patients, therapeutic tests will be more reliable and can be made for longer period of time.

5.5. Cornified envelope proteins

A remarkable feature of the adult skin graft and of the *Alox12b*$^{fl/fl/K14\text{-}Cre\text{-}ERT2}$ mice as compared to the newborn mutant skin is the restoration of profilaggrin processing. As previously shown, 12R-LOX deficient newborn skin completely lacks mature filaggrin monomers, a defect that considerably might contribute to the early neonatal death [55]. Disturbance of profilaggrin processing is also observed in several other mouse models with defective barrier function and in humans a lack of proteolytically processed filaggrin monomers has been shown to underlie ichthyosis vulgaris and suggested to be a major predisposing factor for atopic dermatitis [75, 86-90]. The processing of profilaggrin to filaggrin and the final proteolytic steps of filaggrin degradation is a complex and poorly understood cascade during late differentiation that requires the coordinated activity of various enzymes including phosphatases, proteases and protease inhibitors. It is currently unknown how 12R-LOX deficiency affects these pathways. The reappearance of filaggrin monomers in adult skin grafts could possibly be explained by a diffusible host factor that compensates for the defect evoked by 12R-LOX deficiency in the neonatal KO skin, but this explanation can not be applied to the of the *Alox12b*$^{fl/fl/K14\text{-}Cre\text{-}ERT2}$ mice. As the deletion of *Alox12b* in our model occurs slowly and over a long period of time and in a patchy way, as seen in the immunofluorescens staining of the tongue epithelia, it could be that neighbouring keratinocytes are able to overproduce filaggrin monomers or factors necessary for the correct profilaggrin processing thus counteracting the defects evoked by 12R-LOX deficiency. As already discussed, this problem will be hopefully overcome by diminution of the cre activity leakiness by changing either diet

or genetic background of the mice, thus being able to produce then a general time-specific deletion of *Alox12b*.

Western blot analysis not only indicated unimpaired profilaggrin processing in the adult KO skin grafts as well as in the *Alox12b*$^{fl/fl/K14\text{-}Cre\text{-}ERT2}$ epidermis but also, as compared to control, a strong upregulation of filaggrin and repetin, whereas involucrin was only found to be overexpressed in skin grafts but not in *Alox12b*$^{fl/fl/K14\text{-}Cre\text{-}ERT2}$ mice. Keratins 5 and 10 expression was unchanged. Involucrin represents a major CE scaffold protein while repetin, another member of the multifunctional fused gene family profilaggrin belongs to, is a minor structural CE component commonly expressed in toughened epithelia and during wound healing [91, 92]. Compensatory up-regulation of repetin in response to barrier disturbance has previously been observed in the skin of loricrin deficient mice [93]. The genes of filaggrin, involucrin and repetin are localised close together within the highly conserved epidermal differentiation complex (EDC) suggesting a coordinate up-regulation of these genes, which has also could be linked to deregulation of AP-1.

5.6. Involvement of 12R-LOX in skin differentiation pathways

To date, very little is known about the molecular pathways in which 12R-LOX is involved and its implication in keratinocytes proliferation and differentiation. In order to unravel the molecular mechanisms of LOX action responsible for ichthyosis, we performed global gene expression analysis of epidermis isolated from 12R-LOX deficient newborn mice. Enormous individual differences in the KOs gene expression profile were observed that might be due to the rapid dramatic changes happening directly after birth. However some genes were identified showing differential expression in all KO samples as compared with samples from wild-types and heterozygotes. As a consequence we have focussed on several candidate genes, which were previously described to play an important role in keratinocytes proliferation and differentiation.

Among them, two keratin genes, K6 and K16, have been found up-regulated in absence of 12R-LOX. Keratins are a family of proteins that form the intermediate filament cytoskeleton in epithelial cells. The first step in keratin intermediate filament (KIF) assembly is the formation of heterodimers between one type I and one type II keratins. K16 and its partner, K6, are expressed in various stratified epithelia including those of the oral cavity, esophagus, genital tract, and epidermis. In the epidermis, they are normally confined to the hair follicles, sweat and sebaceous glands, although they are also expressed in the suprabasal layer of palmoplantar epidermis[94]. The enhanced expression of these two keratins is of particular interest since they are expressed in hyperproliferative situations such as benign and malignant tumors, keratinocytes in culture, in hyperproliferative skin diseases such as psoriasis, and during wound healing [95]. Interestingly, although K16 and K6 were

robustly up-regulated in 12R-LOX deficient epidermis, no obvious hyperproliferative cutaneous phenotype could be observed in the 12R-LOX deficient newborn. Moreover, hyperproliferation and hyperkeratosis was first visible in 4 weeks old KO skin grafts and 3 to 4 weeks old *Alox12b*$^{fl/fl/K14\text{-}Cre\text{-}ERT2}$ conditional animals. This phenotype is also seen in other deficient mice suffering from severe skin barrier defects as well as in skin from ichthyosis patients and has been proposed to result from a typical compensatory mechanism[3, 5]. In 12R-LOX deficient skinup-regulation of K16 and K6 may be due to a compensatory effect rather than a direct consequence.

Another class of genes whose expression was increased in KO epidermis is the family of small proline rich proteins (SPRR). This family includes at least 15 different proteins and all members are part of the epidermal differentiation complex (EDC) which in addition encodes other structural proteins of the skin (loricrin, filaggrin, involucrin) as well as 13 different S100 and 18 late envelope proteins (*Lep*) genes [96, 97]. The primary role of the SPRR proteins is to serve as precursors for the CE functioning as cross-bridging proteins [98]. The coordinated up-regulation of the EDC genes has been reported from mice with targeted ablation of the transcription factor klf14 where 12 of the 15 members of the SPRR family were found to be deregulated in response to the severe barrier dysfunction in these mice [99]. Deregulation of the *sprr* genes has also been described in other transgenic mouse models with epidermal permeability barrier dysfunction [93, 100], suggesting that this could be a general response to barrier dysfunction.

Lastly, the group of deregulated genes that attracted our attention was the family members of the activating protein-1 (AP-1). Not only were JunB and Fos highly expressed in the 12R-LOX deficient epidermis but also the expression of other members such as c-Jun, Fra-1 and FosB was affected. AP-1 is known to mediate gene regulation in response to a variety of extracellular stimuli including growth factors, cytokines, and oncogenes [62, 63, 101]. The role of AP-1 in skin biology has been intensively studied in the past years and it became clear that each individual AP-1 subunit plays a different critical role in cell proliferation and differentiation. A general concept suggests that c-Jun is a positive regulator of cell proliferation, while JunB acts as an attenuator of cell cycle progression and favours differentiation. However, it has been recently postulated that this concept may not account for cells in the epidermis, at least in humans [62], and our results would corroborate this observation as well in mice. This would suggest that in mice, as well as in humans, the AP-1 subunits expressed in keratinocytes are predominantly involved in the regulation of the differentiation program rather than in the proliferation control. However, the expression pattern of Fos and Jun proteins in mice may point to a critical role of c-Jun in keratinocyte proliferation or in the early stages of differentiation [62]. The AP-1 target genes in the epidermis include transglutaminase and different keratins, all of them being critical players of skin homeostasis [102-104]. Thus, increased activity of AP-1 could explain the higher expression levels of K6 and K16

observed in 12R-LOX KO epidermis. In humans, high basal level expression of the profilaggrin gene in epidermal keratinocytes depends on c-Jun/c-Fos heterodimers [105], whereas co-operative action of AP-1 and Sp1 is required for maximal expression of the human involucrin promoter [106]. However, since c-Jun expression levels were diminished in absence of 12R-LOX, some other AP-1 subunits, e.g. Fra-1 and JunB which are up-regulated in 12R-LOX deficient mice, might be responsible for the upregulation of involucrin [107]. Functional synergism between AP-1 and ETS transcription factors proteins was found to mediate expression of the keratinocyte terminal differentiation markers SPRR-1A and SPRR-3 [108]. In contrast, expression of SPRR-2 members is negatively regulated by c-Jun [109]. Therefore, the decreased expression of c-Jun in 12R-LOX deficient epidermis might be causative of increased SPRR expression.

There is strong evidence that signal transduction pathways modulating AP-1 activity are main regulators of keratinocyte proliferation and differentiation [110]. AP-1 activity is regulated by multiple signaling pathways including the Erk MAPK. In line with the dysregulated expression of AP-1 members, especially with increased Fos levels, Erk1/2 were found to be highly activated in the epidermis of 12R-LOX deficient mice. Erk1/2 activation has been previously described in hyperproliferative conditions of human skin (acanthosis nigrans and squamous cell carcinoma), as well as in healing skin wounds in mice and in psoriatic skin [69, 111-113]. Our data suggests that Erk1/2 activation and AP-1 deregulation are also implicated in a broad range of skin diseases including ichthyosis thus indicative as a broad functional marker of disturbed proliferation and/or differentiation of keratinocytes.

In order to determine whether deregulated AP-1activity is responsible for the improper proliferation-differentiation status observed in the pathology of ichthyosis, cell culture models as well as KO mouse models will be analyzed. By using siRNA technology against AP-1 members in immortalized keratinocytes isolated from 12R-LOX KO mice we could analyze proliferation and differentiation ability. In addition, it will be very interesting and challenging to analyse double conditional KO animals with epidermal deletion of AP-1 subunits in addition to 12R-LOX in order to decipher the interaction of both components during the development of the diseased phenotype.

Finally, we demostrated that 12R-LOX plays a critical role in postnatal survival by regulating the skin barrier function. A few interesting candidate genes which might be responsible for this phenotype could be characterized. However, due to the rapid dramatic changes happening directly after birth, which brings enormous individual difference between KO mice, it will be challenging to precisely decipher the molecular mechanism responsible for the phenotype. Therefore, it will be very interesting to analyze as well the changes produced by 12R-LOX deletion during embryogenesis. To this end, we will perform global gene expression analysis with epidermis isolated at different time points of embryonic development, such as embryonic day 15,5, 16.5, when 12R-LOX expression starts, until embryonic day 18.5 just before birth. Thus, deciphering the molecular mechanisms responsible for the development of the

diseased phenotype will allow us to develop novel strategies towards novel appropriate therapies for ichthyosis. Furthermore, therapeutic consequences also could be directly investigated in our conditional 12R-LOX KO mouse model.

In summary, this study shows that mature 12R-LOX-deficient mouse skin as analysed in skin garfts and in a conditional KO model develops an ichthyosiform phenotype that closely resembles the phenotype observed in ichthyosis patients. This indicates that *Alox12b*$^{fl/fl/K14\text{-}Cre\text{-}ERT2}$ conditional mice represent a suitable animal model for ARCI forms associated with an impaired LOX metabolism and a perfect model for future therapeutic approaches.

Supplementary table

Symbol	Genename	mean_ko	mean_wt	FC
Sprr2e	small proline-rich protein 2E	2134,82	103,62	20,6
Sprr2g	small proline-rich protein 2G	2557,37	135,11	18,93
Sprr1b	small proline-rich protein 1B	9671,02	557,06	17,36
Sprr2i	small proline-rich protein 2I	1154,6	90,22	12,8
Krt1-16	keratin complex 1, acidic, gene 16	3904,18	320,87	12,17
Epgn	epithelial mitogen	1634,27	157,38	10,38
Areg	amphiregulin	3140,54	319,85	9,82
Cxcl1	chemokine (C-X-C motif) ligand 1	1112,41	142,87	7,79
Slpi	secretory leukocyte peptidase inhibitor	569,15	80,53	7,07
Arc	activity regulated cytoskeletal-associated protein	978,85	138,61	7,06
Junb	Jun-B oncogene	2973,14	442,21	6,72
NA	NA	874,96	136,06	6,43
Phlda1	pleckstrin homology-like domain, family A, member 1	8544,41	1354,55	6,31
Sprr2d	small proline-rich protein 2D	9065,13	1632,01	5,55
Serpinb2	serine (or cysteine) peptidase inhibitor, clade B, member 2	2758,35	520,18	5,3
Hbegf	heparin-binding EGF-like growth factor	541,81	109,35	4,96
Ccl20	chemokine (C-C motif) ligand 20	404,82	84,63	4,78
Ier3	immediate early response 3	4633,96	1059,84	4,37
Fosl1	fos-like antigen 1	366,45	88,66	4,13
NA	NA	695,17	170,1	4,09
Sprrl1	small proline rich-like 1	3904,17	962,44	4,06
Tnfaip3	tumor necrosis factor, alpha-induced protein 3	529,18	137,98	3,84
Rptn	repetin	7815,7	2061,17	3,79
Sprr1a	small proline-rich protein 1A	1336,48	355,21	3,76
Axud1	AXIN1 up-regulated 1	391,01	113,41	3,45
Fosb	FBJ osteosarcoma oncogene B	635,3	200,33	3,17
Cyp3a13	cytochrome P450, family 3, subfamily a, polypeptide 13	1098,6	355	3,09
Krt2-6b	keratin complex 2, basic, gene 6b	611,79	202,75	3,02
Pim3	proviral integration site 3	4969,23	1655,48	3
Ldlr	low density lipoprotein receptor	4851,06	1635,49	2,97
Epha2	Eph receptor A2	422,65	142,59	2,96
Dusp6	dual specificity phosphatase 6	2294,14	774,28	2,96

Symbol	Genename	mean_ko	mean_wt	FC
Ptpre	protein tyrosine phosphatase, receptor type, E	1682,76	585,8	2,87
Krt2-6a	keratin complex 2, basic, gene 6a	950,79	331,23	2,87
NA	NA	370,3	130,01	2,85
Sprr2j	small proline-rich protein 2J	194,81	68,47	2,85
Sertad1	SERTA domain containing 1	1239,15	441,77	2,8
Cyp1a1	cytochrome P450, family 1, subfamily a, polypeptide 1	262,49	94,81	2,77
Krt2-6b	keratin complex 2, basic, gene 6b	229,23	83,19	2,76
Neu2	neuraminidase 2	971,41	353,49	2,75
NA	NA	563,41	207,17	2,72
NA	NA	261,43	96,13	2,72
NA	NA	1752,66	647,83	2,71
Gtse1	G two S phase expressed protein 1	326,2	122,05	2,67
2310040C09Rik	RIKEN cDNA 2310040C09 gene	4863,13	1822,1	2,67
Dnase1l3	deoxyribonuclease 1-like 3	500,07	187	2,67
Gm1279	NA	248,1	93,61	2,65
Dusp1	dual specificity phosphatase 1	6956,81	2633,46	2,64
Adam28	a disintegrin and metallopeptidase domain 28	276,39	105,42	2,62
Egr1	early growth response 1	5600,44	2143,07	2,61
Ptprs	protein tyrosine phosphatase, receptor type, S	247,67	95,24	2,6
Prkg1	protein kinase, cGMP-dependent, type I	201,64	77,59	2,6
Rptn	repetin	1320,14	509,45	2,59
Olfr994	olfactory receptor 994	190,02	73,29	2,59
Cklf	chemokine-like factor	267,88	103,73	2,58
4930526D03Rik	RIKEN cDNA 4930526D03 gene	223,56	86,73	2,58
D930030D11Rik	RIKEN cDNA D930030D11 gene	282,07	109,8	2,57
Pdhb	pyruvate dehydrogenase (lipoamide) beta	257,99	101,16	2,55
Dach2	dachshund 2 (Drosophila)	241,53	95,36	2,53
Tnfrsf12a	tumor necrosis factor receptor superfamily, member 12a	2278,75	901,09	2,53
Fcrla	Fc receptor-like A	243,7	96,68	2,52
NA	NA	357,05	141,93	2,52
Sat1	spermidine/spermine N1-acetyl transferase 1	2513,99	1000,05	2,51
Hes7	hairy and enhancer of split 7 (Drosophila)	258,52	104,4	2,48
NA	NA	264,25	107,02	2,47

Symbol	Genename	mean_ko	mean_wt	FC
Ccdc86	coiled-coil domain containing 86	359,98	145,59	2,47
Cspg6	chondroitin sulfate proteoglycan 6	197,09	80,06	2,46
Bcl10	B-cell leukemia/lymphoma 10	1547,8	635,22	2,44
Gm1341	NA	219,69	90,68	2,42
NA	NA	1031,96	427,11	2,42
NA	NA	266,25	109,81	2,42
Fas	Fas (TNF receptor superfamily member)	305,38	127,03	2,4
Cdk5r1	cyclin-dependent kinase 5, regulatory subunit (p35) 1	908,81	380,57	2,39
NA	NA	202,77	85,21	2,38
Fpr-rs6	formyl peptide receptor, related sequence 6	251,36	105,8	2,38
1500041J02Rik	RIKEN cDNA 1500041J02 gene	604,02	254,25	2,38
Cars	cysteinyl-tRNA synthetase	248,73	104,88	2,37
Gse1	genetic suppressor element 1	244,92	103,74	2,36
Cish	cytokine inducible SH2-containing protein	2334	987,43	2,36
Gjb2	gap junction membrane channel protein beta 2	1609,72	684,42	2,35
Nfkbiz	nuclear factor of kappa light polypeptide gene enhancer in B-cells inhibitor, zeta	794,18	338,1	2,35
Tnrc4	trinucleotide repeat containing 4	259,81	110,94	2,34
Pnmt	phenylethanolamine-N-methyltransferase	261,6	111,93	2,34
Calu	calumenin	207,49	89,14	2,33
Klhl12	kelch-like 12 (Drosophila)	280,37	120,5	2,33
Itpkc	inositol 1,4,5-trisphosphate 3-kinase C	3698,6	1587,65	2,33
Tas1r2	taste receptor, type 1, member 2	223,38	96,16	2,32
Phlda2	pleckstrin homology-like domain, family A, member 2	293,09	126,29	2,32
Rapgef1	Rap guanine nucleotide exchange factor (GEF) 1	228,58	98,92	2,31
V1rc7	vomeronasal 1 receptor, C7	239,46	104,34	2,3
Tapbp	TAP binding protein	253,93	111,38	2,28
Olfr1395	olfactory receptor 1395	232,92	102,3	2,28
Cldn4	claudin 4	3874,77	1707,19	2,27
Hk2	hexokinase 2	3640,77	1605,69	2,27
NA	NA	261,95	115,42	2,27
2310042E22Rik	RIKEN cDNA 2310042E22 gene	361,05	159,46	2,26
NA	NA	478,18	211,45	2,26

Symbol	Genename	mean_ko	mean_wt	FC
1810008K16Rik	RIKEN cDNA 1810008K16 gene	224,03	99,68	2,25
Chl1	cell adhesion molecule with homology to L1CAM	203,55	90,74	2,24
Slc16a5	solute carrier family 16 (monocarboxylic acid transporters), member 5	321,54	144,03	2,23
Mdm2	transformed mouse 3T3 cell double minute 2	2488,9	1120,56	2,22
Grtp1	GH regulated TBC protein 1	242,76	109,74	2,21
Iars	isoleucine-tRNA synthetase	236,03	107,36	2,2
Veph1	ventricular zone expressed PH domain homolog 1 (zebrafish)	211,39	96,67	2,19
Klk6	kallikrein 6	498,77	227,68	2,19
2310040C09Rik	RIKEN cDNA 2310040C09 gene	1958,27	901,16	2,17
NA	NA	781,11	360,09	2,17
Siglech	sialic acid binding Ig-like lectin H	218,43	101,05	2,16
Psors1c2	psoriasis susceptibility 1 candidate 2 (human)	432,07	200,66	2,15
Sfn	stratifin	774,35	362,02	2,14
Ak3	adenylate kinase 3	291,68	136,24	2,14
Rassf1	Ras association (RalGDS/AF-6) domain family 1	1833,86	858,49	2,14
Atf3	activating transcription factor 3	371,77	173,82	2,14
Mbd3l1	methyl-CpG binding domain protein 3-like 1	239,85	112,08	2,14
Maff	v-maf musculoaponeurotic fibrosarcoma oncogene family, protein F (avian)	502,77	235,47	2,14
NA	NA	225,55	105,86	2,13
NA	NA	1091,93	512,92	2,13
Mdga1	MAM domain containing glycosylphosphatidylinositol anchor 1	284,83	133,99	2,13
St6galnac4	ST6 (alpha-N-acetyl-neuraminyl-2,3-beta-galactosyl-1,3)-N-acetylgalactosaminide alpha-2,6-sialyltransferase 4	250,17	117,33	2,13
Cyp3a13	cytochrome P450, family 3, subfamily a, polypeptide 13	316,1	149,09	2,12
Pla2g4e	phospholipase A2, group IVE	531,63	251,25	2,12
Il5	interleukin 5	191,44	90,46	2,12
Suv420h1	suppressor of variegation 4-20 homolog 1 (Drosophila)	1121,71	530,49	2,11

Symbol	Genename	mean_ko	mean_wt	FC
Olfr541	olfactory receptor 541	226	107,17	2,11
Krt1-12	keratin complex 1, acidic, gene 12	305,45	144,8	2,11
Fos	FBJ osteosarcoma oncogene	3366,45	1598,28	2,11
Tjap1	tight junction associated protein 1	237,31	113,45	2,09
9030607L17Rik	RIKEN cDNA 9030607L17 gene	334,92	160,06	2,09
Slc28a2	solute carrier family 28 (sodium-coupled nucleoside transporter), member 2	233,41	112,3	2,08
Rph3al	rabphilin 3A-like (without C2 domains)	228,17	109,69	2,08
Zfp353	zinc finger protein 353	203,57	98,24	2,07
1700109H08Rik	RIKEN cDNA 1700109H08 gene	813,08	392,86	2,07
Fga	fibrinogen, alpha polypeptide	221,62	107,63	2,06
Fbxl14	F-box and leucine-rich repeat protein 14	210,42	102,17	2,06
Foxd2	forkhead box D2	257,07	125,26	2,05
Ccr3	chemokine (C-C motif) receptor 3	209,83	102,22	2,05
Colec10	collectin sub-family member 10	206,12	100,53	2,05
Chn2	chimerin (chimaerin) 2	200,52	98,07	2,04
NA	NA	221,54	108,55	2,04
Olfr1365	olfactory receptor 1365	219,6	108,01	2,03
Barhl1	BarH-like 1 (Drosophila)	240,12	118,3	2,03
Folr4	folate receptor 4 (delta)	210,7	104,47	2,02
Slc5a1	solute carrier family 5 (sodium/glucose cotransporter), member 1	452,19	223,46	2,02
Zfp641	zinc finger protein 641	255,84	126,94	2,02
Per2	period homolog 2 (Drosophila)	899,96	446	2,02
0610040J01Rik	RIKEN cDNA 0610040J01 gene	219,2	108,55	2,02
1190003J15Rik	RIKEN cDNA 1190003J15 gene	10802,7	5351,69	2,02
Olfr1453	olfactory receptor 1453	221,18	109,56	2,02
Ippk	inositol 1,3,4,5,6-pentakisphosphate 2-kinase	727,51	362,17	2,01
Entpd6	ectonucleoside triphosphate diphosphohydrolase 6	226,5	113,06	2
Hsd3b2	hydroxysteroid dehydrogenase-2, delta<5>-3-beta	213,17	106,5	2
Klf3	Kruppel-like factor 3 (basic)	161,82	325,06	-2,01
Nudt16	nudix (nucleoside diphosphate linked moiety X)-type motif 16	203,81	413,45	-2,03
2510042P03Rik	RIKEN cDNA 2510042P03 gene	112,29	229,91	-2,05
Clec2d	C-type lectin domain family 2, member d	966,13	1975,77	-2,05

Symbol	Genename	mean_ko	mean_wt	FC
Gata3	GATA binding protein 3	960,14	1974,09	-2,06
NA	NA	315,77	653,89	-2,07
NA	NA	167,27	349,5	-2,09
Acsl1	acyl-CoA synthetase long-chain family member 1	129,99	271,45	-2,09
Bcl11a	B-cell CLL/lymphoma 11A (zinc finger protein)	223,55	467,9	-2,09
NA	NA	173,45	362,65	-2,09
Trps1	trichorhinophalangeal syndrome I (human)	274,42	575,23	-2,1
Hsp90ab1	heat shock protein 90kDa alpha (cytosolic), class B member 1	571,39	1199,17	-2,1
NA	NA	119,6	253,85	-2,12
2310079G19Rik	RIKEN cDNA 2310079G19 gene	91,34	196,61	-2,15
Foxq1	forkhead box Q1	202,84	439,46	-2,17
Hoxd4	homeo box D4	162,42	354,03	-2,18
NA	NA	9574,69	20889,01	-2,18
9930028C20Rik	RIKEN cDNA 9930028C20 gene	566,33	1240,84	-2,19
2810003C17Rik	RIKEN cDNA 2810003C17 gene	1123,63	2465,35	-2,19
NA	NA	1738,21	3824,4	-2,2
NA	NA	127,45	282,31	-2,22
Hsp90ab1	heat shock protein 90kDa alpha (cytosolic), class B member 1	255,6	572,53	-2,24
Cpa3	carboxypeptidase A3, mast cell	186	417,98	-2,25
Hmgcs2	3-hydroxy-3-methylglutaryl-Coenzyme A synthase 2	156,58	352,13	-2,25
Ppp1r3c	protein phosphatase 1, regulatory (inhibitor) subunit 3C	284,01	647,56	-2,28
Snrpb	small nuclear ribonucleoprotein B	371,89	854,91	-2,3
Cobl	cordon-bleu	115,39	267,03	-2,31
Txnip	thioredoxin interacting protein	2862,5	6609,7	-2,31
NA	NA	371,74	862,75	-2,32
1110055J05Rik	RIKEN cDNA 1110055J05 gene	5043,14	11719,23	-2,32
NA	NA	176,7	411,78	-2,33
MTERF	NA	157,48	366,91	-2,33
Sprrl5	small proline rich-like 5	10061,24	23880,9	-2,37
NA	NA	168,38	403,19	-2,39
NA	NA	444,88	1088,69	-2,45
NA	NA	115,13	286,96	-2,49
Ecm1	extracellular matrix protein 1	752,5	1880,32	-2,5
NA	NA	529,31	1381,06	-2,61
Sprrl7	small proline rich-like 7	4196,75	11531,76	-2,75

Symbol	Genename	mean_ko	mean_wt	FC
2300008B03Rik	RIKEN cDNA 2300008B03 gene	144,77	400,37	-2,77
Gpsm1	G-protein signalling modulator 1 (AGS3-like, C. elegans)	601,66	1753,85	-2,92
NA	NA	145,67	444,68	-3,05
NA	NA	1623,91	4989,29	-3,07
Gba2	glucosidase beta 2	405,17	1256,9	-3,1
1110058A15Rik	RIKEN cDNA 1110058A15 gene	277	916,83	-3,31
Sprrl2	small proline rich-like 2	2631,41	9281,1	-3,53
1110008K04Rik	RIKEN cDNA 1110008K04 gene	521,53	2227,56	-4,27
Sprrl9	small proline rich-like 9	190,25	854,72	-4,49
1110031B11Rik	RIKEN cDNA 1110031B11 gene	509,9	3182,56	-6,24
NA	NA	182,8	1254,17	-6,86
2310069N01Rik	RIKEN cDNA 2310069N01 gene	668,35	4781,63	-7,15
NA	NA	408,16	3745,83	-9,18

6. References

1. Hengge, U.R. and B. Volv-Platzer, *The skin and gene therapy*. 2001: Springer.
2. Nouri, K., *Skin Cancer*. 2008: Mc Graw Hill Medical.
3. Segre, J.A., *Epidermal barrier formation and recovery in skin disorders.* J Clin Invest, 2006. 116(5): p. 1150-8.
4. Porter, R.M. and E.B. Lane, *Phenotypes, genotypes and their contribution to understanding keratin function.* Trends Genet, 2003. 19(5): p. 278-85.
5. Oji, V. and H. Traupe, *Ichthyoses: differential diagnosis and molecular genetics.* Eur J Dermatol, 2006. 16(4): p. 349-59.
6. Lefevre, C., et al., *Mutations in a new cytochrome P450 gene in lamellar ichthyosis type 3.* Hum Mol Genet, 2006. 15(5): p. 767-76.
7. Huber, M., et al., *Mutations of keratinocyte transglutaminase in lamellar ichthyosis.* Science, 1995. 267(5197): p. 525-8.
8. Jobard, F., et al., *Lipoxygenase-3 (ALOXE3) and 12(R)-lipoxygenase (ALOX12B) are mutated in non-bullous congenital ichthyosiform erythroderma (NCIE) linked to chromosome 17p13.1.* Hum Mol Genet, 2002. 11(1): p. 107-13.
9. Lefevre, C., et al., *Mutations in the transporter ABCA12 are associated with lamellar ichthyosis type 2.* Hum. Mol. Genet., 2003. 12(18): p. 2369-2378.
10. Lefevre, C., et al., *Mutations in ichthyin a new gene on chromosome 5q33 in a new form of autosomal recessive congenital ichthyosis.* Hum. Mol. Genet., 2004. 13(20): p. 2473-2482.
11. Funk, C.D., *Molecular biology in the eicosanoid field.* Prog Nucleic Acid Res Mol Biol, 1993. 45: p. 67-98.
12. Funk, C.D., *The molecular biology of mammalian lipoxygenases and the quest for eicosanoid functions using lipoxygenase-deficient mice.* Biochim Biophys Acta, 1996. 1304(1): p. 65-84.
13. Shibata, D. and B. Axelrod, *Plant lipoxygenases.* J Lipid Mediat Cell Signal, 1995. 12(2-3): p. 213-28.
14. Brash, A.R., Boeglin, W. E., Chang, M. S., and Shieh, B.-H. , J. Biol. Chem. , 1996. 271: p. 20949-20957.
15. Krieg, P., et al., *12-Lipoxygenase isoenzymes in mouse skin tumor development.* Mol Carcinog, 1995. 14(2): p. 118-29.
16. Heidt M., F.G., Vogel S.,Marks F., Krieg P., *Diversity of mouse lipoxygenases: identification of a subfamily of epidermal isozymes exhibiting a differentiation-dependent mRNA expression pattern.* Lipids, 2000. 35: p. 701-707.
17. Furstenberger, G., et al., *What are cyclooxygenases and lipoxygenases doing in the driver's seat of carcinogenesis?* Int J Cancer, 2006. 119(10): p. 2247-54.
18. Brash, A.R., *Lipoxygenases: occurrence, functions, catalysis, and acquisition of substrate.* J Biol Chem, 1999. 274(34): p. 23679-82.
19. Jisaka, M., et al., *Molecular cloning and functional expression of a phorbol ester-inducible 8S-lipoxygenase from mouse skin.* J Biol Chem, 1997. 272(39): p. 24410-6.

20. Chen, X.S., et al., *cDNA cloning, expression, mutagenesis, intracellular localization, and gene chromosomal assignment of mouse 5-lipoxygenase.* J Biol Chem, 1995. 270(30): p. 17993-9.
21. Krieg, P., et al., *Murine 12(R)-lipoxygenase: functional expression, genomic structure and chromosomal localization.* FEBS Lett, 1999. 446(1): p. 142-8.
22. Kinzig, A., et al., *cDNA cloning, genomic structure, and chromosomal localization of a novel murine epidermis-type lipoxygenase.* Genomics, 1999. 58(2): p. 158-64.
23. Gillmor, S.A., et al., *The structure of mammalian 15-lipoxygenase reveals similarity to the lipases and the determinants of substrate specificity.* Nat Struct Biol, 1997. 4(12): p. 1003-9.
24. Piomelli, D., et al., *Lipoxygenase metabolites of arachidonic acid as second messengers for presynaptic inhibition of Aplysia sensory cells.* Nature, 1987. 328(6125): p. 38-43.
25. O'Flaherty, J.T., J.S. Taylor, and M.J. Thomas, *Receptors for the 5-Oxo Class of Eicosanoids in Neutrophils.* J. Biol. Chem., 1998. 273(49): p. 32535-32541.
26. Tang, D., Y. Chen, and K. Honn, *Arachidonate lipoxygenases as essential regulators of cell survival and apoptosis.* PNAS 1996(93): p. 5241-5246.
27. Yu, K., et al., *Differential Activation of Peroxisome Proliferator-activated Receptors by Eicosanoids.* J. Biol. Chem., 1995. 270(41): p. 23975-23983.
28. Yu, Z., et al., *Epidermal Lipoxygenase Products of the Hepoxilin Pathway Selectively Activate the Nuclear Receptor PPARα.* Lipids, 2007. 42(6): p. 491-497.
29. Rapoport, S. and T. Schewe, *The maturational breakdown of mitochondria in reticulocytes.* Biochim Biophys Acta, 1986. 864(3-4).
30. Thorburn, D. and E. Beutler, *The loss of enzyme activity from erythroid cells during maturation.* Adv Exp Med Biol. , 1991. 307: p. 15-27.
31. Muga, S.J., et al., *8S-Lipoxygenase Products Activate Peroxisome Proliferator-activated Receptor {{alpha}} and Induce Differentiation in Murine Keratinocytes.* Cell Growth Differ, 2000. 11(8): p. 447-454.
32. Thuillier, P., et al., *Inhibition of peroxisome proliferator-activated receptor (PPAR)-mediated keratinocyte differentiation by lipoxygenase inhibitors.* Biochem. J., 2002. 366(3): p. 901-910.
33. Lysz, T., et al., *12(S)-hydroxyeicosatetraenoic acid regulates DNA synthesis and protooncogene expression induced by epidermal growth factor and insulin in rat lens epithelium.* Cell Growth Differ, 1994. 5(10): p. 1069-1076.
34. Shillabeer, G., et al., *Arachidonic acid metabolites of the lipoxygenase as well as the cyclooxygenase pathway may be involved in regulating preadipocyte differentiation.* Metabolism, 1998. 47(4): p. 461-466.
35. Jira, W., G. Spiteller, and A. Richter, *Increased levels of lipid oxidation products in low density lipoproteins of patients suffering from rheumatoid arthritis.* Chemistry and Physics of Lipids, 1997. 87(1): p. 81-89.
36. Feinmark, S.J. and J.A. Cornicelli, *Is there a role for 15-lipoxygenase in atherogenesis?* Biochemical Pharmacology, 1997. 54(9): p. 953-959.

37. Hiltunen, T., et al., *Induction of 15-Lipoxygenase mRNA and Protein in Early Atherosclerotic Lesions.* Circulation, 1995. 92(11): p. 3297-3303.
38. Drazen, J.M., E. Israel, and P.M. O'Byrne, *Treatment of Asthma with Drugs Modifying the Leukotriene Pathway.* N Engl J Med, 1999. 340(3): p. 197-206.
39. Hammarström S., H.M., Samuelson B., Duell E.A., Stawiski M., Voorhees J.J., *Increased concentrations of nonesterified arachidonic acid, 12L-hydroxy-5,8,10,14-eicosatetraeonic acid, prostaglandin E_2, and prostaglandin F_2a in epidermis of psoriasis.* Procc. Natl. Acad. Sci. U. S. A., 1975. 72: p. 5130-5134.
40. Krieg, P., F. Marks, and G. Furstenberger, *A Gene Cluster Encoding Human Epidermis-type Lipoxygenases at Chromosome 17p13.1: Cloning, Physical Mapping, and Expression.* Genomics, 2001. 73(3): p. 323-330.
41. Eckl, K.-M., et al., *Molecular Analysis of 250 Patients with Autosomal Recessive Congenital Ichthyosis: Evidence for Mutation Hotspots in ALOXE3 and Allelic Heterogeneity in ALOX12B.* J Invest Dermatol, 2009.
42. Grazzini, E., et al., *Inhibition of oxytocin receptor function by direct binding of progesterone.* Nature, 1998. 392(6675): p. 509-512.
43. Picard, D., *Molecular endocrinology. Steroids tickle cells inside and out.* Nature, 1998. 392(6675): p. 8.
44. Logie, C. and F.A. Stewart, *Ligand-regulated site-specific recombination.* PNAS, 1995. 92: p. 5.
45. Metzger, D., et al., *Conditional site-specific recombination in mammalian cells using a ligand-dependent chimeric Cre recombinase.* PNAS, 1995. 95(12): p. 6.
46. Brocard, J., et al., *A chimeric Cre recombinase inducible by synthetic,but not by natural ligands of the glucocorticoid receptor.* Nucl. Acids Res., 1998. 26(17): p. 4086-4090.
47. Kaczmarczyk, S.J. and J.E. Green, *Induction of cre recombinase activity using modified androgen receptor ligand binding domains: a sensitive assay for ligand-receptor interactions.* Nucl. Acids Res., 2003. 31(15): p. e86-.
48. Kellendonk, C., et al., *Regulation of Cre recombinase activity by the synthetic steroid RU 486.* Nucl. Acids Res., 1996. 24(8): p. 1404-1411.
49. Schwenk, F., U. Baron, and K. Rajewsky, *A cre-transgenic mouse strain for the ubiquitous deletion of loxP-flanked gene segments including deletion in germ cells.* Nucl. Acids Res., 1995. 23(24): p. 5080-5081.
50. Feil, R., et al., *Ligand-activated site-specific recombination in mice.* Proc Natl Acad Sci U S A, 1996. 93(20): p. 4.
51. Indra, A., et al., *Temporally-controlled site-specific mutagenesis in the basal layer of the epidermis: comparison of the recombinase activity of the tamoxifen- inducible Cre-ER(T) and Cre-ER(T2) recombinases.* Nucl. Acids Res., 1999. 27(22): p. 4324-4327.
52. Vasioukhin, V., et al., *The magical touch: Genome targeting in epidermal stem cells induced by tamoxifen application to mouse skin.* Proc Natl Acad Sci U S A, 1999. 96(15): p. 6.

53. Seibler, J., et al., *Rapid generation of inducible mouse mutants.* Nucl. Acids Res., 2003. 31(4): p. e12-.
54. Kühbandner, S., et al., *Temporally controlled somatic mutagenesis in smooth muscle.* Genesis, 2000. 28(1): p. 15-22.
55. Epp, N., et al., *12R-lipoxygenase deficiency impairs epidermal barrier function.* Journal of Cell Biology, 2007.
56. Metzger, D. and P. Chambon, *Site- and Time-Specific Gene Targeting in the Mouse.* Methods, 2001. 24(1): p. 71-80.
57. Schultze, J.L. and D. Eggle, *IlluminaGUI: Graphical User Interface for analyzing gene expression data generated on the Illumina platform.* Bioinformatics, 2007. 23(11): p. 1431-1433.
58. Lichti, U., J. Anders, and S.H. Yuspa, *Isolation and short-term culture of primary keratinocytes, hair follicle populations and dermal cells from newborn mice and keratinocytes from adult mice for in vitro analysis and for grafting to immunodeficient mice.* Nat. Protocols, 2008. 3(5): p. 799-810.
59. Barrandon, Y., V. Li, and H. Green, *New Techniques for the Grafting of Cultured Human Epidermal Cells onto Athymic Animals.* J Investig Dermatol, 1988. 91(4): p. 315-318.
60. Indra, A.K., et al., *Targeted somatic mutagenesis in mouse epidermis.* Horm Res, 2000. 54(5-6): p. 296-300.
61. Hess, J., P. Angel, and M. Schorpp-Kistner, *AP-1 subunits: quarrel and harmony among siblings.* J Cell Sci, 2004. 117(25): p. 5965-5973.
62. Angel, P., A. Szabowski, and M. Schorpp-Kistner, *Function and regulation of AP-1 subunits in skin physiology and pathology.* Oncogene, 2001. 20(19): p. 2413-2423.
63. Angel, P. and A. Szabowski, *Function of AP-1 target genes in mesenchymal-epithelial cross-talk in skin.* Biochemical Pharmacology, 2002. 64(5-6): p. 949-956.
64. Eckl, K.M., et al., *Mutation spectrum and functional analysis of epidermis-type lipoxygenases in patients with autosomal recessive congenital ichthyosis.* Hum Mutat, 2005. 26(4): p. 351-61.
65. Yu, Z., et al., *Mutations associated with a congenital form of ichthyosis (NCIE) inactivate the epidermal lipoxygenases 12R-LOX and eLOX3.* Biochim Biophys Acta, 2005. 1686 3: p. 238-47.
66. Moran, J.L., et al., *A Mouse Mutation in the 12R-Lipoxygenase, Alox12b, Disrupts Formation of the Epidermal Permeability Barrier.* J Invest Dermatol, 2007. 127(8): p. 1893-1897.
67. Li, M., et al., *RXR-alpha ablation in skin keratinocytes results in alopecia and epidermal alterations.* Development, 2001. 128(5): p. 675-688.
68. Hirrlinger, P.G., et al., *Temporal control of gene recombination in astrocytes by transgenic expression of the tamoxifen-inducible DNA recombinase variant CreERT2.* Glia, 2006. 54(1): p. 11-20.

69. Stratis, A., et al., *Localized Inflammatory Skin Disease Following Inducible Ablation of I Kappa B Kinase 2 in Murine Epidermis.* J Invest Dermatol, 2006. 126(3): p. 614-620.
70. Li, M., et al., *Skin abnormalities generated by temporally controlled RXR[alpha] mutations in mouse epidermis.* Nature, 2000. 407(6804): p. 633-636.
71. Herrmann, T., et al., *Disturbed Epidermal Structure in Mice with Temporally Controlled Fatp4 Deficiency.* J Investig Dermatol, 2005. 125(6): p. 1228-1235.
72. Penttinen, P., et al., *Diet-Derived Polyphenol Metabolite Enterolactone Is a Tissue-Specific Estrogen Receptor Activator.* Endocrinology, 2007. 148(10): p. 4875-4886.
73. Segre, J., *Complex redundancy to build a simple epidermal permeability barrier.* Current Opinion in Cell Biology, 2003. 15(6): p. 776-782.
74. Kuramoto, N., et al., *Development of ichthyosiform skin compensates for defective permeability barrier function in mice lacking transglutaminase 1.* Journal of Clinica Investigation, 2002. 109(2): p. 243-250.
75. Descargues, P., et al., *Spink5-deficient mice mimic Netherton syndrome through degradation of desmoglein 1 by epidermal protease hyperactivity.* Nat Genet, 2005. 37(1): p. 56-65.
76. Furuse, M., et al., *Claudin-based tight junctions are crucial for the mammalian epidermal barrier: a lesson from claudin-1-deficient mice.* J Cell Biol, 2002. 156(6): p. 1099-111.
77. Stone, S.J., et al., *Lipopenia and Skin Barrier Abnormalities in DGAT2-deficient Mice.* J. Biol. Chem., 2004. 279(12): p. 11767-11776.
78. Lesueur, F., et al., *Novel Mutations in ALOX12B in Patients with Autosomal Recessive Congenital Ichthyosis and Evidence for Genetic Heterogeneity on Chromosome 17p13.* J Invest Dermatol, 2006.
79. Harting, M., et al., *Self-healing collodion membrane and mild nonbullous congenital ichthyosiform erythroderma due to 2 novel mutations in the ALOX12B gene.* Archives of dermatology, 2008. 144: p. 351-356.
80. Dahlqvist, J., et al., *Congenital ichthyosis: mutations in ichthyin are associated with specific structural abnormalities in the granular layer of epidermis.* J Med Genet, 2007. 44(10): p. 615-620.
81. Meixner, A., et al., *Epidermal JunB represses G-CSF transcription and affects haematopoiesis and bone formation.* Nat Cell Biol, 2008. 10(8): p. 1003-1011.
82. Grigoriadis, A.E., Z.-Q. Wang, and E.F. Wagner, *Fos and bone cell development: lessons from a nuclear oncogene.* Trends in Genetics, 1995. 11(11): p. 436-441.
83. Takayanagi, H., et al., *RANKL maintains bone homeostasis through c-Fos-dependent induction of interferon-[beta].* Nature, 2002. 416(6882): p. 744-749.
84. Clowes, J.A., B.L. Riggs, and S. Khosla, *The role of the immune system in the pathophysiology of osteoporosis.* Immunological Reviews, 2005. 208(1): p. 207-227.

85. Paul, E., et al., *Disruption of Supv3L1 damages the skin and causes sarcopenia, loss of fat, and death.* Mammalian Genome, 2008.
86. Leyvraz, C., et al., *The epidermal barrier function is dependent on the serine protease CAP1/Prss8.* J. Cell Biol., 2005. 170(3): p. 487-496.
87. List, K., et al., *Matriptase/MT-SP1 is required for postnatal survival, epidermal barrier function, hair follicle development, and thymic homeostasis.* Oncogene, 2002. 21(23): p. 3765-3779.
88. Presland, R.B., et al., *Loss of Normal Profilaggrin and Filaggrin in Flaky Tail (ft//ft) Mice: an Animal Model for the Filaggrin-Deficient Skin Disease Ichthyosis Vulgaris.* 2000. 115(6): p. 1072-1081.
89. Sandilands, A., et al., *Prevalent and Rare Mutations in the Gene Encoding Filaggrin Cause Ichthyosis Vulgaris and Predispose Individuals to Atopic Dermatitis.* J Invest Dermatol, 2006. 126(8): p. 1770-1775.
90. Smith, W.L. and D.L. Dewitt, *Prostaglandin endoperoxide H synthases-1 and -2.* Adv Immunol, 1996. 62: p. 167-215.
91. Cooper, L., et al., *Wound healing and inflammation genes revealed by array analysis of 'macrophageless' PU.1 null mice.* Genome Biology, 2004. 6(1): p. R5.
92. Krieg, P., et al., *Repetin (Rptn), a New Member of the "Fused Gene" Subgroup within the S100 Gene Family Encoding a Murine Epidermal Differentiation Protein.* Genomics, 1997. 43(3): p. 339-348.
93. Koch, P.J., et al., *Lessons from Loricrin-deficient Mice: Compensatory Mechanisms Maintaining Skin Barrier Function in the Absence of a Major Cornified Envelope Protein.* J. Cell Biol., 2000. 151(2): p. 389-400.
94. Quinlan, R.A., et al., *Patterns of Expression and Organization of Cytokeratin Intermediate Filaments.* Annals of the New York Academy of Sciences, 1985. 455(Intermediate Filaments): p. 282-306.
95. Stoler, A., et al., *Use of monospecific antisera and cRNA probes to localize the major changes in keratin expression during normal and abnormal epidermal differentiation.* J. Cell Biol., 1988. 107(2): p. 427-446.
96. Marshall, D., et al., *Differentially expressed late constituents of the epidermal cornified envelope.* PNAS, 2001. 98: p. 13031-13036.
97. Song, H.-J., et al., *MouseSprr2Genes: A Clustered Family of Genes Showing Differential Expression in Epithelial Tissues.* Genomics, 1999. 55(1): p. 28-42.
98. Hohl, D., et al., *The Small Proline-Rich Proteins Constitute a Multigene Family of Differentially Regulated Cornified Cell Envelope Precursor Proteins.* J Investig Dermatol, 1995. 104(6): p. 902-909.
99. Patel, S., T. Kartasova, and J.A. Segre, *Mouse Sprr locus: a tandem array of coordinately regulated genes.* Mammalian Genome, 2003. 14(2): p. 140-148.
100. Turksen, K. and T.-C. Troy, *Permeability barrier dysfunction in transgenic mice overexpressing claudin 6.* Development, 2002. 129(7): p. 1775-1784.
101. Karin, M., Z.-g. Liu, and E. Zandi, *AP-1 function and regulation.* Current Opinion in Cell Biology, 1997. 9(2): p. 240-246.

102. Chuanshu Huang, J.L., Nanyue Chen, Wei-ya Ma, G. Tim Bowden, Zigang Dong,, *Inhibition of atypical PKC blocks ultraviolet-induced AP-1 activation by specifically inhibiting ERKs activation.* Molecular Carcinogenesis, 2000. 27(2): p. 65-75.
103. Eckert, R.L. and J.F. Welter, *Transcription factor regulation of epidermal keratinocyte gene expression.* Molecular Biology Reports, 1996. 23(1): p. 59-70.
104. Navarro, J.M., J. Casatorres, and J.L. Jorcano, *Elements Controlling the Expression and Induction of the Skin Hyperproliferation-associated Keratin K6.* J. Biol. Chem., 1995. 270(36): p. 21362-21367.
105. Jang, S.-I., P.M. Steinert, and N.G. Markova, *Activator Protein 1Activity Is Involved in the Regulation of the Cell Type-specific Expression from the Proximal Promoter of the Human Profilaggrin Gene.* J. Biol. Chem., 1996. 271(39): p. 24105-24114.
106. Lopez-Bayghen, E., et al., *Transcriptional Analysis of the 5`-Noncoding Region of the Human Involucrin Gene.* J. Biol. Chem., 1996. 271(1): p. 512-520.
107. Welter, J.F. and R.L. Eckert, *Differential expression of the fos and jun family members c-fos, fosB, Fra-1, Fra-2, c-jun, junB and junD during human epidermal keratinocyte differentiation.* Oncogene, 1995. 21: p. 2681-2687.
108. Fischer, D.F., et al., *Structure and Evolution of the HumanSPRR3Gene: Implications for Function and Regulation.* Genomics, 1999. 55(1): p. 88-99.
109. Lohman, F., et al., *Involvement of c-JUN in the regulation of terminal differentiation genes in normal and malignant keratinocytes.* Oncogene, 1997. 14: p. 1623-1627.
110. Rincón, M., R.A. Flavell, and R.J. Davis, *Signal transduction by MAP kinases in T lymphocytes.* Oncogene, 2001. 20(19): p. 2490-2497.
111. Albanell, J., et al., *Activated Extracellular Signal-regulated Kinases: Association with Epidermal Growth Factor Receptor/Transforming Growth Factor {alpha} Expression in Head and Neck Squamous Carcinoma and Inhibition by Anti-Epidermal Growth Factor Receptor Treatments.* Cancer Res, 2001. 61(17): p. 6500-6510.
112. Chaturvedi, V., et al., *Role of INK4a/Arf Locus-Encoded Senescent Checkpoints Activated in Normal and Psoriatic Keratinocytes.* Am J Pathol, 2003. 162(1): p. 161-170.
113. Haase, I. and N. Hunzelmann, *Activation of Epidermal Growth Factor Receptor//ERK Signaling Correlates with Suppressed Differentiation in Malignant Acanthosis Nigricans.* 2002. 118(5): p. 891-893.

FIGURES

Acknowledgments

At the end of my PhD, I would like to thank all the people who helped me on my way to success and made my PhD work possible, fruitful and enjoyable.

First, my biggest thank you goes to Peter Krieg, my supervisor, not only for his constructive comments and suggestions, but also for sharing knowledge and teaching me many techniques. I am very grateful to Gerd Fürstenberger for giving me the possibility of joining his lab for my PhD thesis.

I am very thankful to Rainer Zawatsky and Karin Müller-Decker who agreed to supervise my thesis.

Thanks a lot too to all the members of the Lab: particularly to Nico for teaching me many things about the project, to Ina for helping me to make a great start, to Timo, Markus, Susy and Lena.

I would like to express a very special thank you to Mareen, who was a great help throughout these three years not only for her excellent technical but also for her personal support.

I am very happy to have shared this experience with other PhD students from the neighbour´s lab, but specially: thank you Sara for being there everyday with a great mood and the best morning smile!

Finally a big thank you to my parents for making me somebody they can be proud of and for being my all and everything for many years. Their unconditional support and love always travel with me. Thanks to my brother for his encouragement and his ability to make out of every hurdle a new challenge.

And thank you Alex, so much, for sharing everything with me, for being there day and night, for being you… with me.